Comparative analysis of the Seasonal Sea Surface Temperature & Wind Stress in the four major Eastern Boundary Current Systems

Tarron Lamont

Submitted in fulfilment of the requirement for the degree of Master of Science in the Faculty of Science (Department of Oceanography).

January 2006

Supervisors: Prof. F. A. Shillington
Dr. C. Roy

Department of Oceanography
University of Cape Town

Acknowledgements

I wish to thank my supervisors, Prof. Frank Shillington from the Department of Oceanography at the University of Cape Town and Dr. Claude Roy from the Institut de Recherche pour le Développement, Brest, France, for their continual support and encouragement throughout the research and write-up of this thesis.

Abstract

The coastal upwelling regions along northwest Africa (the Canary system), southwest Africa (the Benguela system), North America (the California system), and South America (the Peru-Chile system) were studied and compared on a seasonal timescale. A 17-year NOAA Pathfinder Sea Surface Temperature (SST) dataset with a spatial resolution of 9km was used to describe the large-scale temporal and spatial variability of upwelling within the four regions. An upwelling index (DSST) was derived in order to add to the patterns of upwelling variability described from the sea surface temperature. The upwelling index was also used to describe the similarities and differences between the four upwelling regions. A 10-year ERS wind stress dataset with a spatial resolution of 1° x 1° was used to derive the offshore Ekman Transport in each of the regions. The offshore Ekman Transport was used to supplement the description of SST's in each system. Principal Component Analysis was used to investigate the variance structure of the anomalies of the sea surface temperature in each of the four regions. The results of the principal component analysis are interpreted in terms of the underlying physical dynamics.

In certain areas, the large-scale spatial and temporal variability was described very well by the Upwelling Index (for example, the Luderitz upwelling cell). In other areas (for example, the Cape Peninsula Upwelling cell), the index failed completely. This was likely due to the monthly averaged dataset not capturing the shorter, event-scale (3-10 days) upwelling. The upwelling index was also influenced by the suppression of the surface expression of upwelling during intense solar insolation. Results from the principal component analysis indicated that there are similarities between the four upwelling regions with regard to the variability in spatial extent and temporal structure of upwelling within the regions. Principal component 1 accounts for 42% of the total variance in the Benguela, 53% in the Peru-Chile, 47% in the Canary, and 50% in the California systems. The pattern exhibited by principal component 1 was better represented in the central part of the Benguela, Canary and California systems. In the Peru-Chile system, the pattern was better represented in the northern part of the region, along the Peruvian coast. Principal component 2 explains 18% of the total variance in the Benguela, 13% in the Peru-Chile, 12% in the Canary, and 12% in the California regions. The north-south dipole structure is suggestive of the seasonal polarity of the tropical and subtropical areas in each of the four systems. It seems that the pattern of variability described by principal component 2 can be related to the oceanic circulation, rather than to the solar irradiance received within each of the four systems.

Table of Contents

List of figures

Introduction

The Benguela, Humboldt, California, and Canary Current Systems are all Eastern Boundary Currents (EBC's), which flow equatorward to complete the large, basin-scale subtropical gyral circulations in the Atlantic and Pacific oceans. Generally, EBC's are slow moving, broad, and shallow (Wooster & Reid, 1963). The atmospheric forcing over EBC's is largely regulated by the subtropical anticyclonic systems in the mid-latitudes, which comprises the descending limb of the Hadley circulation cell (Hill et al., 1998). The trade winds blow equatorward over the sea surface, completing the lower branch of the Hadley cell. It is this meridional wind flow that powers the upwelling process by forcing the surface waters of EBC's equatorward. Once in motion, the surface waters become subject to Coriolis force, resulting in a deflection of the water 90° to the left (right) of the wind in the Southern (Northern) Hemisphere (Smith, 1968; Brink, 1983). Compensation for the divergence in the surface waters of the coastal ocean comes in the form of upwelled water. The water, which is upwelled, is rich in nutrients and typically comes from depths of 50-250m (Hill et al., 1998). During coastal upwelling, nutrients from depth are supplied to the euphotic zone, and consequently, upwelling regions are characterised by high levels of primary productivity (Carr, 2002) and relatively large populations of fish, seabirds, and other marine mammals. It is thus important to understand the nature and variability of the upwelling in each of these regions.

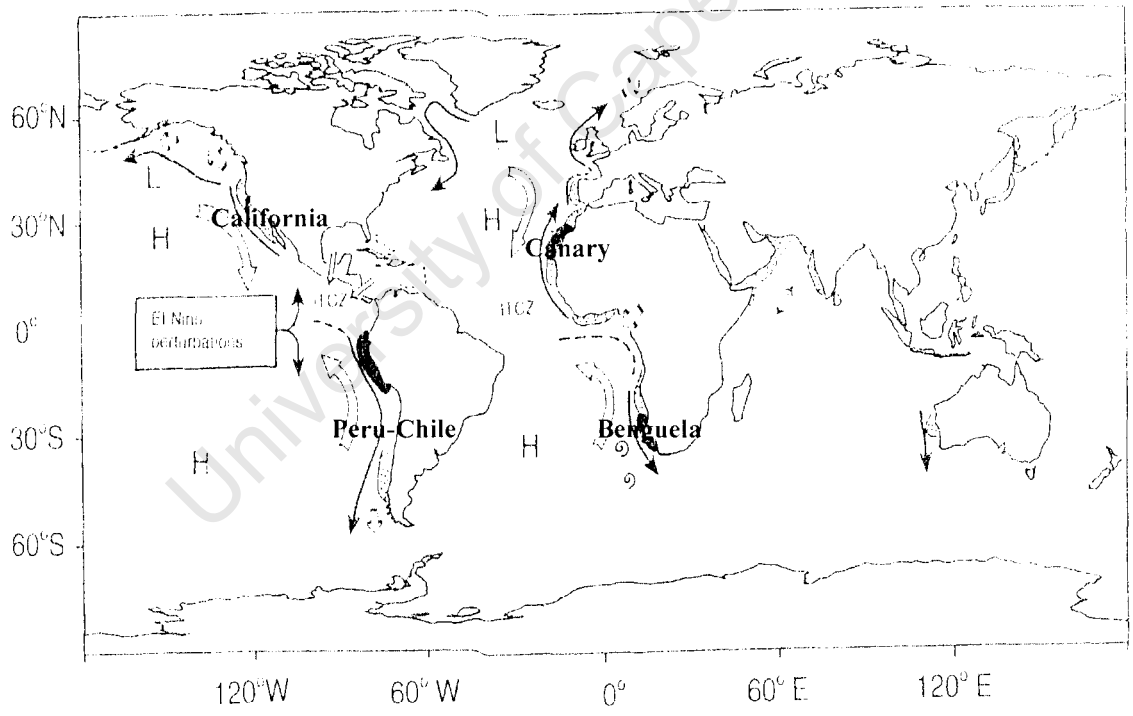

Figure 1: Global map showing the four major upwelling systems. (Adapted from Hill et al, 1998).

Variability in upwelling systems occurs on a variety of spatial and temporal scales (Abbot & Barksdale, 1995; Shillington, 1998). In this study attention is given to the mean seasonal pattern of sea surface temperatures (SST's) and upwelling favourable wind conditions within each region.

This study aims to:

- Describe the large-scale temporal and spatial variability of upwelling within the four main upwelling regions using satellite SST and wind data.
- Derive an upwelling index from the SST data to confirm and also add to the patterns of upwelling variability identified and described from the SST.
- Describe the similarities and differences between the four upwelling regions, using the upwelling index.

Due to its unique characteristics, the fifth major upwelling system located in the Indian Ocean is not included in this study.

Following this introduction, Chapter 1 provides an overview of the four main upwelling systems. The physical features, meteorology and associated upwelling variability of the four systems is described. Chapter 2 describes the data used and outlines the methodology applied in preparing and analysing the data. The results of this study are presented and discussed in Chapter 3. Chapter 4 summarises the similarities and differences between the four upwelling systems, and Chapter 5 follows with some concluding remarks.

Chapter 1 - Literature Review

This chapter provides an overview of the four main upwelling systems. The physical features of each system, the meteorology, the large scale ocean circulation, as well as the associated upwelling variability is reviewed.

1.1. The Benguela Upwelling System

The Benguela Current system extends along the southwestern coast of Africa and comprises the equatorward limb of the South Atlantic Subtropical gyre. It consists of an upwelling system extending from about Cape Frio (18°S) to Cape Agulhas (34°S) (Shillington, 1998).

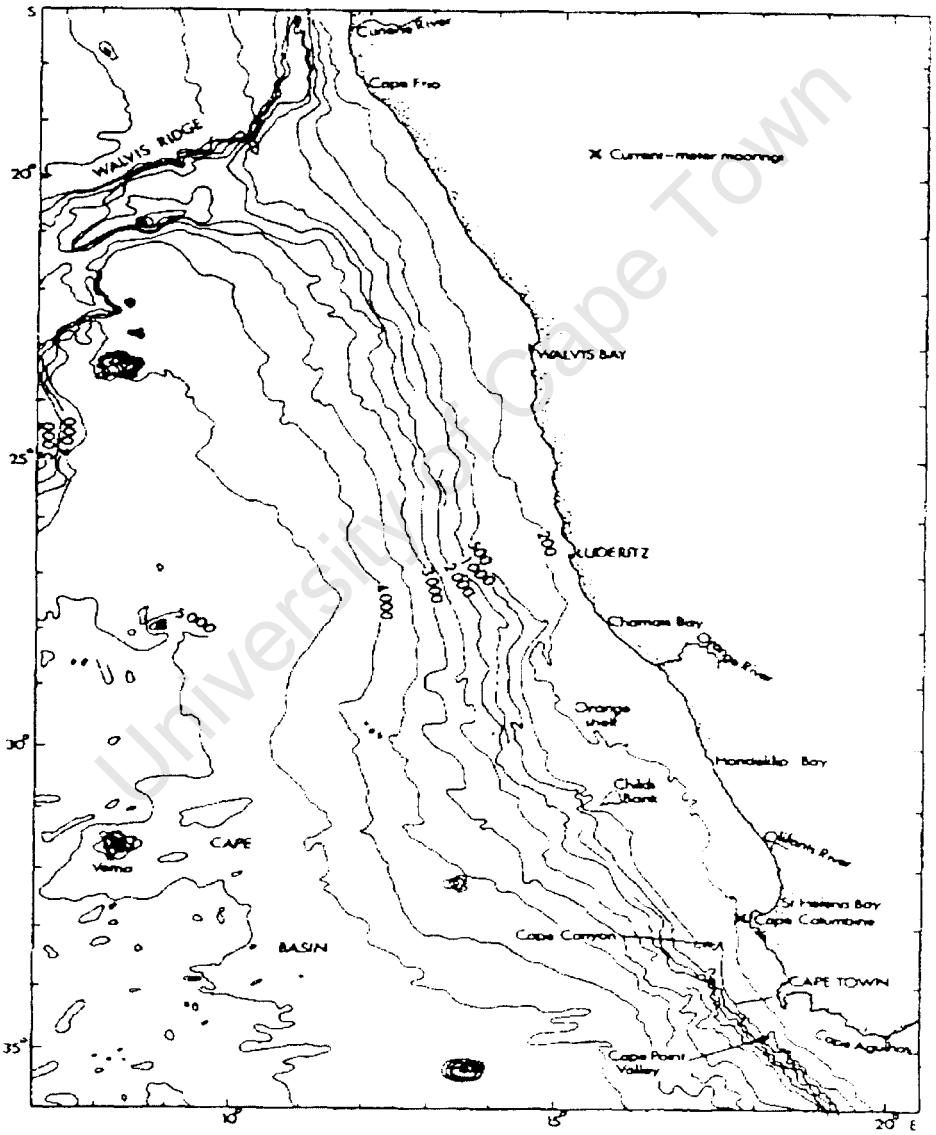

Figure 2: Bathymetry of the continental shelf off Southwest Africa between 10°S and 36°S. Depth contours in metres. (Taken from Shillington, 1998).

1.1.1. Shelf Topography

The west coast of southern Africa is characterised by a relatively narrow coastal plain which rises to the main continental escarpment situated 50-200km inland (Shannon, 1985; Shannon & Nelson, 1996). Off the Cape Peninsula, the coastal plain rises rapidly to form an escarpment 1000m high. This coastal elevation enhances horizontal air pressure and temperature gradients, resulting in stronger alongshore winds. The southwestern coastline of Africa is relatively straight, with only a few topographic irregularities in the southern region. At topographic irregularities such as capes (e.g. Cape Columbine, Cape Peninsula, Cape Hangklip) and canyons (e.g. Cape Canyon), upwelling is enhanced due to the modification of local wind patterns and the funnelling of cold water to the surface (Shannon & Nelson, 1996). For most of its length north of Cape Columbine, the coastline is low-lying and highly arid, with the Namib Desert extending between 14-31°S. The aridity increases the land-sea temperature gradient, resulting in stronger alongshore winds. These winds decrease the sea surface temperature (SST) by enhancing upwelling and thus reinforcing the temperature and pressure gradients across the coastline. The continental shelf, defined by the 200m isobath, varies in width from about 20km off southern Angola to 180km opposite the Orange River where the shelf widens to form the Orange River Cone. Around Walvis Bay (23°S), inner and outer shelf breaks are located at depths of about 140m and 400m. Between 31-33°S, inner and outer shelf breaks are located between 200-380m and at 500m. South of 33°S, a single shelf break is located at a depth of about 500m (Shannon & Nelson, 1996; Shannon, 1985). At about 20°S, the Walvis Ridge extends from the continental shelf in a southwesterly direction toward the Mid-Atlantic Ridge, separating the Southeast Atlantic abyssal plain into the Cape and Angola Basins. The Ridge forms a barrier to the northward and southward flow of water below 3000m (Shannon & Nelson, 1996; Shannon & Chapman, 1991).

1.1.2. Meteorology

Numerous studies of the wind field over the Southern Benguela have been published (Kamstra, 1985; Hutchings &Taunton-Clark, 1990; Jury, 1985b; Jury et al, 1985b; Jury 1988; Johnson &Nelson, 1999). Comparatively fewer studies exist for the Northern Benguela (Nelson & Hutchings, 1983; Shannon, 1985; Shannon & Nelson, 1996; Boyd, 1987; Boyd et al, 1987).

Prevailing winds over the Benguela system are influenced by the semi-permanent South Atlantic High pressure system, the seasonal low pressure field over the adjacent continent, and by eastward moving cyclones crossing the southern part of the continent (Preston-Whyte & Tyson, 1988; Shannon & Nelson, 1996). During summer, the high pressure system is situated further southeast (centred around 31°S). This results in strong southerly to southeasterly winds along the coast, which are upwelling-favourable. During winter, the high pressure system is situated further northwest (centred around 25°S). This allows the polar frontal systems to exert a greater influence on the wind field over the Southern Benguela, resulting in strong northwesterly to southwesterly winds which blow for a few hours at a time, over a period of 3-10 days (Jury et al, 1990; Shannon & Nelson, 1996). This causes upwelling-favourable winds to be suppressed during winter. Thus, upwelling-favourable winds reach a maximum during spring and summer in the Southern Benguela (Shannon, 1985; Andrews & Hutchings, 1980). In the Northern Benguela, there is less

seasonality in the wind fields and therefore less seasonality is observed in the upwelling conditions.

Associated with the cyclonic systems which pass south of the continent, there are low pressure cells which develop around Luderitz and travel southward around the subcontinent as coastally trapped waves (Jury et al, 1990; Jury & Brundrit, 1992)). These low pressure cells are best observed in summer when modulation by the South Atlantic High pressure system is weaker. As the wave travels along the coast, upwelling is suppressed locally by the cyclonic rotation of air around the cell.

1.1.3. Large-scale Current Circulation

Stramma & Peterson (1989) provide an overview of the geostrophically balanced current circulation of the Benguela system. Shannon & Nelson (1996) and Shillington (1998) review the large-scale current circulation of the South Atlantic Ocean. According to Shillington (1998), the Benguela upwelling system is largely influenced by its boundaries. Shillington (1998) considers 5 boundaries, namely, the upper surface boundary, the northern boundary, the southern boundary, the open ocean boundary and the bottom boundary.

- The upper surface boundary

At the surface, cyclonic wind stress curl patterns supply the Ekman pumping, which enhances coastal upwelling. Near the shelf break, west of Cape Town, a strong equatorward baroclinic jet current is confined to the surface layers. Bang & Andrews first measured this in 1974, by suspending a current meter over the side of a ship at various depths. Nelson (1985) improved this work by using better ship positioning and acoustic current meters suspended at various depths. The jet was shown to lie over the 300-400m isobaths and stretch from Cape Point to Child's Bank. In March 1990, the jet current was found to be further offshore. It appears to be enhanced by the presence of an Agulhas ring or warm water filament offshore of the Cape Peninsula (Shillington et al, 1992; Shillington, 1998). The jet current has been shown to play an important role in the transport of pelagic fish eggs and larvae from the spawning grounds on the Agulhas Bank to the nursery areas along the west coast (Parada, 2003; Hugget et al., 2003).

- The northern boundary

In the north, the Benguela system is bounded by the Angola-Benguela surface front. This front is a permanent feature and lies between 15-17°S, separating the warm Angolan Current from the cooler Benguela upwelling system. The front is well defined in the upper 50m and is most intense within 250km of the coast (Shannon & Nelson, 1996; Shannon et al, 1987). The average position of the front migrates seasonally over about 2° latitude from its northernmost position in winter (August) to its southernmost position in late summer (March) (Shannon et al, 1987; Meeuwis & Lutjeharms, 1990). Veitch et al (2005) found that the Angola-Benguela Front is broader during summer (spanning ~1.5° of latitude) and narrower during winter (spanning ~1° of latitude). Significant frontal movement (frontal eddies and tongue-like intrusions of warm water into the Benguela system) and variability is evident on shorter time-scales of days to weeks. Near the coast, there is a typical horizontal temperature gradient of 4°C per degree latitude, with temperatures ranging between 17-21°C. The orientation of the front is usually zonal, especially in winter and is maintained through a combination of

factors including bathymetry, stratification, coastal orientation, wind stress curl, as well as the opposing flows of the Angolan and Benguela Currents (Shannon & Nelson, 1996). Gordon & Bosley (1991) confirmed the presence of the Angola Dome, centred near 13°S, 5°E. This cyclonic circulation feature is situated in a region of anticyclonic wind stress curl.

- The southern boundary

In the south, the Benguela system is bounded by the Agulhas Retroflection area. Although the southern boundary of coastal upwelling is usually found south of Cape Town (Hart & Currie, 1960; Andrews & Hutchings, 1980), Schumann et al (1982) and Shannon et al (1983) and others have shown that upwelling occasionally extends as far south and east as Cape Agulhas (25°E). Evidence of warm water intrusions from the Agulhas Current into the Benguela system was first described by Bang (1971). These intrusions occur in the form of warm water filaments and Agulhas rings. The Agulhas Retroflection area shows a high degree of variability. Lutjeharms & van Ballegooyen (1988) provides a comprehensive overview of the kinematics and processes of the Retroflection region. Extreme circulation events in the Retroflection in 1985 and 1986 have been documented by Lutjeharms (1988) and Shannon et al (1990). At times, e.g. April 1984 (Walker, 1986) and August 1989 (Brundrit & Shannon, 1989), the Agulhas Current retroflects further west than normal, thereby exerting a greater influence on the southern part Benguela upwelling system.

- The open ocean boundary

The process of coastal upwelling results in an offshore zone of sharp, near-surface horizontal density gradients (Brink, 1983). This zone (or front) forms the boundary between the warmer oceanic water and the cooler upwelled water along the coast (Shillington et al, 1990; Shillington, 1998; van Foreest, 1984, Lutjeharms & Stockton, 1987). Upwelling filaments, which have a typical life span of a few days to several weeks, are characteristic of the oceanic front. These filaments are typically zonal in orientation and are on the order of 200km in length. In extreme cases, they may extend up to 1000km or more offshore (Lutjeharms et al, 1991). Lutjeharms & Stockton (1987) found that there are three preferred sites for filament formation, near 20°S, 26-27°S, and 30°S.

- The bottom boundary

Nelson (1989) concluded that the Benguela system has a definite poleward flow of the near-bottom water on the shelf. This poleward undercurrent is located at the shelf edge and comprises the deep compensating flow in the coastal upwelling model. The mean speed of this flow is about 5km.day $^{-1}$ (Nelson, 1989; Nelson & Polito, 1987). There are indications that further south, the flow becomes weaker and the core of the current deeper. Processes which may account for the poleward undercurrent in the Benguela system are tidal rectification, wind stress (Clarke, 1989) and forcing by mean density fields (Shannon & Nelson, 1996).

Low dissolved oxygen concentrations are characteristic of this bottom boundary flow. Chapman & Shannon (1985) suggest two source regions for this oxygen-depleted water:

- Off Angola, there is a southward-flowing wedge of low oxygen water at about 300m depth.
- On the shelf between the Cunene River and Luderitz, the near-bottom water is oxygen-depleted due to biochemical action.

1.1.4. Upwelling and Upwelling Variability

In the Benguela system, variability occurs at a variety of spatial and temporal scales (Shillington, 1998; Abbot & Barksdale, 1995). In the Southern Benguela, wind variability is dominated by the 3-10 day atmospheric synoptic scale, which sometimes extends to a few weeks (Shillington, 1998).

- Seasonal Variability

Hart & Currie (1960) found that the seasonality of wind is more pronounced in the Southern Benguela, where prevailing winds change from southerly and southeasterly winds in summer to northwesterly and southwesterly winds in winter. As a result, wind induced upwelling is more seasonal, reaching a maximum during spring and summer (September-March) and a minimum in late autumn and winter (Andrews & Hutchings, 1980). Wind variability in the Northern Benguela has a much less pronounced seasonal component, resulting in a smaller seasonal component in the upwelling cycle. Here, upwelling is more perennial. Characteristics of the principle upwelling centres have been described by various authors (Nelson & Hutchings, 1983; Shannon, 1985; Lutjeharms & Meeuwis, 1987). Six upwelling centres were identified by Shannon (1985):

- Cape Frio (18°S)
- Northern Namibia (20°S)
- Luderitz (24-27°S)
- Hondeklip (30°S)
- Cape Columbine (33°S)
- Cape Peninsula (34°S)

Lutjeharms & Meeuwis (1987) identified an additional cell along Central Namibia (23°S). The upwelling cells are generally located near regions of cyclonic wind stress curl and, in most cases, occur where there is a change in the orientation of the coastline.

In the Northern Benguela upwelling centres, upwelling occurs throughout the year, but reaches a maximum during winter (June-August). During summer (December-February), stratification of the water column suppresses the upwelling slightly. Off Central Namibia, the continental shelf is narrower and shallower than further south. Here, the shelf break occurs at around 140m depth. The upwelled water is thus slightly warmer than that further south. In the Cape Frio centre, upwelled water is about 19.5°C on average and that in the Central Namibian centre is about 18.5°C. The offshore extent of upwelled water is about 150km.

The semi-permanent upwelling centre in the vicinity of Luderitz is the most intense in the Benguela system. It comprises the environmental barrier that essentially divides the Benguela system into the Southern and Northern systems. Here, the shelf break is rather deep and water is upwelled from about 200-300m depth. The average temperature of the upwelled water is about 16.5°C. The offshore extent of upwelled water is greater here, reaching up to 300km off Luderitz. In the bight just south of the Orange River, where the shelf becomes narrow and deep, cyclonic wind stress curl is at a maximum and upwelling is continuous.

A persistent tongue of cold water extends offshore from the Hondeklip upwelling centre. Upwelling reaches a maximum during October-December and is at a minimum during May-July. In the Cape Columbine and Cape Peninsula centres, upwelling

occurs mainly during summer (December-February). Off Cape Columbine, filaments of upwelled water extend about 500-700km offshore and about 200-300km alongshore. Off Cape Peninsula, they reach approximately half that extent.

- Interannual Variability

Occasionally, interannual variations in the synoptic wind fields are larger than normal, resulting in unusually warm and cold periods (Shillington, 1998; Shannon & Nelson, 1996). The most significant of these variations appears to be related to the El Niño Southern Oscillation (ENSO). Although, according to Philander (1990), much of the interannual variability in the Atlantic is independent of the Southern Oscillation. Shannon et al (1986) refers to this Southeast Atlantic counterpart of the Pacific El Niño as "Benguela Niños". Benguela Niños are less intense and occur less frequently (at least once in ten years according to Shannon et al, 1986) than Pacific El Niños and are characterised by an intrusion of warm, saline tropical and equatorial water from the north and northwest (Shannon et al, 1986; Boyd et al, 1987; Gamelsrød et al, 1998). Benguela Niños have the strongest influence in the Northern Benguela and little or no effect in the Southern Benguela. However, the Southern Benguela seems to be affected more by El Niño Southern Oscillation (ENSO) events. The Northern Benguela appears to be out of phase with regard to ENSO events (Shannon et al, 1986). During Benguela Niños, local winds change. The 1949, 1972, and 1963 warmings were associated with significantly lower equatorward wind stress (Taunton-Clark, 1990). The Benguela Niños that have occurred during 1934, 1949, 1963, 1984, and 1995 are well documented (Shannon & Nelson, 1996; Shannon et al, 1992; Gamelsrød et al, 1998). Florenchie et al (2003) found that Benguela Niños were large-scale events, which extend meridionally from the equator to ~20°S along the west coast of Africa, and that they are not restricted to the sea surface, but are evident in deeper layers as well. Florenchie et al (2004) found that although warm and cold anomalies develop regularly off Angola and Namibia, Benguela Niños are most likely to occur when major warm events are in phase with late summer, since extremely high sea surface temperatures are induced. Cool events in the Benguela system are less well documented. Cool events have occurred during 1928, 1955, 1970-71, 1982. Clarke (1990) has suggested that the 1928 and 1955 cool events may have been associated with changes in the subtropical convergence and easterly winds. The cool event during 1970-71 was oceanic in origin while the 1982 event was confined to the shelf (Shannon & Nelson, 1996).

1.2. The Canary Upwelling System

The Canary Current System is located on the eastern boundary of the Central North Atlantic Ocean. It forms the poleward limb of the North Atlantic Subtropical gyre and consists of an upwelling system extending from the northern tip of Iberia (43°N) to south of Dakar (~10°N) (Barton, 1998).

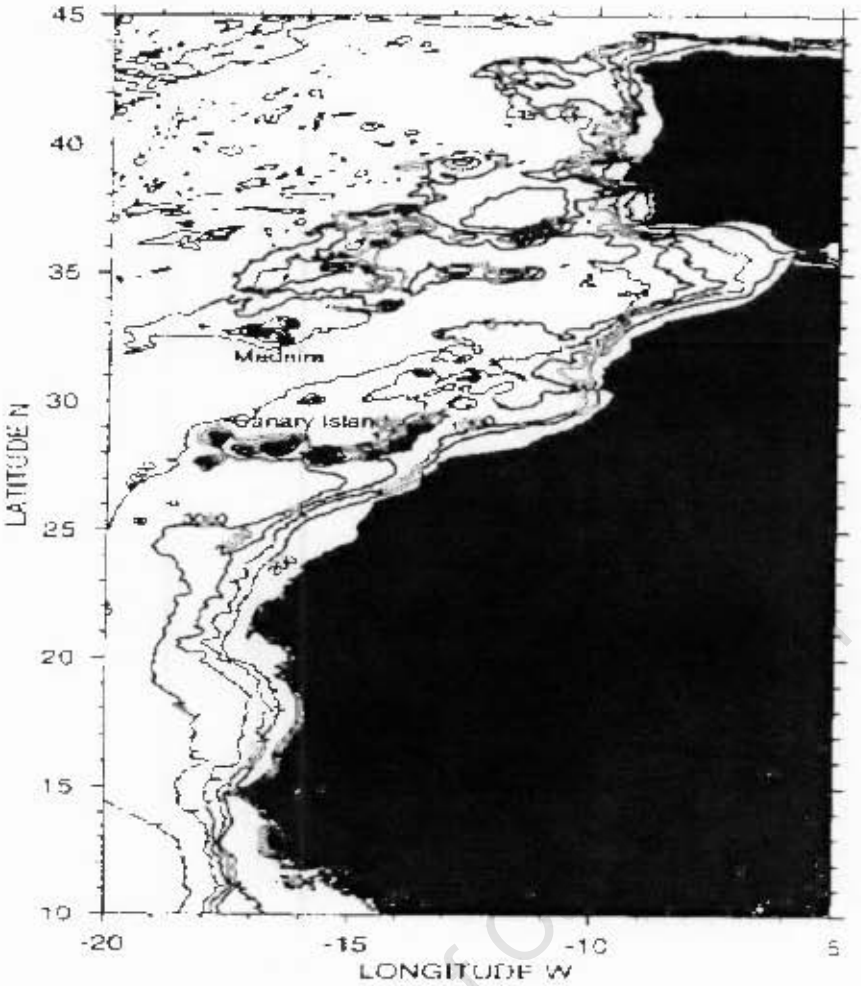

Figure 3: Bathymetry of the continental shelf off northwest Africa and Iberia. Depth contours in metres. (Taken from Barton, 1998).

1.2.1. Shelf topography

The continental shelf off Northwest Africa is the most extensive of the Eastern Boundary Current systems and is typically on the order of 50-150km wide (Hagen, 2001). Between the Strait of Gibraltar and Cape Vert, the average width of the shelf is about 50-60km. The widest areas occur in the Cape Ghir-Cape Jubi, and the Cape Bojador-Cape Blanc bights. Around 25°N, the shelf reaches a maximum width of 100-120km, and has its minimum width of 20-30km around Cape Vert.

Two major topographic features, the Strait of Gibraltar and the Canary Islands archipelago, distinguish the Canary system from the other Eastern Boundary Current systems. Through the Strait of Gibraltar at about 36°N, exchange of water occurs with the Mediterranean Sea. In the adjacent Gulf of Cadiz, the coastline is at a large angle to the direction of the dominant trade winds (Barton, 1998). The Canary Island Archipelago comprises seven major islands lying between 100-600km offshore at about 28°N (Davenport et al, 2002). The Canary Islands interact with upwelling as well as alongshore flow to produce localised effects (Barton, 1998). Between 40-41°N, the most significant topographic feature is the Aveiro Canyon (Peliz et al, 2003). The northern and southern edges of the canyon are places of recurrent filament activity (Haynes et al, 1993).

1.2.2. Meteorology

Coastal upwelling in the Canary system is related to the large-scale variation of the trade winds. During summer and autumn, the trade winds move northward in response to the northward migration of the Azores High, which reaches it's northernmost location in July-August (Van Camp et al, 1991; Mittelstaedt, 1991). The trade winds blow parallel to the coast throughout the year, reaching a maximum during summer between about 20-32°N. Winds tend to be weaker and less upwelling-favourable off the Southern Portuguese coast (Barton, 1998). South of 20°N, northerly winds occur during this season, but they are generally weaker and often replaced by moderate southwesterly and sometimes southerly monsoon winds (Mittelstaedt, 1991). South of about 15°N, southwest monsoon winds become dominant during summer.

During winter (January-February), the trade winds are well developed in the southern part of the region between about 10°N and 25°N, in response to the southward shift of the Azores High. Occasionally, during winter, between 15°N and 28°N, very dry, warm winds blow offshore from between Mauritania and Senegal (Mittelstaedt, 1983). Blowing from northeast to east, these continental trade winds, termed Harmattan, carry aeolian dust from the Sahara over the ocean (Van Camp et al, 1991). Between 30°N-36°N, coastal winds are weak and blow onshore due to the orientation of the coastline.

1.2.3. Large-scale Current Circulation

- **Near-surface circulation**

Near 33°N, the eastward flowing Azores Current separates into three branches as it approaches the coast. Two branches flow west of Madeira and form the interior of the southward recirculation of the North Atlantic Subtropical gyre. The third branch flows north around Madeira and feeds the Canary Current (Barton, 1998; Stramma, 1984). The Canary Current extends from Cape Finnisterre (43°N) to Cabo Blanco (21°N), where it separates from the African coast. By 15°N (Cape Vert) all the flow in the Canary Current has turned west to supply the North Equatorial Current (Barton, 1998). Stramma & Siedler (1988) found that there is some seasonal variation in the Canary Current. It is stronger in the summer near the African coast, while in the winter it is stronger west of the Canary Islands. This is related to the Azores Current being situated further south in summer and further north in winter (Stramma & Isemer, 1988). Mittelstaedt (1983, 1991) provides a summary of the circulation pattern in the near-shore region south from 35°N. Where the Canary Current separates from the coast at about 21°N, a large permanent cyclonic recirculation feature is located between the offshore-moving Canary Current and the African Coast. The recirculation feature extends equatorward to about 10°N. Barton (1987) demonstrates the confluence between the poleward flow and the equatorward-flowing Canary Current. The eastern boundary along the African upwelling coast can be divided in two regions with respect to the large-scale surface circulation:

  - The northern region, north of Cape Blanc
  - The southern region, south of Cape Blanc.

The northern region is part of the Canary Current System, while the southern region is influenced by the Canary Current System offshore and by the tropical circulation.

Around the Canary Islands, Mittelstaedt (1991) suggests that the Canary Current form an anticlockwise meander. Frouin et al (1990) and Haynes & Barton (1990)

demonstrated the existence of a well-defined surface poleward flow along the shelf edge off western Iberia and around Cape Finnisterre during the non-upwelling season. The eastward flowing North Equatorial Counter Current (NECC) is located south of 10°N. The NECC is strong in summer and early autumn, forming a continuous flow extending over practically the entire tropical Atlantic between 5°N and 10°N. Part of the NECC branches off toward the north while another part continues eastward to feed the Guinea Current. The northern boundary of the surface poleward flow originating from the NECC occurs at about 14°N in early spring and migrates north to about 20°N in early autumn. The NECC becomes weak and irregular as it is pushed back towards the equator by the well-established trade winds in the south. (Mittelstaedt 1991). Between 10-15°N, large-scale interaction occurs between the Canary Current, the North Equatorial Current and the NECC.

Over the continental shelf up to ~21°N, flow is predominantly equatorward throughout the year (Barton, 1998). In the near-shore region, flow is predominantly poleward, especially during summer when the trade winds are located further north. When the trades extends further south during winter, a shallow equatorward current (25-50 $cm.s^{-1}$) is associated with the coastal upwelling that occurs over continental shelf. During this season, over the continental slope flow remain polewards (Hamann et al, 1981; Mittelstaedt, 1991). Cross-shelf circulation associated with coastal upwelling does not extend offshore beyond the continental slope. Off Morocco, coastal currents are less well studied. At ~32°N, inshore currents may flow north during winter, while further south and offshore, they flow southwest (Mittelstaedt 1991). During strong northerly winds, the seas within the Bay of Agadir (southeast of Cape Ghir) are relatively calm due to sheltering effect of the Atlas Mountains. Off Cape Ghir, alongshore equatorward currents flow southwest without rounding the Cape. Where the coastline runs almost zonally, northeast of Cape Jubi the trade winds and the southwestward currents are predominantly onshore.

Poleward alongshore countercurrents are associated with seasonally occurring cyclonic eddies, which are on the order of 100-300km in length. These cyclonic eddies form along the continental slope, on the coastal boundary of the Canary Current. They appear in spring and summer between 23°N-30°N, just north of Cape Jubi, and in winter and spring off Cape Bojador. Between Cape Jubi and the eastern Canary Island, Fuerte Ventura, the equatorwards surface flow increases over $50cm.s^{-1}$. Local flow may exceed $200cm.s^{-1}$ around the Cape, especially during northerly winds. South of Cape Jubi-Cape Bojador the coastal flow decreases again to below $50cm.s^{-1}$. Countercurrents in the surface layer, which flow polewards against the prevailing trades, occur offshore along the continental slope between 17°N-23°N ranging between $5\text{-}15cm.s^{-1}$. In summer, poleward-flowing currents occur over the slope and the whole shelf south of Cape Blanc. A northward compensation flow along the African coast is initiated by the interaction between the seasonally intensified NECC and the southwest monsoon at low latitudes, and the relaxation of the equatorward blowing trade winds south of 21°N. Warm, less saline surface water is carried from the tropics about as far north as Cape Blanc. This warm surface water cannot advance north of the Cape for an extended period during the summer due to the strong trade winds located north of the Cape during this season.

- **Poleward undercurrent**

Barton (1989) reviews the poleward flow along Northwest Africa and Iberia. Off Northwest Africa, the poleward undercurrent is relatively narrow (30- 60 wide). It flows along the continental slope with mean maximum speed $5\text{-}20cm.s^{-1}$ (Mittelsteadt, 1983).

It has been noted that there are periods during which the undercurrent advances onto the continental shelf. When the undercurrent moves onto the shelf it becomes indistinguishable from the near-surface countercurrent. (Mittelsteadt, 1991).

In general, subsurface poleward flow does not extent onto the continental shelf during the upwelling season (Mittelsteadt, 1983; Barton, 1998). The existence of the poleward undercurrent has been reliably proven from lower latitudes up to about 26°N (Mittelsteadt, 1991). South of Cape Blanc (15°-21°N) the core of the undercurrent lies between 100-200m depth. The undercurrent appears to originate from two regions:

- a subsurface current branch flowing along the continental slope from the Gulf of Guinea.
- a subsurface current branch of the North Equatorial Countercurrent, which joins the undercurrent along the continental slope between 10-15°N. (Mittelsteadt, 1991).

North of Cape Blanc, the undercurrent encounters the Canary Current (between 21-22°N) (Barton 1998). The part of the undercurrent within the upper 400m flows southwest, parallel to the Canary Current. The deeper part of the undercurrent continues to flow north along the continental slope (Mittelsteadt, 1991). There is some evidence that below 500m depth, the undercurrent extends to north of the Canary Islands (Mittelsteadt, 1989). Hughes and Barton (1974) traced the undercurrent as far north as 28°N by anomalous temperature-salinity and nutrient characteristics along the coast. Further north, these anomalies are indistinguishable due to dilution of the surrounding waters by freshwater input. Where it has not yet submerged (north of ~24°N), the poleward undercurrent is an important source of water which is upwelling from 100-300 depth.

1.2.4. Upwelling and Upwelling Variability

- Seasonal Variability

Upwelling is essentially confined within a 20-30km strip along the coast, but the relatively low sea surface temperatures that result, may extend as far offshore as 200-300km (Mittelstaedt, 1991). According to Bakun & Nelson (1991), the nearshore region from Iberia to about 15°N is characterized by cyclonic wind stress curl during the upwelling season. This implies that coastal upwelling is increased by open-ocean upwelling within a few hundred kilometres of the coast. Wooster et al. (1976) have shown that seasonal variations in the trade winds induce upwelling seasons along the Northwest African coast.

At 12°N, upwelling-favourable winds occur for only 1-2 months (Mittelstaedt, 1991). Between 12-20°N, upwelling occurs during winter and spring (January-May) (Wooster et al., 1976). During the rest of the year, the region south of Cape Blanc is characterized by weak southwesterly (sometimes southerly) monsoon winds, and a warm poleward flow at the sea surface (Barton, 1998). South of Cape Blanc (21°N), the seasonality of upwelling is thus most pronounced, with a distinct seasonal change from upwelling to non-upwelling. Due to the strong and steady trade winds that prevail between 20-25°N, upwelling occurs throughout the year, reaching a maximum during spring and autumn (July-September).

North of 25°N, upwelling generally occurs during summer and early autumn (June-October). Orographically induced weak winds occur throughout the year at Agadir

(~30°N) (Mittelsteadt, 1991), resulting in a relative maximum upwelling during summer and early autumn (Mittelsteadt, 1983). Between 30-36°N, coastal winds are weak and tend to blow onshore due to the orientation of the coastline (Mittelstaedt, 1991). Haynes et al. (1993) described the seasonal development of upwelling off the Iberian Peninsula. Strong coastal upwelling occurs off Western Iberia during summer. This is associated with the equatorward flow due to the Portuguese Trade winds (Barton, 1998). The duration of the upwelling season increases from 1 month at about 10°N in February, to 6 months at about 15°N (November-May), to 12 months between 20-25°N. North of 25°N, the duration of the upwelling season decreases as latitude increases (Mittelstaedt, 1983). Major upwelling centres in the northern region are located:

- between Cape Bojador -Cape Jubi (26-28°N)
- between Cape Ghir-Cape Beddouzza (30.6-32.5°N).

The southernmost upwelling cell at Cape Vert (15°N) extends to about 13°N off southern Senegal. Here, upwelling is restricted to winter and no upwelling occurs further south where the coast bends eastward to form the Gulf of Guinea. At Cape Timiris (19°N), a submarine canyon enhances the local upwelling.
At Cape Blanc (21°N), the greatest intensity and frequency of upwelling occurs between January-June. Its effects extend far south to incorporate both the upwelling cells further south into a single feature.

- Interannual Variability

Much of the interannual variability is attributed to the El Nino Southern Oscillation (ENSO). The ENSO effect in the Atlantic-European region is roughly half as strong as it's counterpart in the Pacific region (May & Bengtsson, 1996, as cited in Hagen, 2001). According to Ward & Hoskins (1996), the related anomalies are well manifested by changes in the core pressure of the atmospheric centres (the Icelandic Low, the Azores High, and the Sahara Low).

The North Atlantic Oscillation (NAO) results from differences in sea level air pressure between the Azores and Iceland. The intensity of the northeast trade wind system is modified by subsequent fluctuations, which result in inter-annually occurring changes in coastal upwelling off Northwest Africa. Sedykh (1978), as cited in Hagen, 2001, reported a clear statistical relationship between inter-annually changed Ekman-offshore transports and fluctuating fish catches. This correlation was confirmed by other authors in different coastal upwelling regions (Schwartzlose et al., 1999).

The non-symmetric locations of the equator and the Intertropical Convergence Zone (ITCZ), and the zonal orientation of the coastline in the Gulf of Guinea influence the El Niño effect. However, El Niño-like fluctuations are well-documented (Servain et al., 1982). There is a negative correlation between inter-annual SST anomalies along the northern part of the Gulf of Guinea and off NW-Africa (Cape Blanc). This correlation suggests that pronounced wind-driven upwelling along the NW-African coast coincides with relaxed upwelling in the Gulf of Guinea (Hagen, 2001). Michelchen (1989, as cited in Hagen, 2001) showed that strong upwelling off NW-Africa corresponds to relaxed upwelling in the Gulf of Guinea and off SW-Africa and vice versa. Abnormally high SST's in the Gulf of Guinea coincide with relaxed southeast trade winds.

1.3. The Peru-Chile Upwelling System

The Peru-Chile Upwelling System is located on the eastern boundary of the South Pacific Ocean. This upwelling system has the greatest north-south extent of all the upwelling systems, extending from about 4°S off Peru to about 42°S off southern Chile (Strub et al 1998).

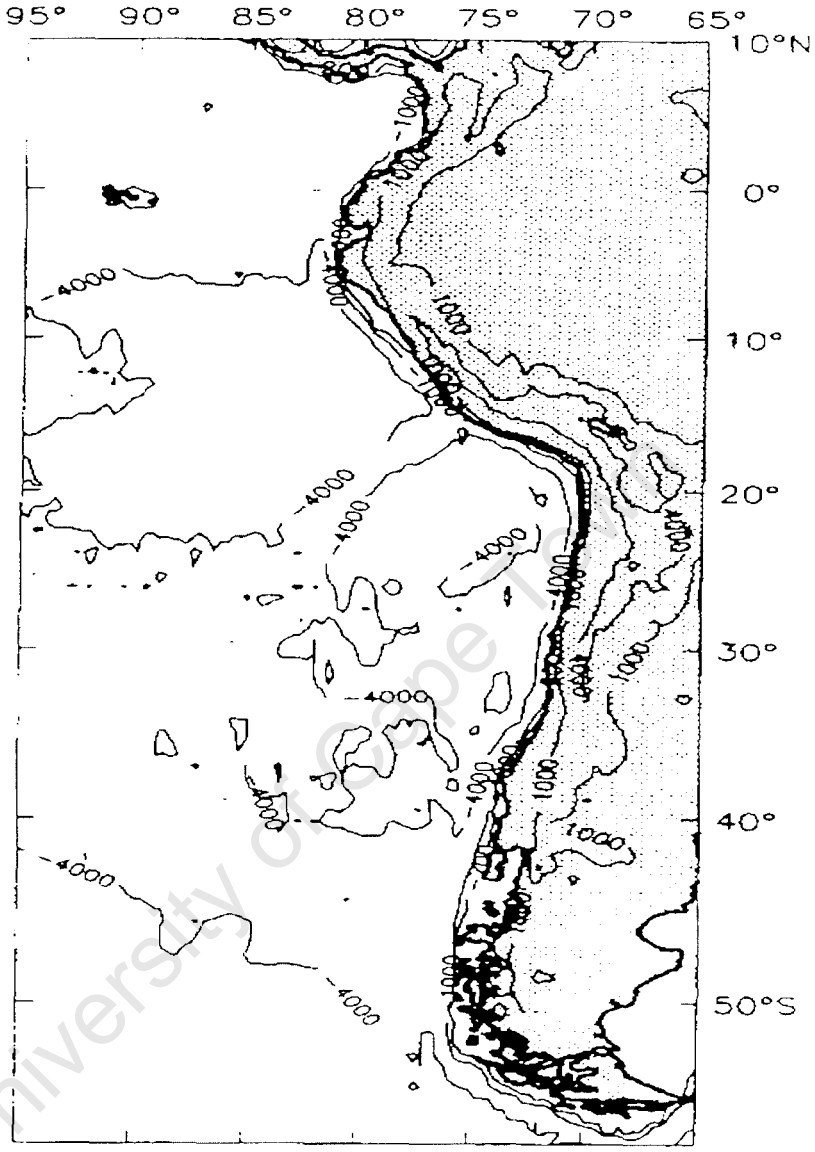

Figure 4: Coastal geometry, bottom topography and mountain elevations off South America. Contours are drawn for the depths of 200, 1000, and 4000m to show the shelf, slope, and deep ocean. The Andes Mountains are indicated by 1000 and 4000m contours. (Taken from Strub et al., 1998).

1.3.1. Shelf topography

Along the west coast of South America, the continental shelf is generally very narrow. Near Panama, the shelf is very complex. Here, some regions are wider than 100km. The shelf is narrower off Columbia and Ecuador. Off Peru, the shelf widens up to 100km and becomes very narrow off Northern Chile. Off northern and central Chile, there is virtually no shelf (at 30°S, the depth drops to 800m at about 8km offshore). It widens again off Southern Chile. Near Concepcion (36-37°S), the shelf is about 20-

60km wide. South of 42°S, the shelf is several hundred kilometres wide and is scattered with islands offshore of the fjords.

Along most of the coast of Peru and Chile, the Andes Mountains are situated about 100-200km from the coast. This results in a layered atmospheric system that supports poleward propagation of coastally trapped waves (Strub et al, 1998). Between 0-5°S, the Sierra de Ametape mountain range runs parallel to the coastline, enhancing alongshore winds.

The offshore regions of the ocean are divided into the Panama, Peru, and Chile Basins. The Panama Basin is located north of the equator, while the Peru Basin lies between 0-15°S, and the Chile Basin is located south of 15°S. The Carnegie Ridge stretches west from the coast near the equator to the Galápagos Island separating the Panama and Peru Basins. The Nazca Ridge stretches southwest from the coast at about 15°S, separating the Peru and Chile Basins.

1.3.2. Meteorology

Off the west coast of South America, the marine climate results from the interaction between basin-scale atmospheric systems; the Pacific subtropical high pressure system, the ITCZ in the north, and the polar frontal zone in the south. The climate is also influenced by regional and local effects caused by topography and coastal orientation (Strub et al, 1998). Associated with the arid region inshore of upwelling centres, local semi-permanent lows occur along the coasts of Peru and northern Chile. The high aridity and clear sky conditions on land result in stronger alongshore winds, which produces enhanced upwelling.

The South Pacific High pressure system is bounded by the ITCZ in north. The ITCZ is situated ~10°N during winter (June – September) and migrates to between ~2-5°N during summer (December - March). During winter when the ITCZ is located in its northernmost position, southeast trade winds become easterly off northern Ecuador and Columbia. These easterly winds are downwelling-favourable along the coast (Strub et al 1998). During austral summer, when the ITCZ is located in its southernmost position, winds north of 4°N are upwelling favourable. From south of 4°S to central Chile, winds are upwelling favourable throughout the year off Peru (10-20°S) maximum upwelling favourable winds occurs during the austral autumn and winter (April-October) (Bakun & Nelson, 1991).

Between 20-35°S, winds are upwelling-favourable throughout the year due to the location of the South Pacific High, which is centred off 20°S in winter, and strengthens and migrates to 30°S in austral summer. Equatorward winds along the coast are maximum in austral spring and summer between 25-35°S. This maximum is out of phase with the maximum winds off Peru. Bakun & Nelson (1991) demonstrate a weak seasonal maximum during austral winter offshore of 30°S. This reflects the seasonality of the large-scale oceanic trade winds (Strub et al. 1998). During winter, south of 27°S, the effects of polar frontal disturbances become more pronounced on a timescale of 7-10 days. Coastal atmospheric lows, which propagate poleward as coastally trapped waves (CTW's), are triggered by these polar frontal disturbances between 27-32°S. Between 35-45°S, winds alternate between the northerlies associated with polar frontal systems during winter and the southerlies associated with the South Pacific High during summer. Between 35-45°S, upwelling-favourable winds are highly variable on the synoptic time-scale, even in summer (Djurfeldt, 1989). South of 45°S, winds are

downwelling-favourable throughout the year due to the polar frontal synoptic disturbances.

1.3.3. Large-scale Current Circulation

At about 43°S, the West Wind Drift reaches the South America coastline where the flow is partially directed into the equatorward-flowing Peru Current & partially into the poleward-flowing Cape Horn Current along Southern Chile. The Peru Current system has been described as a complex system of inter-leaving currents. Near the equator, the Peru Current flows into the South Equatorial Current. Strub et al. (1998) quotes that the equatorward Peru Current has little direct effect on the coastal current associated with upwelling.

Cucalón (1987) suggests that the equatorward surface flow in the Peru Coastal Current is strongest during winter when equatorward winds are maximum. The Peru Coastal Current carries a cooler, more saline tongue of upwelled water northward. Its confluence with the warm fresh water flowing south (out of the Panama Bight) results in the formation of the strong Equatorial Front. During spring and summer when the trade winds are weaker in the equatorial Pacific, the cool tongue of upwelled water collapses. During this season the Equatorial Front is weak or sometimes absent. Offshore, a warm tongue extends southwest from the equator to northern and central Chile (Strub et al, 1995a).

Off Peru, equatorward flow is rather shallow and poleward currents dominate below this layer. This situation is in direct contrast to the circulation in other eastern boundary current systems. Lukas (1986) suggested that the eastward-flowing Equatorial Undercurrent splits into two at the Galapagos Islands. One branch flows southeast of the Galapagos Islands and approaches the coast at ~6-7°S, forming the Peru–Chile Countercurrent. The other branch continues eastwards and reaches South America near the equator, and turns south to becomes the Poleward Undercurrent. Both these currents flow south from Peru to northern and central Chile. The Poleward Undercurrent is located over the continental slope and outer shelf (Fonesca, 1989). Shaffer (1982) suggests that between 7-10°S, the Poleward undercurrent is concentrated over the inner shelf region. It is more saline, richer in nutrients and lower in oxygen than the surrounding water. Silva & Neshyba (1979) have traced the Poleward Undercurrent from about 10°S to 48°S with a marked decrease in strength of flow south of about 33°S, using geostrophic velocities and T-S characteristics. Huyer et al (1991) found the Poleward Undercurrent to be maximum over the continental slope at 150-200m depth all along the South America coast and showed the undercurrent to be within 40km from the coast off Chile (~30°S), often extending to the surface. The Poleward Undercurrent is important in the southward transport of oxygen-depleted water and is an important source of the nutrient-rich upwelled water (Brink et al., 1983).

The Peru-Chile Countercurrent is located 100-300km offshore and is less well documented than the Poleward Undercurrent. Off Peru, the current appears to be about 200km offshore (Huyer et al., 1991; Lukas, 1986). As reported in Strub et al. (1998), the Peru-Chile Countercurrent was originally thought to flow straight south of 15°S, between ~ 75-77°W. Near the upwelling centre at 15°S, it was noted that the Poleward Undercurrent is the dominant alongshore feature on the shelf. This poleward flow was noted to disappear for a few days during the onset of an upwelling event (Brink et al., 1980). Strub et al. (1995b) demonstrate a continuous band of poleward

currents following the coastline at about 100-300km offshore and extending from ~8-35°S. The equatorward surface currents associated with coastal upwelling are located inshore of the Peru-Chile Countercurrent.

1.3.4. Upwelling and Upwelling Variability

- Seasonal Variability

Between 0-42°S, upwelling is a permanent or seasonal feature. Between 42-45°S, winds are downwelling-favourable resulting in high sea surface temperatures and heavy precipitation. The interaction between the South Atlantic High pressure system, the ITCZ, and the polar frontal system produces upwelling throughout the year off Peru, which reaches a maximum during winter. Southward flowing equatorial surface water is upwelled from between 50-150m depth (Strub et al., 1998). Major upwelling centres off Peru are located at Point Negro (6°S), Chimbate (9°S), Callao (12°S), and Cape Nazca (15°S).

Off Peru, upwelling plumes are rather shallow (up to 50m) and limited in horizontal extent (25-50km). Over the shelf, equatorward flow associated with upwelling is confined a shallow upper layer (20-50m). A feature of the Peruvian system is the lack of a strong upwelling front during maximum upwelling in winter. This appears to be the result of strong offshore advection (Strub et al., 1998).

Off northern Chile (18-35°S), upwelling is weaker but still favourably persistent, being stronger during spring and summer. Off central Chile (35-42°S), strong upwelling occurs during spring and summer while downwelling occurs during autumn and winter. Upwelling plumes off northern Chile have a horizontal extent of 50-125km, while they are larger off central Chile (150 km or more) (Strub et al., 1998). Off northern Chile, the Peru-Chile Countercurrent confines the upwelling system as it impacts the coast. During El Niño conditions, the upwelling system may be confined to an even narrower region along the coast. Off central Chile, the area of upwelling water appears to be more extensive in summer (Strub et al 1998). Over the continental slope, water appears to upwell from between 150-250m depth. Upwelling is intensified around capes and is characterised by water from the Poleward Undercurrent. This has been observed at 23°S in Mejillones Bay, at 30°S near Coquimbo, and at 33°S, south of Valparaiso Bay (Strub et al., 1998, Johnson et al., 1980). Off Northern Chile, localised semi-permanent upwelling centres have been identified at:

- Punta Angamas (23°S)
- Punta Media (27°S)
- Punta Lengua de Vaca (30°S)
- Punta Curaumilla (33°S)

Off central Chile, the most intense and persistent upwelling occurs between 35-38°S. During winter when strong northern winds drive flow onshore, Subantarctic Water predominates. During summer, Equatorial Subsurface Water predominates as southerly winds cause the Poleward Undercurrent to spread along the bottom of the shelf and upwell. During strong upwelling, fish kills result from the very low oxygen concentrations in the upwelled water.

- Interannual Variability

In the Pacific Basin, much of the interannual variability is caused by the El Niño Southern Oscillation (ENSO) cycle. Persistent warm water conditions during El Niño were first thought to be a local phenomenon off Ecuador and Peru. Now, it is known to

be part of the primary basin-scale variability for the couple ocean-atmosphere system in the Pacific.

During the warm El Niño phase, there is an eastward propagation of the sea level and SST signal along the equator. Poleward propagation of the sea level signal occurs along the coast away from the equator toward the midlatitudes (Enfield & Allen, 1980, Chelton & Davis, 1982). Smith (1983) and Huyer et al. (1991) report a stronger poleward flow along the coast of Peru for a two-month period as temperatures and sea levels are rising. A persistent deepening of the thermocline occurs. This reduces (or reverses) the normal land-sea temperature difference caused by upwelling. The ITCZ shifts southward, resulting in heavy precipitation in normally arid regions. The southward migration of the ITCZ also shifts the location of maximum upwelling-favourable winds (Huyer et al., 1987, 1991). The influence of the Subtropical High pressure system on coastal winds weakens. Off central Chile, there is a shift in storm tracks, resulting in an equatorward shift of the area influenced by coastal lows. Upwelling-favourable winds are not greatly reduced during El Niño conditions. Enfield (1981) discusses how a reduction in coastal cloudiness due to warmer water at the coast may enhance insolation, thereby reducing the atmospheric pressure over the land. This would result in maintaining the pressure difference and winds over the coast.

Cucalón (1987) describes the changes off Ecuador, while Enfield et al (1987) describes the source of the increase in the energy of sea level fluctuations along the Peru coast during the 1982-1983 El Niño. Huyer et al. (1987,1991) describe the sea level, vertical temperature structure and the coastal circulation during the 1982-1983 El Niño. The strong positive sea level anomaly during the 1982-1983 El Niño was observed as far south as 33°S (Fonesca, 1985, as cited in Strub et al, 1998).

1.4. The California Upwelling System

The California Upwelling system is located on the west coast of North America between the Strait of Juan de Fuca and the tip of Baja, California (Hickey, 1998).

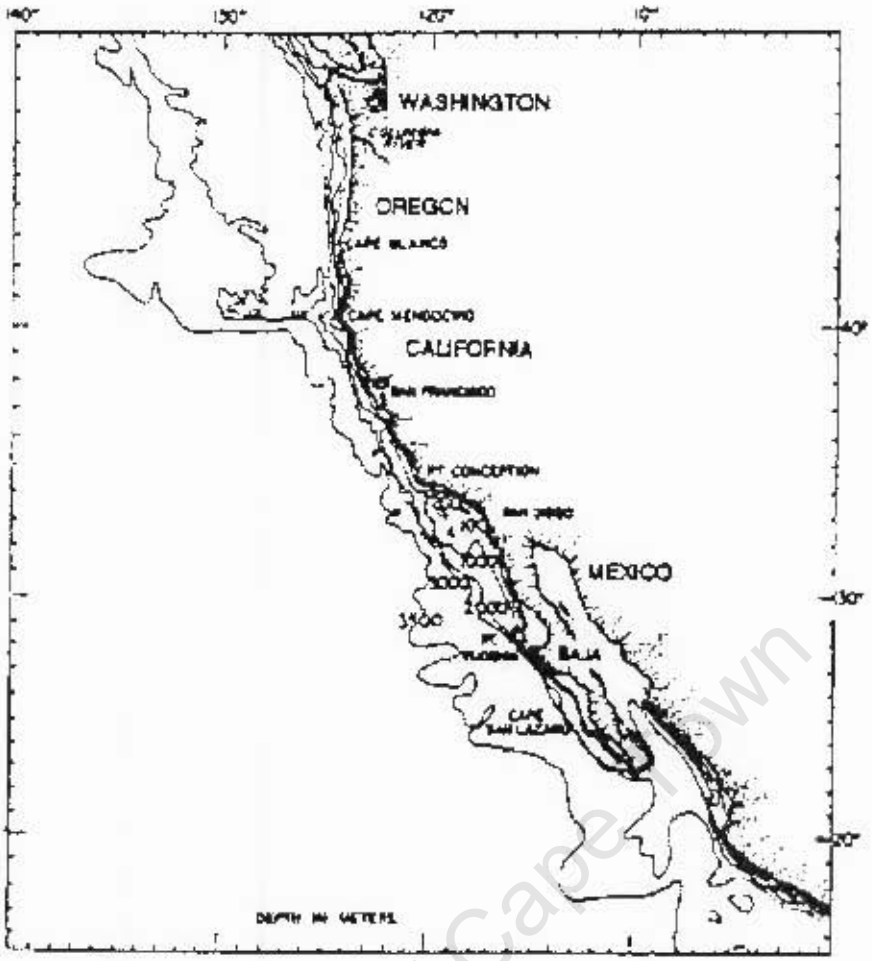

Figure 5: Bathymetry of the continental shelf off North America (Taken from Hickey, 1998).

1.4.1. Shelf topography

Between the Strait of Juan de Fuca and the tip of Baja, California, the coastline is relatively straight with only a few promontories interrupting it. The largest of these is the Southern California Bight. The Southern California Bight extends from Point Conception (34.3°N) to Cabo Colnett, Baja California (31°N) (Schiff et al., 2000). This Bight causes the California Current to deviate far offshore and it consists of a number of shallow banks, deep basin and small islands. The shelf is generally very narrow (10-75km wide) (Hickey, 1992, 1998).

Irregularities in the topography such as abrupt widening or narrowing of the shelf or the existence of submarine canyon can cause dramatic alterations in the structure of coastal currents (Wilkin & Chapman, 1990). Freeland & Denman (1982) discuss the enhanced seasonal productivity, which results from the topographically controlled upwelling at the Juan de Fuca Canyon. The Astoria Canyon intersects the shelf edge just offshore of the Columbia river. The Hecata bank exists on the west coast of North America of the Strait of Juan de Fuca (44°N). Fishing success in the region suggest that like the broad bank just Strait of Juan de Fuca, upwelling and hence productivity, are probably enhanced near this bank. Near Cape Mendocino, there are several major promontories and a major ridge along the coast. Largier et al. (1993) discusses the effect of the Mendocino Ridge on the local circulation patterns. A semi-permanent

offshore squirt of coastal water occurs in the area as a result of flow converging on the ridge from both sides.

In the Southern California Bight, the continental shelf is relatively wide (20km) in several areas (such as Santa Monica Bay, the San Pedro Shelf) and very narrow in other areas. Because of the numerous islands and ridges offshore, much of the water column flow in the northern half of the bight is confined to broad (50km wide) channels. At the north end of the bight, an island chain forces both surface and subsurface flow to divide at the entrance to the Santa Barbara Channel. At deeper depths, the flow is cut off by basin sills. The depth of these sills varies from basin to basin, typically between 500 – 1000m.

1.4.2. Meteorology

The North Pacific High pressure system migrates from its southernmost position at 28°N (February) to its northernmost position at 38°N (August) (Huyer, 1983).
Atmospheric pressure over the western United States is higher in winter, when the surface is cold, than in summer, when the surface is warm. Therefore, the offshore pressure gradient along the west coast of California is strongest in winter.

Equatorward wind stress is maximum off northern California where the centre of the North Pacific High is closest to the Thermal Low over California's central valley during spring and summer (Bakun & Nelson, 1991; Huyer, 1983). During autumn and winter, wind stress becomes poleward and unfavourable for upwelling north of San Francisco (~38°N).
South of ~38°N, wind stress is equatorward and upwelling-favourable throughout the year, reaching a maximum during spring or summer. In the Southern California Bight during summer, equatorward wind stress is reduced during summer (Hickey, 1992).

1.4.3. Large-scale Current Circulation

The west coast of North America between the Strait of Juan de Fuca and the tip of Baja, California is essentially divided into three geographical regions: the region north of Point Conception, the Southern California Bight, and the Baja Peninsula (Hickey, 1998). Dynamics of circulation patterns within the Southern California Bight differs significantly from regions north and south of it (Hickey 1992). Along the west coast of North America, the California Current flows equatorward throughout the year between the shelf break and about 1000km offshore. The current moves progressively closer to the coast further south reaching 850km off Cape Mendocino and 500km off Cape San Lazaro. The California Current is stronger at the surface and extends to ~500m depth (Hickey, 1998). The main core of the current lies about 200-400km offshore. A separate narrower flow occurs within 100-150km from the coast. This inshore current partially reverses with seasons.

The California Current carries cooler, fresher Subarctic water equatorward along the coast. In the upper 20m of the water column, some fresher water within about 300km of the coast is associated with a local plume from the Columbia River (around 45°N). South of Point Conception (~35°N), a portion of the California Current (called the Southern California Countercurrent) turns southeast and then shoreward when the flow successfully rounds Point Conception. When the flow recirculates within the Bight, it is known as the Southern California Eddy (Hickey, 1998). In the near shore region of the

Southern California Bight, the upper water column is dominated by the surface poleward-flowing Southern California Countercurrent and the subsurface California Undercurrent (Hickey, 1979, 1992; Tsuchiya, 1980; Lynn & Simpson, 1987,1990). The California Current, the California Undercurrent and the Southern California Eddy are at a maximum in summer and early autumn, while the California Countercurrent is maximum during winter. This coincides with the development of the Davidson Current north of Point Conception during winter.

The California Undercurrent is relatively narrow (10-40km wide) and flows poleward over the continental shelf between Baja California and Vancouver Island (Hickey, 1998, Huyer, 1989). Within the Southern California Bight, poleward flow at the northwestern end of the Santa Monica Basin separates into two components:

- A northwestern flow through the Santa Barbara Channel
- A westward flow south of the Islands forming the southern side of the Channel (Hickey, 1998).

Subsurface poleward flow over the continental slope is at a maximum during summer or early autumn when the California Current is strongest. Minimum subsurface poleward flow occurs during spring. Sometimes, during spring, flow within the Southern California Bight becomes equatorward (Hickey, 1979, 1992). Hickey & Pola (1983) and Hickey (1989) suggest that the seasonal variation in the California Undercurrent is related to the seasonal variation in the alongshore pressure gradient. Largier et al. (1993) has confirmed this relationship off Northern California.

It has been suggested that the Davidson Current, which flows poleward in autumn and winter, from Point Conception (35°N) to Vancouver Island (50°N), is due to the surfacing of the California Undercurrent during late autumn (Huyer & Smith, 1974; Pavlova, 1966). The surface-trapped Davidson Current is broad (~100km in width) and extends seaward of the slope (Hickey, 1979; Chelton, 1984).

1.4.4. Upwelling and Upwelling Variability

- Seasonal Variability

From Oregon to British Columbia (42-48°N) wind stress is highly variable throughout the year. During summer offshore Ekman transport is rather weak but still significant. During strong upwelling, the Columbia River plume is advected far offshore. Off central Oregon, the offshore limit of water influenced by upwelling seems to be regulated by the location of the inner boundary of the Columbia River plume during summer. Between these latitudes, maximum upwelling occurs during spring-summer. Seasonal estimates of Ekman transport suggest that upwelling should occur throughout the year south of about 38°N. However, cool SST's are not observed off Northern Baja despite the prevailing upwelling-favourable winds. Huyer (1983) suggests that the surface expression of upwelling may be suppressed by surface heating. Upwelling is strongest from Point Conception to Cape Mendocino. Topographically enhanced upwelling occurs at the strait of Juan de Fuca, the Hecata Bank, Cape Blanco (43°N), and Cape Mendocino (41.5°N). These cells often form filaments that generally meander equatorward and may stretch several hundred kilometres offshore (Kelly, 1985; Huyer & Kosro, 1987).

Shipboard surveys demonstrated that filaments extend from the surface to depths of over 200m separating fresher, warmer chlorophyll-depleted water from colder, saltier, chlorophyll-rich, recently upwelled water (Huyer et al., 1991; Strub et al., 1991). Large-

scale surveys confirmed that filaments are more common in spring and summer than during autumn and winter. North of about 43°N, where the coastline is straighter, fewer filaments have been observed. This is probably due to the association of filaments with coastal promontories. Strub et al. (1991) suggests that the filaments occur as a result of separation of the coastal jet (formed over the shelf during upwelling events) from the shelf. Satellite imagery suggests that the coastal jet, which frequently separates from the coast near Cape Blanco, meanders equatorward and can be traced throughout the California current as a continuous feature (Strub et al., 1991; Strub & James, 1995).

In the Southern California Bight (32-33°N), upwelling occurs in small, localised coastal cells and at offshore banks throughout the year. Although winds are relatively weak in the northern part of the Bight, upwelling is stronger in a narrow zone along the coast from March to May (Tsuchiya, 1980). South of Point Conception, seaward of the shelf, 20 to 30-day period fluctuations are the most dominant signal within the Santa Barbara Channel (Brink & Muench, 1986) and the Santa Monica and San Pedro Channels (Hickey, 1992). Christensen & Rodriguez (1979) have observed similar signals along the Baja Peninsula. Using coastal sea level data, Hickey (1992) demonstrates that these signals have propagation characteristics consistent with those of freely-propagating coastal trapped waves. Off Baja California (22-31°N) coastal winds are weaker but upwelling favourable throughout the year.

- Interannual Variability

Interannual variability is significant along the west coast of North America. Much of this variability can be attributed to El Niño (Hickey, 1998). During an El Niño event, the California Current is weak while the California Undercurrent is anomalously strong (Schiff et al., 2000; Chelton et al., 1982). The water in the upper 500m of the water column is anomalously warm. El Niño is generally associated with less saline conditions in the upper water column. This is probably due to onshore advection of subarctic water and a deepening of the nearshore thermocline (Ramp et al., 1997). Huyer & Smith (1984) show that poleward flow over the shelf off Oregon increases during the 1982-1983 El Niño. Johnson & O' Brien (1990) demonstrate the continuity of the El Niño signal from the western equatorial Pacific ocean along the equator and then poleward along the coast to about 50°N. Roemmich & McGowan (1995) attribute the 80 % decline of macrozooplankton biomass off Southern California since 1951 to a warming trend in the upper ocean. This warming resulted in increased stratification, thereby inhibiting upwelling despite prevailing upwelling-favourable winds over a similar time period.

Chapter 2 – Data and Methodology

This chapter describes the data used and outlines the methodology applied in preparing and analysing the data.

2.1. Sea Surface Temperature (SST)

Full resolution images are continuously transmitted and recorded in High Resolution Picture Transmission (HRPT) format from the AVHRR sensors on board the NOAA series polar-orbiting satellites (NOAA-7, NOAA-9, NOAA-11, NOAA-12, NOAA-14 and NOAA-16). The AVHRR sensor has a 110.8° cross-track scan equates to a swath width of about 2700 km. This swath width is greater than the 25.3° separation between successive orbital tracks, thus providing overlapping coverage. Coverage by the AVHRR sensors is global, twice daily, at an instantaneous field of view (IFOV) of ~1.4 milliradians. This IFOV gives a ground field of view of ~1.1 km at nadir for a nominal altitude of 833 km. Global Area Coverage (GAC) data are subsampled to approximately 4 km IFOV, recorded internally, and downlinked daily. The GAC AVHRR data are radiometrically-corrected and calibrated in physical units at full instrument resolution, and then quality controlled and assembled into discrete datasets. Multichannel sea surface temperatures (MCSST's) are computed from the GAC AVHRR radiances, using the Pathfinder Sea Surface Temperature (SST) algorithm (Kilpatrick et al, 2001; McClain et al., 1985). The Pathfinder SST data is subsampled and distributed on an equal-angle projection, in a variety of spatial resolutions and temporal averages.

For the purposes of this study, monthly averaged AVHRR Pathfinder SST data (JPL PODAAC) was used to describe the large-scale temporal and spatial variability of upwelling within the four major upwelling regions. Attention was given to the variability of the intensity of upwelling as well as the offshore extent of the upwelled water on a seasonal timescale. The monthly averages used were provided on an equal-angle projection with a spatial resolution of 9km. For each region, monthly SST maps for a 17-year period from January 1985 to December 2001 were extracted from the global dataset. The standard deviation was used to identify contaminated data in each of the monthly images. For each of the monthly images, data with a standard deviation greater than 2°C was flagged as contaminated data. The contaminated data was then removed and a boxcar average was used to apply a spatial smooth to each of the monthly images in order to replace the contaminated data and also fill in any missing data. The SST of each pixel was multiplied by one hundred to remove the decimal for more accurate and easier computation. All SST images are thus presented in units of °C.

The 17 year time-series (January 1985 – December 2001) of extracted monthly SST maps was used to compute a monthly climatology for each upwelling region. The mean seasonal pattern of SST, as well as the spatial changes of this distribution within and between seasons in each region was described from the monthly climatology maps. For each of the regions, the first three pixels (representing ~27km) of the SST at the coast were extracted and zonally averaged. The average at the coast was then plotted as a function of latitude and time. It was expected that this average would reveal the seasonal variability of SST at the coast.

2.2. Upwelling Index (DSST)

An upwelling index (DSST) was derived in order to quantify the patterns of upwelling variability identified from the sea surface temperature and also to describe the similarities and differences between the four upwelling regions in a consistent framework. The upwelling index is defined as:

$$DSST_{(c, lat)} = SST_{(o, lat)} - SST_{(c, lat)}$$

- **DSST**–the difference between a fixed offshore pixel and subsequent shoreward pixels
- **o** – longitude of the offshore pixel
- **c** – longitude of the shoreward pixel
- **lat** – latitude of the pixel

Wind-driven upwelling at the coast results in cooler water at the surface close to the coast, with warmer oceanic waters at some distance offshore. This is the basis upon which the Upwelling Index (DSST) was derived. The upwelling index is defined as the zonal difference between the SST of a fixed offshore pixel and the SST of the subsequent shoreward pixels. The location of the furtherest offshore pixel was chosen to be 100 pixels offshore so as to minimise the possibility of including upwelled waters entrained in filaments extending offshore. A positive DSST index means that the offshore SST is larger than the shoreward SST, while a negative DSST index means that the shoreward SST exceeds the offshore SST. Thus, a positive DSST index indicates the occurrence of cooler water at the coast, while a negative index indicates warmer water at the coast (that is, water which is warmer than that further offshore). An index of zero would indicate uniform sea surface temperatures of the inshore and offshore regions, suggesting very limited or zero upwelling at the time. The value of the upwelling index depends firstly on the amount of upwelling that occurs. Secondly, the index is affected by the temporal resolution of the data (monthly time scales mask event-scale features due to the temporal averaging of the data). The seasonal cycle of solar insolation also has an effect on the upwelling index.

This upwelling index (DSST) was calculated from the extracted monthly SST maps and the monthly climatology for the new DSST maps was computed. The climatology maps were then used to describe the seasonal variation of the DSST in each of the study regions. Similar to the extraction performed for the SST, the first three pixels of the DSST at the coast were extracted and zonally averaged. This average at the coast was then presented as a function of latitude and time. It was expected that this average would reveal the seasonal variability of the DSST at the coast.

2.3. Principal Component Analysis

Principal Component Analysis is a mathematical technique commonly used for image analysis in remote sensing. Generally, it is used for data compression between highly correlated spectral bands but it can also be used for change detection studies (Fung & LeDrew, 1987; Lillesand & Kiefer, 1987; Eastman, 1992;Gallaudet & Simpson, 1994; Cole & McGlade, 1998; Hardman-Mountford & McGlade, 2002). The variables derived during principal component analysis are formulated using specific linear combinations of the original variables. The derived variables summarize the original data, thereby

reducing the dimensionality of the dataset. The variables are assumed to be uncorrelated and are computed in decreasing order of importance, with the first variable accounting for the largest portion of the variation in the original dataset. In each of the four major upwelling regions, the Pathfinder sea surface temperature dataset showed a high degree of temporal variability with a strong seasonal signal. A high degree of spatial structure was also identified from the SST images. It therefore seemed appropriate to investigate the different modes of spatial and temporal variability in the SST dataset through the use of principal component analysis.

The monthly and mean monthly SST's were used to calculate SST anomalies for each of the regions. The SST anomalies are defined as the deviations of the monthly SST from the mean monthly SST for a particular month. These SST anomalies were then used to perform the principal component analysis. By using the SST anomalies, it is assumed that the seasonal signal, which would account for the largest portion of the variability in the dataset, has been removed. A correlation matrix was used for the principal component analysis, and the dataset was spatially standardised so that each monthly image had a mean of zero and a variance of one, thereby weighting each monthly image as equally important. Standardising the dataset facilitated the interpretation of the resultant principal component images by presenting them as positive and negative deviations from the mean.

The output from the principal component analysis consisted of principal component images, as well as eigenvalues and eigenvectors for each image. The principal component images denote the spatial output of the analysis while the eigenvalues are a measure of the percentage variance explained by each principal component image. The temporal output (i.e. loadings through time for each principal component image) of the analysis is given by the eigenvectors.

2.4. Wind

Scatterometer data from the European Remote Sensing Satellites 1 and 2 (ERS 1 and ERS 2) for the period January 1992 to December 2000 was used to study upwelling favourable conditions at the coast on a seasonal time-scale. The ERS scatterometer produces wind vectors at a resolution of 50km, with a separation of 25km across a 500km swath. Wind vectors are estimated from the backscatter coefficients of the measured backscatter of the ocean's surface. Zonal and meridional wind components are estimated from the scatterometer wind speed and direction. Statistical interpolation related to the Kriging technique is used to reconstruct synoptic fields of surface winds at basin scales from the discrete observations. Bentamy et al (1996) provides the computational details in reconstructing a regular wind field from polar orbit satellite data. The reconstructed mean wind fields are provided on a rectangular grid with a spatial resolution of 1° x 1°.

For each of the four study regions, monthly averages of the zonal and meridional components of the wind stress at the coast were extracted for the period August 1991 – January 2001. No data was available for the month of February 1992. This was compensated for by using the long-term average (1993-2000) of February as a substitute for February 1992. This substitution did not significantly alter the end results. Components of the ERS 1 and ERS 2 wind stress are provided in north-south and east-west vectors. At the coast, winds are steered by the topography and thus need to be corrected for local topographic effects, especially in mountainous regions. The

vector components of the wind were thus resolved into cross-shore and alongshore components, using the following equations (Emery & Thompson, 2001):

$$u' = u\cos\theta + v\sin\theta$$

$$v' = -u\sin\theta + v\cos\theta$$

- u' - cross-shore component of the wind stress (rotated component)
- v' - alongshore component of the wind stress (rotated component)
- u - east-west component of the wind stress
- v - north-south component of the wind stress
- θ - orientation of the coastline (measured anti-clockwise from the eastward direction).

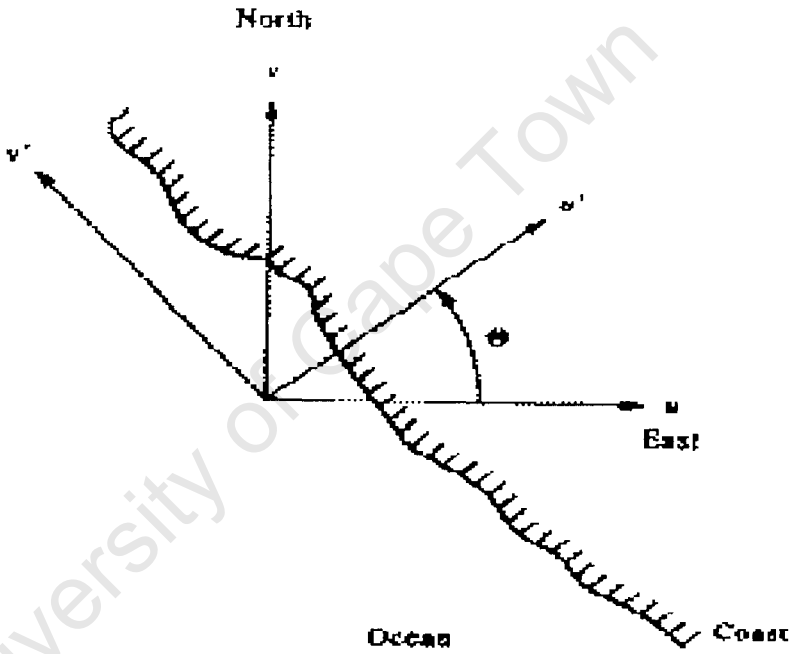

Figure 6: Illustration of the cross-shore and alongshore components of the wind stress. (Taken from Emery & Thompson, 2001).

All analysis was done using the rotated wind components. Since upwelling is caused by the alongshore component of the wind stress, only this component was studied. Similarly to the analysis done on the sea surface temperature maps, the meridional component of the wind stress at the coast was extracted and rotated to obtain alongshore wind stress. The alongshore wind stress was then plotted as a function of latitude and time. Due to the coarser resolution of the wind stress, only the first pixel at the coast was extracted.

2.5. Ekman Transport

Since upwelling is caused by the equatorward, alongshore component of the wind stress, the Ekman Transport perpendicular to the coast was calculated using this component. The following equation was used to calculate the Ekman Transport (Bakun, 1996):

$$U_E = \tau_y / f$$

- U_E is the offshore Ekman Transport
- $f = 2\Omega\sin\phi$ is the Coriolis parameter
  Ω is the earth's angular momentum and ϕ is the latitude
- τ_y is the alongshore component of wind stress

This equation gives the offshore Ekman Transport as a value of kilograms of water per meter of coastline. Dividing this value by the density of seawater (1023 $kg.m^{-3}$) and then multiplying it by 111 000m (1degree = 111km = 111 000m), gives the volume (Sv) of offshore transport along the coast per degree. An extraction of the mean monthly Ekman Transport in first pixel at the coast was performed and then plotted as a function of latitude and time. This was done in order to investigate the variability of the offshore Ekman Transport within and between seasons and to supplement the description of SST's within each region. When the Ekman Transport is positive, it indicates that the flow of water is onshore and unfavourable to upwelling due to convergence of water at the coast. When the Ekman Transport is negative, it indicates that flow is offshore and upwelling favourable due to divergence of water at the coast.

Chapter 3 – Results and Discussion

This chapter presents the results of the Sea Surface Temperature and Ekman Transport in each of the four regions and discusses the similarities and differences between the regions. For each of the four major upwelling systems (Benguela, Peru-Chile, Canary, and California), a detailed climatology showing the spatial characteristic of the SST can be found in Appendices 1, 3, 5, and 7, for each system respectively. A detailed climatology showing the spatial characteristic of the DSST can be found in Appendices 2, 4, 6, and 8, for each system, respectively. The detailed climatologies have been placed in the appendices so as not to interrupt the structure of this chapter. At each latitude within each of the four systems, the first three pixels at the coast were extracted and zonally averaged. This was done for both the SST and the Upwelling Index (DSST). The zonal average of SST is presented as a function of latitude and time in Figure 7a-d, and the zonal average of DSST is presented in Figure 8a-d.

3.1. Sea Surface Temperature (SST)

3.1.1. The Benguela Upwelling System

Appendix 1 describes the mean seasonal pattern of sea surface temperature (SST) in the Benguela region between 10 - 35°S and 3 - 20°E. The onset of spring warming is indicated by the general increase in SST's throughout the region during October. The highest SST's are located north of the Angola-Benguela Front throughout the year. The location of the Angola-Benguela Front is indicated between 15-17°S by the zonal positioning of the isotherms at the coast. At the front, SST varies from a maximum of about 24°C in late summer to mid autumn (February – April) to about 19°C in late winter to mid spring (August – October). North of 15°S, the maximum SST (29°C) occurs during March, while a minimum SST of 21°C occurs in August. South of 15°S, sea surface temperatures are more moderate. The general decrease in SST's throughout the Benguela region during May indicates the onset of winter cooling. The lowest temperatures are located in a band along the coast. This band of lower SST's appears to be concentrated close to the coast during late spring to early autumn (November – March). During late autumn, this band seems to extend further offshore. During the southern hemisphere winter, solar radiation received at the earth's surface is at a minimum. It is at a maximum during summer. The apparent offshore extension of the band of lower SST's along the coast is possibly due to a lesser contrast between coastal and offshore SST's, resulting from less intense solar heating in the Benguela system during autumn and winter. Within this band of lower SST's, the lowest temperatures are located around 25°S throughout the year. This is due to the perennial upwelling occurring at the Luderitz upwelling cell (situated around 25°S). During late autumn to early spring (May – September), there appears to be an intrusion of cooler water into the region from the southwest, as indicated by the northward migration of the isotherms. During August and September, there is an intrusion of slightly warmer water into the region from the southeast. This probably indicates the intrusion of warmer Agulhas Current water into the Benguela system.

Figure 7a is a Hovmöller diagram of the mean monthly SST at the coast for the Benguela region. In general, throughout the region, the highest temperatures occur during summer and autumn, while the lowest temperatures are experienced during winter and spring. This is due to the large influence of the seasonal cycle of solar heating on the sea surface temperatures within the region. The persistent high

temperatures north of ~15°S probably result from a combination of the warm Angolan Current transporting warm water from the north and the considerable amount of solar heating received in this region throughout the year. Here, the SST at the coast closely follows the seasonal cycle of solar heating. Between ~15-20°S, temperatures remain relatively warm throughout the year. The closely spaced isotherms probably indicate the position of the Angola-Benguela Front at the coast. Between ~17-20°S, weak but persistent coastal upwelling has a greater influence on the coastal SST's during winter, when the upwelling is at a maximum, than during the rest of the year. Between ~20-27°S, temperatures are more moderate. Seasonality is not as pronounced as further north. Solar heating is less intense within this region and therefore has less of an influence on SST's at the coast. Winter cooling is enhanced by perennial coastal upwelling, which reaches a maximum during winter. Between about 24-27°S, temperatures are consistently cool (<16°C) except during summer (December – February) when the SST increases slightly, in accordance with the seasonal cycle of solar heating. Here, upwelling is a semi-permanent feature. The smallest seasonal difference in temperatures is observed south of 27°S. The highest temperatures are experienced during summer despite the seasonal upwelling, which is at a maximum during summer and spring. South of about 34°S, the seasonal difference in SST increases slightly.

3.1.2. The Peru-Chile Upwelling System

Appendix 3 describes the mean seasonal pattern of SST in the Peru-Chile region between 0 - 40°S and 90 - 70°W. The general increase in SST's throughout the Peru-Chile region during late spring (November) indicates spring warming of the region. The highest SST's are located in a band extending southwest from offshore at about 5°S to the coast (where the coastline bends eastward roughly around 18°S). Within this band, at ~5°S, SST varies from 28°C during late autumn (March) to ~21°C during mid winter (August) and spring (September and October). Roughly within the region between 18-22°S, where this band of warmer SST's reaches the coast, SST varies between about 24°C during mid summer to mid autumn (January – March) to 18°C during mid winter to early spring (August – September). The general decrease in SST's during May indicates the onset of winter cooling in the Peru-Chile region. Between about 5-18°S, a band of cooler SST's is located along the Peruvian coast. Here, SST's at the coast reach a minimum of ~16°C during mid winter to early spring (August – September), and a maximum of ~22°C during mid summer to mid autumn (January – March). Along the Peruvian coast, the band of cooler SST's appears to be concentrated close to the coast during mid spring to late summer (October – February) and to extend further offshore during autumn to early spring (March – September). Further south, a second band of cooler sea surface temperatures is located along the Chilean coast roughly between 34-40°S. Within this region, SST reaches a maximum of ~16°C at the coast during January – March, and is at a minimum during August – September.

Figure 7c is a Hovmöller diagram of the mean monthly SST at the coast for the Peru-Chile region. In general, throughout the region, the highest temperatures are experienced during summer and autumn, while the lowest temperatures occur during winter and spring. The persistent high temperatures between 0-5°S indicate the persistent warm conditions in the equatorial region throughout the year. Here, the SST at the coast closely follows the seasonal cycle of solar heating. The closely spaced isotherms around 4°S probably indicate the average position of the Equatorial Front at

the coast. At the Front, temperatures range from ~18-25°C. Between 5-10°S, temperatures are relatively warm throughout the year, varying from ~24°C during mid summer (February) to <17°C during early spring (September). Off Peru, upwelling occurs throughout the year and reaches a maximum during autumn and winter due to the interaction between the South Atlantic High pressure system and the Intertropical Convergence Zone (ITCZ).

Between 10-15°S, temperatures become more moderate and seasonality is not as pronounced as further north. This region experiences reduced solar heating and perennial coastal upwelling, which reaches a maximum during autumn and winter, enhances winter cooling. In the southern part of this region, temperatures are cooler, reaching a maximum (>21°C) during late summer to early autumn (February – March). Between 16-28°S, seasonality is large and SST's are warmer, ranging between >23°C during mid summer to early autumn (January – March) and ~15°C during mid winter to mid spring (July – October). The warm temperatures between ~16-23°S during summer and early autumn are probably indicative of the semi-permanent onshore flow of warm Subtropical water. Within this region, upwelling reaches a maximum during spring. Between 28-34°S, temperatures vary between ~19°C during mid to late summer (January – February) and ~14°C during mid winter to mid spring (July – October). Weaker but persistent upwelling reaches a maximum during summer and spring. The region south of 34°S exhibits the smallest seasonal difference in temperatures. During summer (December – February), temperatures within this region reach a maximum of ~16°C. During mid winter to mid spring (July – October), a minimum of <12°C is reached. Seasonal upwelling is at a maximum during late spring to early autumn (November – March).

3.1.3. The Canary Upwelling System

Appendix 5 describes the mean seasonal pattern of SST in the Canary region between 5-45°N and 5-27°W. There is a general increase in SST during late spring (May), indicating summer warming throughout the region. The highest SST's are found south of 10°N throughout the year, varying from about 24-29°C. The general decrease in SST during late autumn indicates winter cooling throughout the region. The lowest temperatures are located north of about 35°N during mid winter to mid spring. Off the Portuguese coast, the isotherms are roughly zonal during mid autumn to early summer (October – June). This suggests that the sea surface temperatures are zonally uniform, from the coast to offshore. From July to November, SST's at the coast are lower. This agrees well with the upwelling off Portugal (37° - 43°N), which is stronger during summer and autumn. Further south, along the northwest African coast, between about 25°-35°N, there is a band of lower SST during summer to mid autumn (June to October). Between ~20°-25°N, the band of lower SST's located along the coast seems to occur throughout the year. South of about 20°N, SST's at the coast are lowest during winter and spring (January – April). This agrees with the season of maximum upwelling at these latitudes described by Mittelsteadt, 1991; Wooster et al, 1976; Van Camp et al, 1991.

Figure 7b is a Hovmöller diagram of mean monthly SST at the coast for the Canary region. South of 12°N, temperatures remain high, (~24-29°C), throughout the year and the seasonal difference in SST is not pronounced. The persistent high temperatures within this region are associated with the considerable amount of solar heating

received here, the seasonally intensified poleward-flowing warm North Equatorial Countercurrent and the southwest monsoon. Between 12-20°N, the seasonal difference in SST is large. High temperatures, ranging from ~24-29°C, occur during summer and autumn (June – November). During summer and autumn, the Azores High is located further north and the southern boundary of the trades is located at about 20°N. South of ~20°N, during this season, upwelling-favourable winds are weak and often replaced by the southwest monsoon. The relaxation of the trade winds south of ~20°N during this season, allows the poleward-flowing North Equatorial Countercurrent to carry warmer, less saline surface water as far north as Cape Blanc (~21°N). During winter and spring, the Azores High is located further south and the southern boundary of the trades is located at about 10°N. During this season, coastal upwelling occurs within this region and temperatures are slightly lower. Between 20-25°N, the seasonal difference in SST is small and temperatures remain relatively low throughout the year. There is a slight warming during late summer and autumn (July – November). The lower temperatures within this region are maintained by perennial upwelling, which reaches a maximum during spring and autumn.

Although the temperatures between 25-32°N are relatively low throughout the year, there is a slight increase in the seasonal difference in SST. A slight warming occurs during summer and autumn (June – November) despite the seasonal upwelling, which reaches a maximum during summer and autumn. Here, the upwelling during summer and autumn has a greater effect on the SST's at the coast than does the seasonal cycle of solar heating. Between 32-36°N, the seasonal variation in SST is more pronounced with relatively low temperatures occurring during winter and spring. There is a slight warming (to >23°C) during summer and autumn, despite the coastal upwelling, which reaches a maximum during this season. Within this region, coastal winds are weak and tend to blow onshore, resulting in weaker upwelling. North of 36°N, the seasonal variation in SST is very pronounced, with low (<14°C) temperatures occurring in the northernmost region during winter and spring (December – April). During summer and autumn there is a slight warming within the region in accordance with the seasonal cycle of solar heating.

3.1.4. The California Upwelling System

Appendix 7 describes the mean seasonal pattern of SST in the California region between 23-57°N and 110-145°W. There is a general increase in SST during May, indicating summer warming throughout the region. The highest SST's (>28°C) are located at the coast, south of 25°S during late summer to mid autumn. The general decrease in SST during November indicates winter cooling throughout the region. The lowest SST's are observed north of 50°N during winter. During mid winter to early spring (January – March), the isotherms throughout the region are more or less zonal, suggesting that SST's are uniform from the coast to offshore. During mid spring, the isotherms at the coast become slightly more meridional and in May, a band of lower SST appears at the coast between about 32-45°S. During summer the band appears to extend further north and south along the coast and further offshore, reaching it's largest extent during July and August. During mid summer and autumn (July – November), another band of slightly lower SST's is visible at the coast between about 45-50°S. This band reaches it's largest north-south and offshore extent during late summer to early autumn. This agrees with the seasonal cycle of upwelling observed off Oregon, which is at a maximum during summer. Further south, in the Southern

California Bight (~31-34°S), a band of higher SST's is visible at the coast during late spring and summer (May – August). During late winter and spring (February – May), the southward extension of the isotherms at the coast suggests a southward flow of water at the surface. This is supported by the findings of Tsuchiya (1980).

Figure 7d is a Hovmöller diagram of the mean monthly SST at the coast for the California region. The highest temperatures, ranging from ~22-28°C, are found along the Baja Peninsula (23-31°N), during summer and autumn (June – November). The high temperatures within this region during summer and autumn are associated with the considerable amounts of solar heating received at these latitudes during this season. Here, the seasonal difference in SST is large. Between 27-34°N, the seasonal variation in SST is slightly reduced, in accordance with the slightly reduced solar heating received here. Within this region, coastal winds are weaker, but upwelling-favourable throughout the year. However, the surface expression of upwelling might be suppressed by surface heating. In the Southern California Bight (31-34°N), the seasonal variation in SST is small. Between 34-50°N, the seasonal variation in SST is less pronounced. Within this region, coastal temperatures are generally low (<14°C), with a slight warming during summer and autumn (June – November) in the southern part of the region. In the northern part of the region, around 45°N, slight warming occurs during summer to mid-autumn (June – October). Although seasonal estimates of Ekman transport suggest that upwelling should occur throughout the year, south of ~38°N, the upwelling reaches a maximum during spring. North of ~38°N, upwelling reaches a maximum during summer. Off Oregon, seasonal upwelling reaches a maximum during summer when the mean Ekman transport is offshore. Downwelling occurs in winter when the mean Ekman transport is onshore.

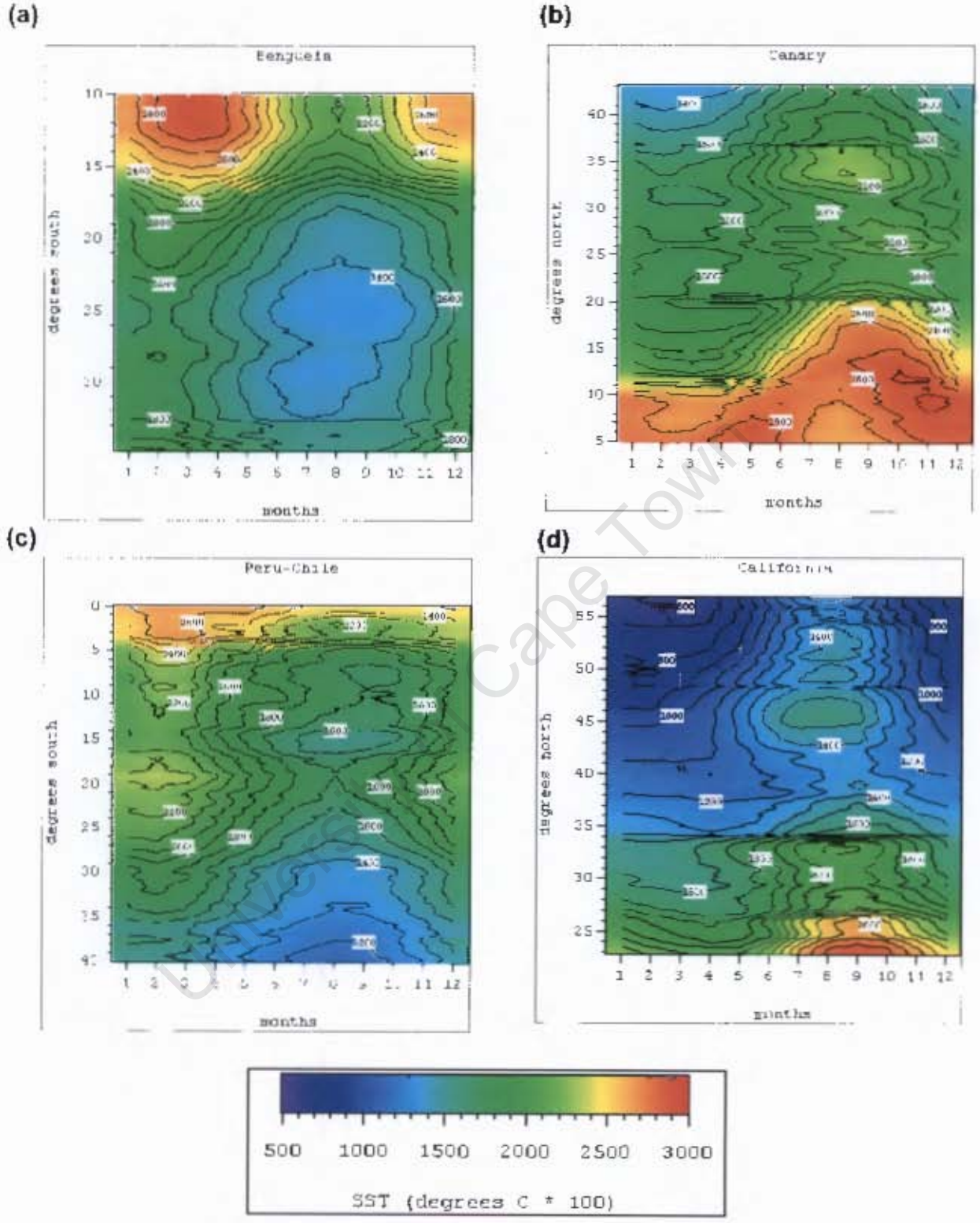

Figure 7: Mean monthly sea surface temperature (SST) at the coast for the **(a)** Benguela, **(b)**Canary, **(c)**Peru-Chile, and **(d)** California regions.

3.2. Upwelling index (DSST)

3.2.1. The Benguela Upwelling System

Appendix 2 describes the mean monthly upwelling index (DSST) for the Benguela region between 10 - 35°S and 3 - 20°E, and figure 8a shows the mean monthly DSST averaged over the first three pixels at the coast for the Benguela region. The hypothesis is that when upwelling occurs, SST at the coast decreases and consequently DSST increases. When the DSST index is negative, it indicates that SST's at the coast are higher than those further offshore. When the index is positive, it indicates that the SST's at the coast are lower than those further offshore. When the index is calculated over the region, the offshore extent and intensity of the upwelling becomes apparent and comparable within and among the four regions.

The upwelling band is visible between about 15-35°S. Around 15°S, the 0°C DSST isoline probably indicates the position of the Angola-Benguela Front. During early summer to mid-autumn (December – April), the 0°C DSST isoline is roughly zonal and centred around 15°S. Where the DSST index is zero, it indicates that there is no difference between the sea surface temperature of the offshore and the subsequent shoreward pixels. During late autumn to late winter (May – August), this isoline migrates north. The northward migration of the isoline is suggestive of the general reduction of sea surface temperatures throughout the Benguela region during autumn and winter. The isoline reaches a maximum northward position of about 10°S further offshore and about 14°S at the coast in winter (June – August). This southward extension of the 0°C DSST isoline along the coast, most obvious in July and August, could be an indication of the southward extension of warmer Angolan current water along the coast. North of 15°S, the upwelling index is negative thoughout the year, indicating warmer water at the coast and the non upwelling conditions prevailing within this region.

Between about 15-34°S, the DSST index at the coast is positive throughout the year, indicating the upwelling conditions within the region. In the northern Benguela upwelling system, the largest positive DSST values, > 6°C, indicating cooler water at the coast, consistently occur in the vicinity of the Luderitz and Central Namibian upwelling cells. Positive DSST values reach a maximum during mid autumn to early winter (April – July), and a minimum during late spring to early summer (November and December). This agrees well with the seasonal cycle of upwelling in the vicinity of the Luderitz and Central Namibian upwelling cells, which reaches a maximum during winter and is at a minimum during summer. In the southern Benguela upwelling system, between ~27-34°S, the DSST index reaches a maximum of >5°C between during April to July. The observed DSST index in the southern Benguela system does not coincide with the maximum upwelling, which occurs during October – December in the vicinity of the Hondeklip upwelling cell, and during December – February further south around the Cape Columbine and Cape Peninsula upwelling cells. It thus appears that the DSST index in the southern Benguela system is more affected by the seasonal cycle of solar heating that the DSST index in the northern Benguela system. It could also result from the influence of warmer Agulhas Current input on the DSST index. South of 34°S, at the coast, the 0°C isoline occurs during spring to early summer (September – December). This isoline possibly indicates intrusion of warmer Agulhas Current water into the Benguela system.

Throughout the year, the upwelling band consistently reaches its maximum offshore extent in the vicinity of the Luderitz and Central Namibian upwelling cells. Considering only the position of the 2°C DSST isoline, the variation in offshore and north-south extent as well as the variation in the intensity of upwelling becomes apparent. Figure 9a shows the maximum offshore extent of the 2°C DSST isoline for the Benguela system. It is expected that when upwelling reaches a maximum, the DSST isoline would be located at a maximum distance offshore, and when upwelling is at a minimum, the location of the DSST isoline would be at a minimum distance offshore. Maximum offshore distance reached coincides with the maximum DSST in the central part of the region. During mid autumn to late winter (April – August), the 2°C DSST isoline consistently reaches a maximum distance offshore (>300km) between ~16-26°S. The isoline reaches its northernmost position during late autumn and winter. This agrees well with the seasonal cycle of upwelling in the northern Benguela system, which reaches a maximum during winter. Between about 27-31°S, during late summer to late winter (February – August), the maximum offshore distance reached by the isoline exceeds 200 km. The southern limit of the isoline reaches it's southernmost position between January – June. This agrees with the seasonal cycle of upwelling in the southern Benguela system, which reaches a maximum during spring and summer. South of 34°S, the isoline reaches a maximum offshore distance during autumn (March – May). This does not agree with the seasonal cycle of upwelling, which is at a maximum during summer, within this part of the region. The maximum offshore distance reached by the 2°C DSST isoline is greater in the northern Benguela upwelling system than in the southern Benguela upwelling system. This could be due to the smaller seasonal signal and the winter upwelling maximum in the Northern Benguela, when the influence of solar heating on the SST structure is at a minimum. Between about 23-26°S, in the vicinity of the Luderitz upwelling cell, the maximum offshore distance reached exceeds 200km throughout the year. This agrees well with the maximum upwelling observed at these latitudes throughout the year.

3.2.2. The Peru-Chile Upwelling System

Appendix 4 shows mean monthly DSST for the Peru-Chile region between 0 - 40°S and 90 - 70°W, and figure 8c shows the mean monthly DSST averaged over the first three pixels at the coast for the Peru-Chile region. Around 4°S, the 0°C DSST isoline is almost zonal during early winter to early summer (June – December). North of this isoline, the DSST index is negative, indicating the prevailing non-upwelling conditions. At the coast, the isoline reaches its northernmost extent (~1°S) during mid to late autumn (March and April) and its southernmost extent (~5°S) during early spring (September). The southward extension of the isoline suggests that there is extension of warmer water from north of the equator southward along the Peruvian coast. South of this isoline, the DSST index is positive, indicating upwelling conditions along the Peruvian and the Northern Chilean coasts. Between 5-11°S, the positive DSST index exceeds 3°C throughout the year, reaching a maximum of >6°C between 6-12°S during mid autumn to early winter (April – July). This agrees well with the stronger upwelling along the Peruvian coast during autumn and winter. The index exceeds 3°C during the first half of the year between 11-14°S, and during late summer to mid spring (February – October) between 14-16°S. Between 16-26°S, the DSST index at the coast is negative during early spring to early autumn (September – March). This indicates non-upwelling conditions within the region. Within this region, during spring and summer, upwelling is weaker and more variable due to the semi-permanent shoreward flow of warmer water.

As indicated by the southward extension of the 0°C DSST isoline just south of this region, there appears to be southward extension of these positive DSST's along the coast during summer (up to 27°S). During autumn (March), the spatial extent of this region of positive DSST decreases, reaching a minimum during late autumn to early winter (May and June).
Along the Northern Chilean coast between 29-34°S, index exceeds 3°C during autumn and winter (March – August). This does not agree with the stronger upwelling which occurs within the region during spring and summer. Between 34-37°S, the index reaches a maximum of >4°C during February to April. This agrees with the seasonal cycle of upwelling, which is stronger within the region during summer.

Along the Peruvian coast between 2-11°S, during early autumn to mid spring (March – October), 12-14°S, during mid autumn to late winter (April – August), ~16°S, during late autumn to early winter (May and June), the location of the 2°C DSST isoline (figure 9c) exceeds 300km offshore. During April and May, a maximum offshore location of >500km is reached between 3-4°S. Between 6-11°S, the maximum offshore location exceeds 400km. This agrees with the stronger upwelling observed at these latitudes during autumn and winter. It also agrees with the location of the major upwelling centres at 6°S, 9°S, and 12°S. Along the Northern Chilean coast, the location of the isoline exceeds 300km offshore between 32-35°S during mid summer to mid autumn (January – April). This agrees with the seasonal cycle of upwelling along the Northern Chilean coast. The maximum offshore location of the 2°C DSST isoline is greater in the Peruvian upwelling system than in the Northern Chilean upwelling system. This is probably due to the lesser seasonality of upwelling conditions in the Peruvian system.

3.2.3. The Canary Upwelling System

Appendix 6 shows mean monthly DSST for the Canary region between 5-45°N and 5-27°W, and figure 8b shows the mean monthly DSST averaged over the first three pixels at the coast for the Canary region. Along the Portuguese coast, the DSST index is negative during winter to early summer (December – June). This indicates higher SST's at the coast and non-upwelling conditions within the region. These negative DSST's extend further south during February. Within the region between 32-37°N, where the coastline bends eastward, the index is negative throughout the year, reaching a maximum during early to mid-summer (June and July). During mid-summer to mid-autumn (July – November), the DSST index along the Portuguese coast is positive, with a maximum during August and September. This indicates that SST's at the coast are lower than those further offshore. The positive DSST at these latitudes is associated with the equatorward flow due to the Portuguese Trades. Further south, along the Northwest African coast, the index is positive throughout the year, indicating lower temperatures and upwelling conditions along the coast. This band of positive DSST has its maximum north-south extent during winter and spring (January – May). The northern limit of this band remains relatively constant at around 32°N. The southern limit of this band is located around 20°N during summer and early autumn (July – October). In November, the southern limit migrates further south along the coast, reaching it's maximum southerly position at about 12°N during late winter to mid-spring (February – April). At the coast, between about 12-20°N, upwelling occurs during winter and autumn, while the rest of the year is characterised by non-upwelling conditions due to weak southwesterly (sometimes southerly) monsoon winds.

Between ~20-25°N, there is a band of consistently large negative DSST index throughout the year. Within this region, the DSST reaches a maximum of >4°C during May – June (spring and early summer) and September – January (autumn and early winter). This agrees with the region of maximum upwelling in the Canary system. However, it does not agree with the season of maximum upwelling within the region. This could be due to the seasonal cycle of solar heating having a more pronounced effect than the upwelling on the SST at coast. Between 25-32°N, the DSST reaches a maximum during late summer and autumn (August – November). This agrees well with the seasonal upwelling, which reaches a maximum in this region during summer and autumn. Between ~32-37°N, the DSST index is negative, indicating higher temperatures at the coast during late winter to early autumn (February – September). These negative DSST's at the coast are related to the onshore winds within this region. At 37°N, there is a sharp change from non-upwelling conditions to upwelling conditions at the coast north of 37°N, during the second half of the year. The sharp change could be a result of straightening out the coastline in this area. The upwelling-favourable DSST north of 37°N is related to the development of the Portuguese Trade winds during summer.

Figure 9b describes the offshore location of the 2°C DSST isoline. Maximum offshore distance reached coincides with the maximum DSST in the central part of the region. Between ~18-25°N, the isoline consistently exceeds a distance of 200km offshore, except during August when it is located less than 200km offshore. Around 20°N, during February and April – June, the isoline reaches a maximum offshore distance of >300km.Around 13-14°N, the location of the DSST isoline exceeds 200km offshore during early to mid-spring (March and April).

3.2.4. The California Upwelling System

Appendix 8 shows mean monthly DSST for the California region between 23-57°N and 110-145°W, and figure 8d describes the mean monthly upwelling (DSST) index averaged over the first three pixels at the coast for the California region. The 0°C DSST isoline is roughly zonal between mid winter and spring (January – May). The isoline is situated just north of 45°S in January and migrates further south to about 42°S in May. During summer, at the coast, the 0°C DSST isoline extends further north along the coast, reaching it's furtherest northward extent of about 51°N during late summer to mid autumn (August – October). North of this isoline, the DSST index is negative, indicating the non-upwelling conditions within the region. South of the isoline, the DSST index is positive, indicating upwelling conditions and lower SST's along the coasts of Oregon and California. Between 34-45°S, the DSST index is positive throughout the year and exceeds 3°C in late spring to late autumn (May – November). The positive DSST index reaches a maximum during mid summer to late autumn (July – November) between 38-41°S. This agrees with the maximum upwelling which occurs off Northern California and Oregon during summer.

Between 30-34°S, there is a cell of negative DSST indicating non upwelling conditions within the Southern California Bight approximately between mid January to mid November. In the southern part of the Southern California Bight (south of 33°S), the index is positive during late autumn to early summer (November – June). This agrees with the stronger southward flow of water and upwelling at the coast during observed

by Tsuchiya (1980) during spring. Between 26-30°S, the DSST index is positive between late autumn to mid summer (November – July). South of 26°S, the index is positive during mid spring to early summer (April – June), and negative throughout the rest of the year.

Figure 9d shows the maximum offshore extent of the 2°C DSST isoline for the California region. The offshore location of the isoline reaches a maximum of >300km offshore between ~36-39°S during mid summer to autumn (July – November) and between ~34-36°S during autumn to early winter (September – December). The region described by the isoline agrees well with the SST pattern between 32-45°S described in Figure 7d. The maximum offshore location (>300km) agrees with the seasonal cycle of upwelling in the California system.

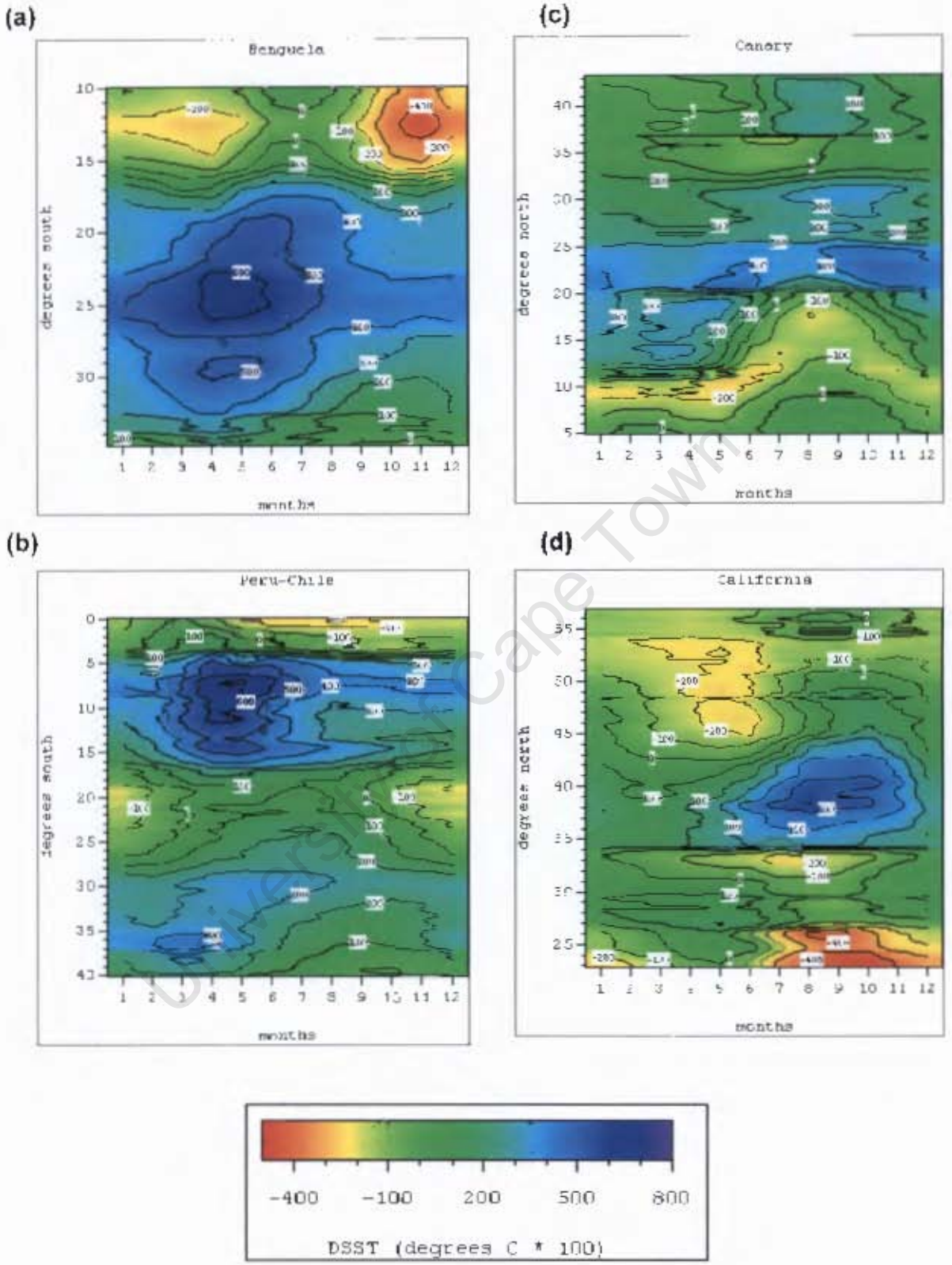

Figure 8: Mean monthly upwelling index (DSST) at the coast for the **(a)** Benguela, **(b)**Canary, **(c)** Peru-Chile, and **(d)** California regions.

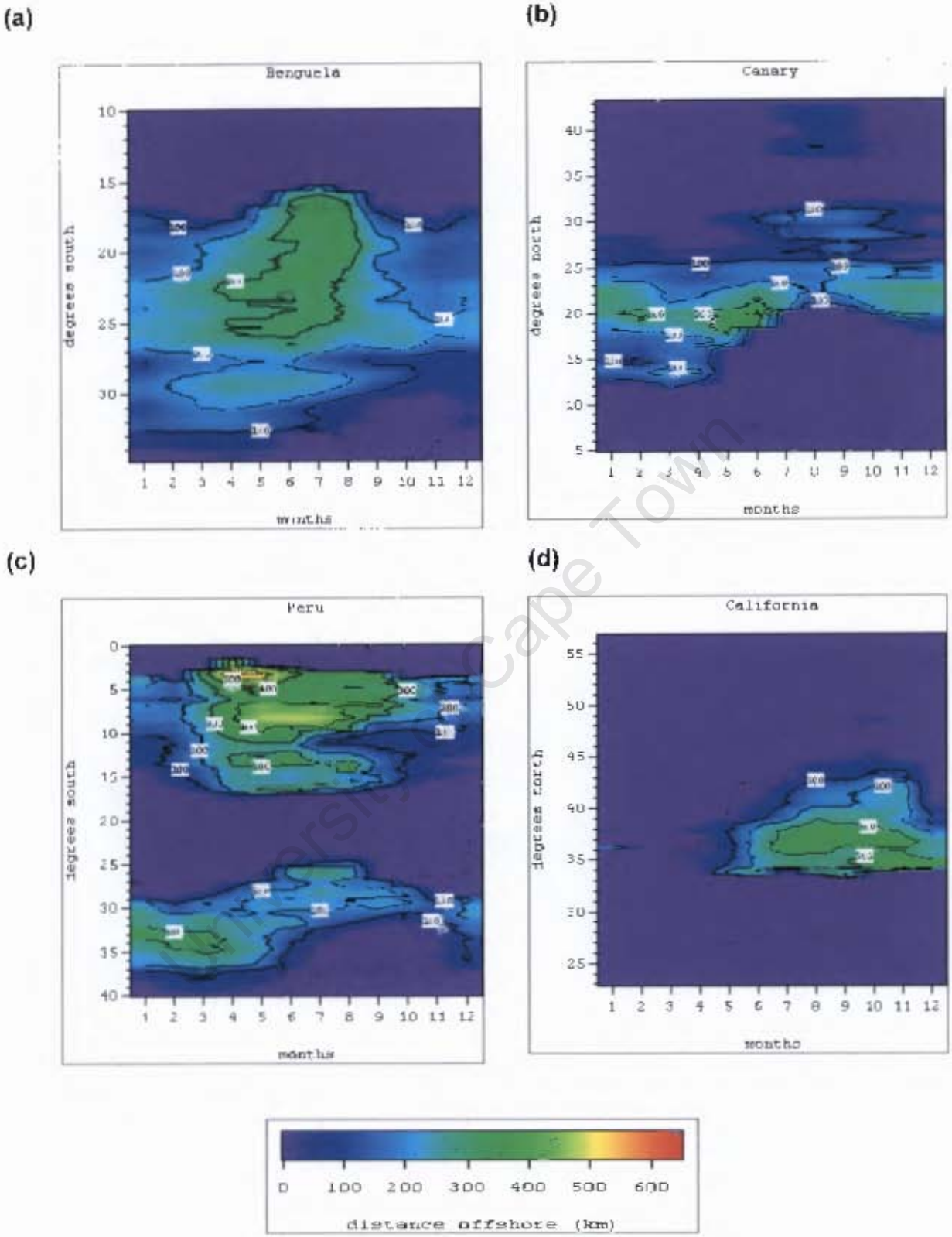

Figure 9: Offshore location of the 2 °C DSST isoline **(a)** Benguela, **(b)**Canary, **(c)** Peru-Chile, and **(d)** California regions.

3.3. Interpretation of Principal Component Analysis

The monthly and mean monthly SST's were used to calculate SST anomalies for each of the regions. The SST anomalies are defined as the deviations of the monthly SST from the mean monthly SST for a particular month. These SST anomalies were then used to perform the principal component analysis. By using the SST anomalies, it is assumed that the seasonal signal, which would account for the largest portion of the variability in the dataset, has been removed. The eigenvalues are presented in figure 10 and the images for principal components 1 and 2 are presented in figure 11.

The eigenvalues shows that the first two eigenvalues have easily interpretable patterns, explaining approximately 60% of the variation in each of the study regions. Only these two components were retained for interpretation, while the other components were discarded on the basis that they explained vary little of the remaining variance. Each of the principal component images (figure 11) are presented in standardised units. It is important to note that the sign of these standardised units is important only for the relative relationship of the pixels in the images. This means that in some of the images, relatively cool areas will be represented by positive pixels, while warm areas will be represented by negative pixels. The intensity of the colour indicates the strength of a pattern in a particular area (i.e., the more intense the colour in a particular area, the stronger the pattern in that area). The lighter shades would represent areas where the pattern is weakly represented. This often occurs close to the boundaries between opposite patterns. Although the sign of the loadings of the component images is arbitrary, the value of the loadings denotes the relative importance of a particular pattern to each individual time step. Thus, loadings with a value close to zero represent times when the pattern described by the component image is not relevant. Loadings with a value closer to 1 represent times when a pattern (or the opposite pattern) in the component image is strongly represented.

Principal component 1 accounts for 42% of the total variance in the Benguela, 53% in the Peru-Chile, 47% in the Canary, and 50% in the California regions. It represents the dominant pattern of variability in each of the regions. In the Benguela, the loadings are negative throughout the region, except in the Cape Peninsula area, where the loadings become weakly positive. This suggests a considerable influence of the Agulhas Retroflection on the southern part of the Benguela system. The loadings are strongest between approximately 15-30°S, suggesting that the pattern indicated by principal component 1 is best represented within this area. To the north and south of this area, the pattern is less well represented. In the Peru-Chile, Canary, and California regions, the loadings are positive throughout the region. In the Peru-Chile region, at ~37-38°S, there is a small patch of weakly negative loadings further offshore. The loadings here are strongest in the northern part of the region, off Peru, and decreases further south. This suggests that the pattern indicated by principal component 1 is best represented along the Peruvian coast. In the Canary, the highest loadings occur in the central part of the region, along the Northwest Africa, while in the California, the loadings are high throughout the region, reaching a maximum around 35°N. This suggests that the pattern is well represented throughout the California region, but is most important in the central part of the region around 35°N. The pattern represented by principal component 1 appears to suggest a zonal gradient. The structure is similar to the structure described by the upwelling index (DSST) and the location of the areas with higher loadings seems to generally coincide with the areas of maximum upwelling found in each of the systems.

Principal component 2 explains 18% of the total variance in the Benguela, 13% in the Peru-Chile, 12% in the Canary, and 12% in the California regions. It represents the main residual pattern in each of the systems once the variability explained by principal component 1 has been removed. In each of the regions, principal component 2 shows positive loadings in the northern part and negative loadings in the southern part. The relative pattern of sea surface temperature can be interpreted in two ways, since the loadings have both positive and negative values. The positive loadings in the north could represent sea surface temperatures which are warmer, suggesting that the SST's in the north are warmer than those in the southern part. Alternatively, the negative loadings could represent SST's which are warmer, suggesting that the SST's in the southern part are warmer than those in the north. The loadings are higher in the Benguela region, suggesting that the pattern indicated by principal component 2 is better represented in the Benguela region than in the others. The pattern appears to be least important in the northern part of the Peru-Chile region, where the loadings are closer to zero. The north-south dipole structure is suggestive of the seasonal polarity of the tropical and subtropical areas in each of the four systems.

The Benguela, Canary, and California systems appear to show three broad regions. The central part of each of these systems has loadings close to zero, while the extreme northern and southern parts of the systems show stronger loadings. In the south, the Benguela system is bounded by the Agulhas Retroflection area, while in the north, it is bounded by the Angola-Benguela surface front, which separates the warm Angolan Current from the cooler water of the Benguela upwelling system. The northern part of the Canary region is part of the Canary Current System, while the southern part is influenced by the Canary Current System offshore and by the tropical circulation. Based on the dynamics of circulation patterns in the California Current system, it appears that the California Current system can be divided into three broad regions. The Peru-Chile system seems to show two broad areas, with strong negative loadings in the southern part and weak positive loadings in the north. In the Peru-Chile system, the region of weak positive loadings in the north, corresponds to the area influenced by the warm tongue extends southwest from the equator to northern and central Chile when the Equatorial Front is weaker or absent during spring and summer. It thus seems that the pattern of variability described by principal component 2 can be related to the oceanic circulation within each of the four systems.

(a)

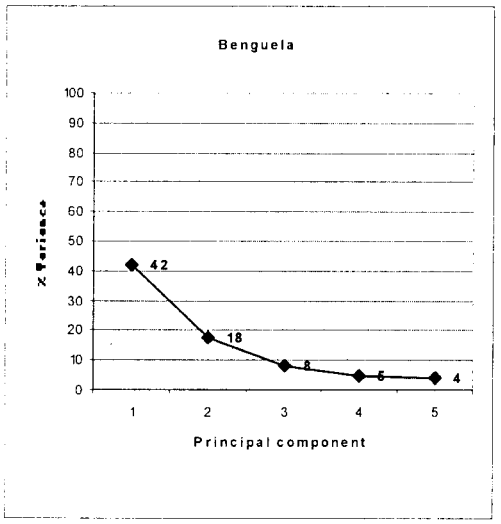

(b)

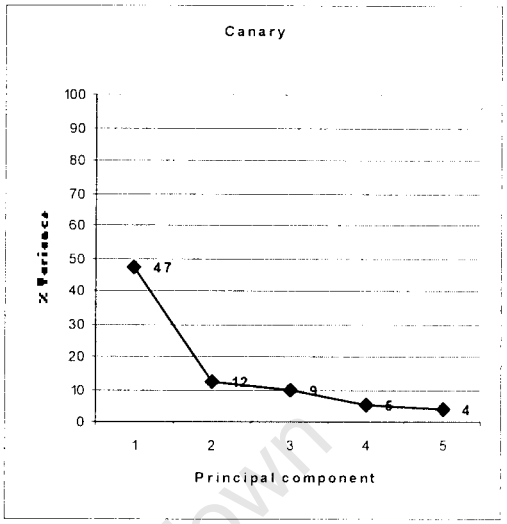

(c)

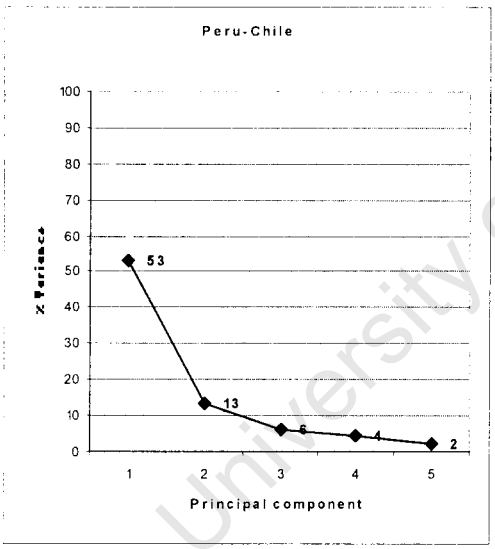

(d)

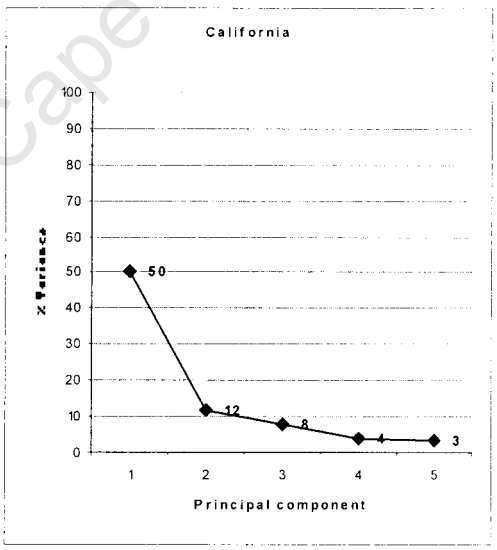

Figure 10: Percentage variance (eigenvalues) explained by the first 5 principal components of the **(a)** Benguela region, **(b)** Canary region, **(c)** Peru-Chile region, **(d)** California region.

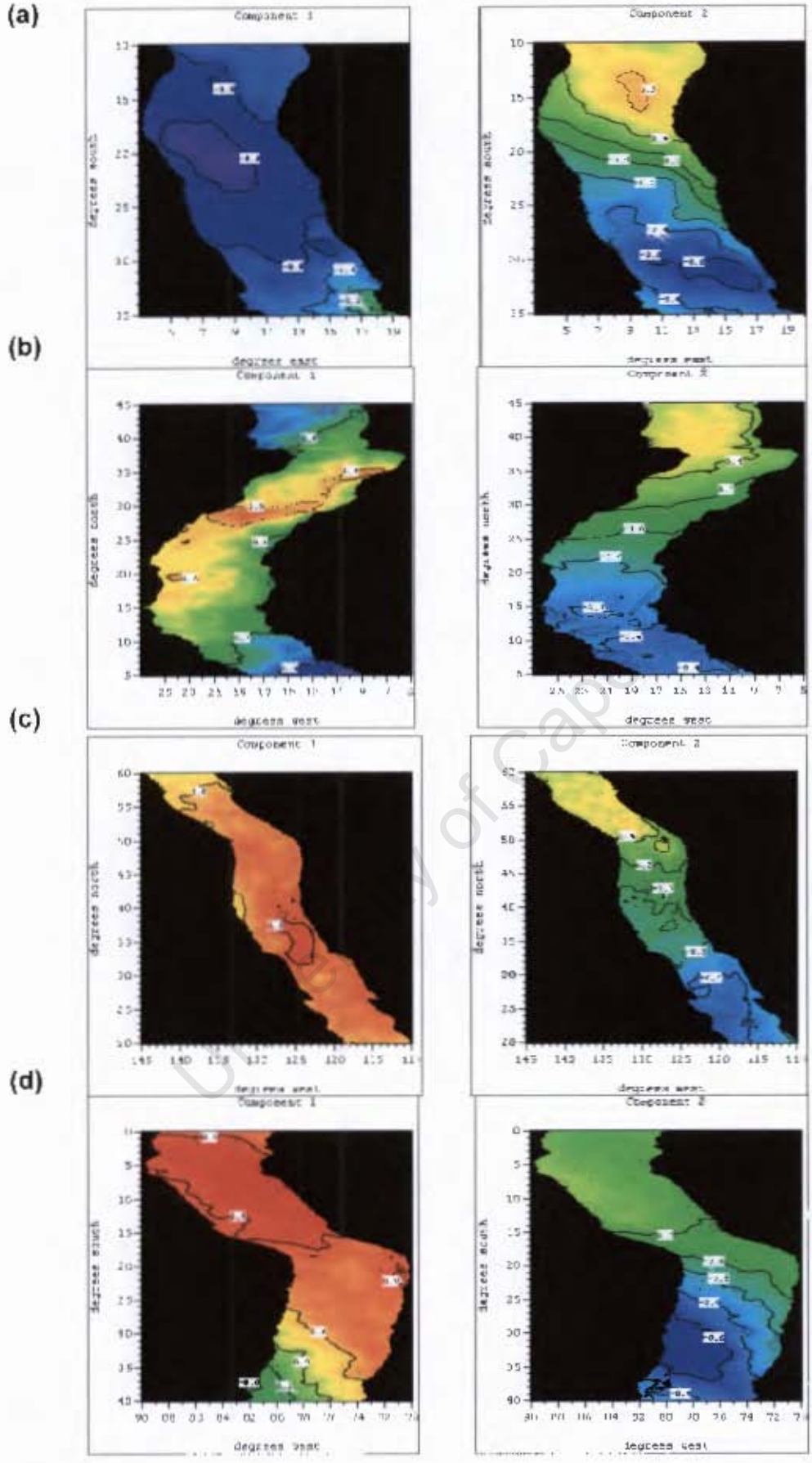

Figure 11: Principal components 1 and 2 for the **(a)** Benguela region, **(b)** Canary region, **(c)** California region, and **(d)** Peru-Chile region.

Figure 12 below shows the loadings for PC 1 and PC 2 for each of the four upwelling systems. Some seasonality is evident in both PC1 and PC2, for each of the regions. This means that there is a residual seasonal signal, which was not completely removed by using the SST anomalies in the principal component analysis. No clear cycles or trends could be identified from the loadings, and they are thus not further discussed.

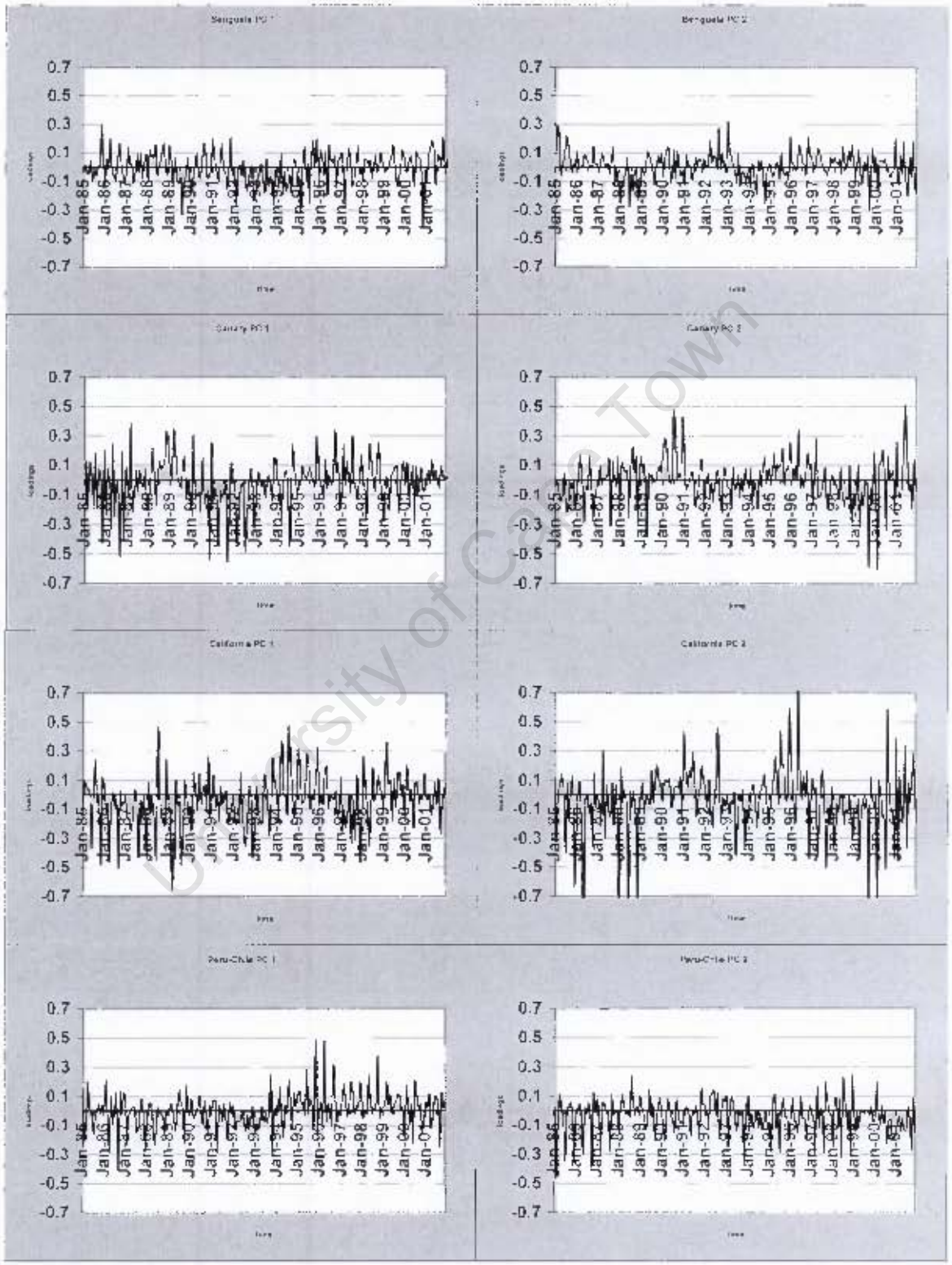

Figure 12: Loadings for principal components (PC) 1 and 2 for the **(a)** Benguela region, **(b)** Canary region, **(c)** California region, and **(d)** Peru-Chile region.

3.4. Ekman Transport

Figure 13a shows the mean monthly offshore Ekman Transport, per degree latitude, at the coast for the Benguela region. When the Ekman Transport is positive, it indicates that flow is onshore and unfavourable to upwelling due to convergence of water at the coast. When the Ekman Transport is negative, it indicates that flow is offshore and upwelling favourable due to divergence of water at the coast.

Around 11-12°S, there is a narrow region where the Ekman Transport is positive throughout the year. This indicates that conditions are unfavourable to upwelling at the coast throughout the year at these latitudes. North of 11°S, Ekman Transport is weakly positive (less than 1Sv). The positive index suggests a poleward flow of air at the surface. Between 12-30°S, Ekman Transport is negative throughout the year, indicating divergence and upwelling-favourable conditions at the coast. Between 18-24°S, Ekman transport is offshore and exceeds 1Sv. Within this region, around 18-19°S, the transport reaches a maximum of more than 2Sv in July, September, and October. This agrees well with the location of the Cape Frio upwelling cell and the season of maximum upwelling experienced here. Further south, between ~24-30°S, Ekman transport is offshore, exceeding 1Sv throughout the year, except around 27°S during May when the transport drops to below 1Sv. It reaches a maximum around 25-27°S during October and November. This agrees with the location of the Luderitz upwelling cell. South of 32°S, the transport exceeds 1Sv during mid-spring and summer (October to February). This agrees with the location of the Cape Columbine and Cape Peninsula upwelling cells. During mid-autumn to mid-winter (April – July), the transport is positive, indicating convergence and conditions unfavourable to upwelling at the coast.

Figure 13b describes the mean monthly offshore Ekman Transport, per degree latitude, at the coast in the Canary region. When the Ekman Transport is positive, it indicates that flow is onshore and unfavourable to upwelling due to convergence of water at the coast. When the Ekman Transport is negative, it indicates that flow is offshore and upwelling favourable due to divergence of water at the coast. North of ~37°N, the Ekman Transport is weakly (less than 1Sv) negative during mid-spring to early winter (April-December), indicating divergence and upwelling-favourable conditions at the coast. During mid-summer to early spring (January – March), the transport is positive, indicating convergence and conditions unfavourable to upwelling at the coast. North of ~47°N, during April-July, and around 35-36°N during November, transport is positive. Between ~17-35°N, the offshore Ekman Transport is slightly stronger (>1Sv) during mid-winter to early autumn (January – September). Within this region, the offshore transport reaches a maximum of >2Sv around 33°N during March. During September to December, the transport exceeds 1Sv between 24-30°N. Between ~15-18°N, there is a small cell of offshore Ekman transport, exceeding 1Sv, during October – December. South of about 9°N during December – April, and south of ~14°N during May – November, the Ekman Transport is positive throughout the year. This indicates onshore flow and conditions unfavourable to upwelling at the coast.

Figure 13c describes the mean monthly offshore Ekman Transport, per degree latitude, at the coast in the Peru-Chile region. Around 2°S, Ekman Transport is zero throughout the year. North of this latitude, transport is positive, indicating onshore flow and conditions unfavourable to upwelling at the coast throughout the year. Between about 2-23°S, Ekman Transport is negative and more or less constant throughout the year.

Within this region, the transport reaches a maximum of >1Sv between 10-15°S during (April to October). Roughly between 23-25°S, the transport reaches zero. South of 25°S, the transport increases again and reaches a maximum of >3Sv between ~30-38°S during mid-winter and summer (July – February). During mid-autumn to mid-winter (April-July), south of 35°S, Ekman Transport is positive, indicating onshore flow and conditions unfavourable to upwelling at the coast.

Figure 13d describes the mean monthly offshore Ekman Transport, per degree latitude, at the coast in the California region. When the Ekman Transport is positive, it indicates that flow is onshore and unfavourable to upwelling due to convergence of water at the coast. When the Ekman Transport is negative, it indicates that flow is offshore and upwelling favourable due to divergence of water at the coast. North of ~50°N, the Ekman Transport is negative during mid-spring to summer (April – August). South of ~50°N, the period of offshore (negative) Ekman Transport increases from March – September at about 50°N to throughout the year at about 38°N. Between about 38-43°N, offshore (negative) Ekman Transport exceeds 1Sv during February to November. Within this region, transport reaches a maximum of >5Sv between 39-41°N during late spring to early summer (May and June). Further south, centred around 35°N, offshore transport exceeds 1Sv during February to October. Between about 27-28°N, during March to May, there is a small cell of transport which exceeds 1Sv.

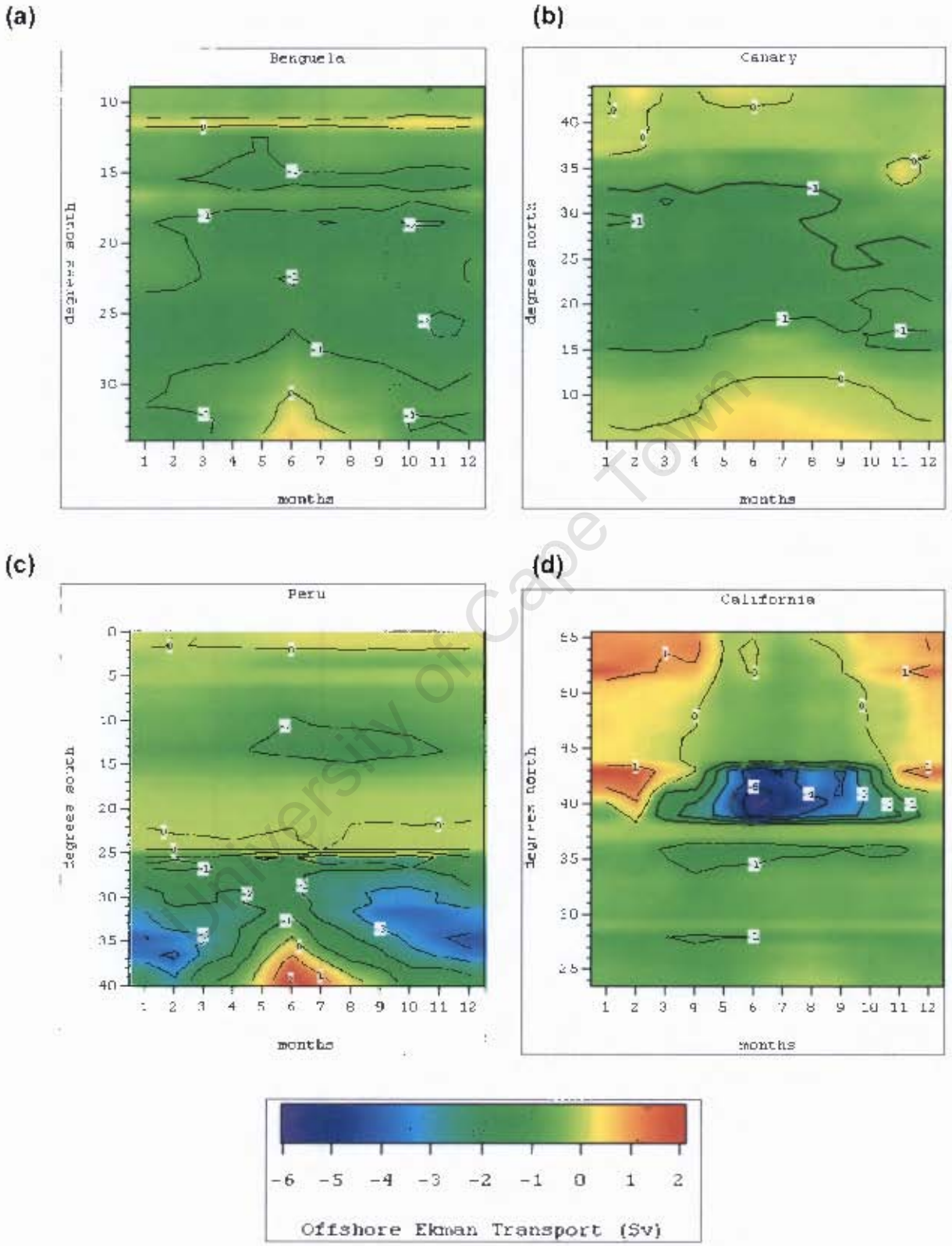

Figure 13: Mean monthly Offshore Ekman Transport at the coast in the **(a)** Benguela, **(b)** Canary, **(c)** Peru-Chile, **(d)** California regions.

Chapter 4 – Summary

This chapter summarises and compares the main features identified from the SST, DSST, and upwelling favourable winds within each of the four major upwelling systems.

4.1. Sea Surface Temperature (SST)

In the Benguela upwelling system, sea surface temperatures reach their maximum value, north of the Angola-Benguela Front. South of this front, the seasonality is reduced as a result of coastal upwelling. Minimum SST's consistently occur in the vicinity of the Luderitz upwelling cell around 25°S. In the southern part of the southern Benguela, around 35°S, the influence of warmer Agulhas current water can be seen and seasonality increases again. In the Peru-Chile upwelling system, SST's are at maximum close to the equator, and at a minimum in the extreme southern part of the region. In the Canary upwelling system, between about 10-20°N, seasonality is large and SST's vary with roughly a 4-5°C difference between winter and summer. In the California upwelling system, south of about 35°N, SST's are generally warm, with a slight cooling during winter. North of 35°N, SST's are generally cool with a slight warming during summer and autumn. The Peru-Chile, Canary, and California systems exhibit similarity in that they are all bounded by warmer water on their equatorial side. In this case, the Benguela system is anomalous since it is bounded by warmer water at both it's northern and southern limits.

4.2. Upwelling Index (DSST)

In the Benguela system, a band of cooler upwelled water is visible along the coast between the Angola-Benguela Front and 35°S. This band appears to be concentrated closer to the coast during late spring to early autumn. During late autumn, the band appears to extend further offshore. The upwelling index appears to be most intense in the vicinity of the Luderitz upwelling cell and also further south at ~30°S, during autumn and winter. The index agrees well with the seasonal maximum of upwelling in the Northern Benguela region. However, further south at the Hondeklip upwelling cell (30°S), as well as at the Cape Peninsula upwelling cell, the index does not agree with the season of maximum upwelling identified by Nelson & Hutchings (1983), Shannon (1985), and Lutjeharms & Meeuwis (1987). The upwelling index in the Southern Benguela system appears to be more affected by the seasonal cycle of solar insolation than in the Northern Benguela system. In the Peru-Chile system, two distinct bands of cooler water are visible along the coast. One band is located along the Peruvian coast, while the other is located along the Northern Chilean coast. In the Peruvian upwelling band, the maximum index occurs during autumn between about 6- 15°S. This agrees with the location of the major upwelling centres off Peru, and with the season of maximum upwelling experienced here. Along the Chilean coast, the index reaches a maximum around 30°S during autumn and winter, and at ~36°S during early autumn. The maximum index along the Northern Chilean coast agrees well with the location of the semi-permanent upwelling cell at Punta Lengua de Vaca. The maximum at ~36°S agrees well with the most intense upwelling along the Central Chilean coast.

In the Canary system, between about 12-20°N, the index indicates upwelling during the first half of the year and downwelling during the second half of the year. Between 20-25°N, upwelling occurs throughout the year, reaching a maximum during autumn and

spring. This agrees well with the season of maximum upwelling experienced in this region. Between 25-33°N, maximum index is experienced during winter and spring. This does not agree with the season of maximum upwelling identified by (Mittelsteadt, 1991, 1983). This may be as a result of the influence of the seasonal cycle of solar heating on the temperature of the region. Off Western Iberia, maximum index is reached during winter and spring. This does not agree with the season of maximum upwelling (summer) experienced along this coast.

In the California system, between ~35-45°N, the maximum index occurs during late autumn to early spring. This does not agree with the season of maximum upwelling (spring and summer) experienced in this region (Hickey, 1998; Huyer et al, 1991). Here, the seasonal cycle of solar heating has a pronounced effect on the upwelling index. Upwelling occurs in small localised cells throughout the year in the Southern California Bight, reaching a maximum from March to May. However, the upwelling index does not resolve this. This is likely the result of the timescale of the data (the monthly timescale tends to mask out event-scale features). Off Baja, California, the index indicates upwelling during the first half of the year. During the second half of the year, the index is negative, suggesting a reduction in upwelling. However, it is more likely the effect of the seasonal cycle of solar heating in the region.

In each of the four regions, the Upwelling index (DSST) highlighted the areas of upwelling along the coast. The Benguela and California systems are similar in the sense that they appear to be single systems situated between ~15-35°S and ~33-45°N, respectively. The Peru-Chile and Canary systems are similar in the sense that they both seem to consist of two separate systems. The Peru-Chile system consists of the upwelling off Peru (~1-17°S) and the upwelling off Chile (~25-36°S). The Canary system consists of the upwelling off Northwest Africa (~12-33°N) and the upwelling off Iberia (~35-43°N). The Benguela, Canary, California, and the upwelling off Chile appear to be similar with respect to the offshore extent of upwelled water (based on the offshore location of the 2°C DSST isotherm). In this case, the upwelling off Peru is anomalous since the 2°C DSST isotherm is located much further offshore.

4.3. Principal Component Analysis

The structure exhibited by Principal component 1 is suggestive of coastal upwelling. This suggests that coastal upwelling is the dominant mode of variability in each of the four upwelling regions. Principal component 1 accounts for 42% of the total variance in the Benguela, 53% in the Peru-Chile, 47% in the Canary, and 50% in the California regions. The pattern exhibited by principal component 1 was better represented in the central part of the Benguela, Canary and California systems. In the Peru-Chile system, the pattern was better represented in the northern part of the region, along the Peruvian coast.

Principal component 2 explains 18% of the total variance in the Benguela, 13% in the Peru-Chile, 12% in the Canary, and 12% in the California regions. The north-south dipole structure is suggestive of the seasonal polarity of the tropical and subtropical areas in each of the four systems. The Benguela, Canary, and California systems appear to show three broad regions. The central part of each of these systems has loadings close to zero, while the extreme northern and southern parts of the systems show stronger loadings. The loadings are higher in the Benguela region, suggesting that the pattern indicated by principal component 2 is better represented in the

Benguela region than in the others. The pattern appears to be least important in the northern part of the Peru-Chile region, where the loadings are closer to zero. It thus seems that the pattern of variability described by principal component 2 can be related to the oceanic circulation within each of the four systems.

4.4. Ekman Transport

In each of the upwelling systems, the regions of maximum offshore Ekman Transport roughly coincide with the regions in which coastal upwelling occurs. In the Benguela and Canary upwelling systems, as well as along the Peruvian coast, the average offshore Ekman Transport is about 1 Sv. Around 24-25°S in the Benguela system during November, the offshore Ekman Transport increases to ~2 Sv. In the Peru-Chile system, along the southern Chilean coast, reaches a maximum of around 4 Sv during spring and summer. In the California upwelling system, between 38-43°N, the offshore Ekman Transport is also large, reaching a maximum of ~5Sv during May and June. Around 30°N and around 27°N, the offshore Ekman Transport is weaker, reaching a maximum of around 1Sv.

Chapter 5 – Concluding Remarks

The main objective of this study was to describe the large-scale temporal and spatial variability of upwelling within the four main upwelling regions using satellite SST and wind data. A key objective was to derive an upwelling index from the SST data to quantify the patterns of upwelling variability identified and described from the SST, and then to use the upwelling index to describe the similarities and differences between the four upwelling regions.

The results obtained during this study are, in general, in agreement with the literature (Nelson & Hutchings, 1983; Shannon, 1985; Lutjeharms & Meeuwis, 1987; Strub et al., 1998; Hickey, 1998; Huyer et al, 1991; Mittelsteadt, 1991, 1983). The sea surface temperature data used has proven useful in describing the large-scale temporal and spatial upwelling variability within the four major upwelling regions. Although the SST upwelling (DSST) index and the offshore Ekman Transport successfully quantified the description of the large-scale temporal and spatial variability of upwelling, it failed to resolve the characteristics of the smaller, more seasonal upwelling cells.

This could be a result of the spatial resolution of the datasets used, especially in the case of the 1°x1° resolution wind stress dataset used to derive the offshore Ekman Transport. It could also be due to the equations employed in this study, especially in the case of the Upwelling Index (DSST), where the index is dependant on the seasonal heat cycle (where solar insolation could suppress the expression of upwelling at the surface). It is also affected by the temporal resolution of the data, since monthly timescales mask out any event-scale upwelling that may occur.

Although there are notable similarities between the four Eastern Boundary Current systems, there are also some major differences. These differences are recognised when considering biological production, fisheries yields, etc. Therefore caution needs to be taken with the comparative approach, since a similar variability in upwelling in the four systems does not necessarily mean a similar variability in biological production.

Chapter 6 – Bibliography

Abbot, M. R. & B. Barksdale, 1995. Variability in Upwelling System as Observed In Satellite Remote Sensing. In: *Upwelling in the Ocean: Modern Processes & Ancient Records*, C. P. Summerhayes, K. –C. Emeis, M. V. Angel, R. L. Smith, & B. Zeitzschel (Eds.), John Wiley & Sons Ltd, pp. 221 – 238.

Andrews, W. R. H. & L. Hutchings, 1980. Upwelling in the Southern Benguela Current. *Prog. Oceanogr.*, **9(1)**, 81 pp.

Bakun A. & C. S. Nelson, 1991. The seasonal cycle of wind stress curl in subtropical eastern boundary current region. *J. Phys. Oceanogr.*, **21,** pp.1815 – 1834.

Bakun, A., 1996. Patterns in the Ocean: Ocean Processes and Marine Population Dynamics. California Sea Grant College System. National Oceanic and Atmospheric Administration.

Bang, N. D., 1971. The Southern Benguela Current region in February 1966. 2. Bathythermography & air-sea interactions. *Deep-Sea Res.*, **18(2)**, pp. 209 – 224.

Bang, N. D. and W. R. H. Andrews, 1974. Direct Current measurements of a shelf-edge frontal jet in the Southern Benguela system. J. Mar. Res., **32(3)**, pp. 405 – 417.

Barton, E. D., 1987. Meanders, eddies and intrusions in the thermohaline front off northwest Africa. *Oceanol. Acta,* **10**, pp. 267 – 283.

Barton, E. D., 1989. The poleward undercurrent on the eastern boundary of the subtropical North Atlantic. In *Poleward Eastern Boundary Currents,* S. Neshyba, C. N. K. Mooers and R. L. Smith, eds. Springer-Verlag, New York, pp. 82 – 92.

Barton, E. D., 1998. Eastern Boundary of the North Atlantic: Northwest Africa and Iberia. In: *The Sea*, **11**, Robinson, A. R., Brink, K. H., (Eds.), John Wiley & Sons Inc., New York, pp. 633 – 657.

Bentamy A., Y. Quilfen, F. Gohin, N. Grima, M. Lenaour and J. Servain, 1996. Determination and validation of average wind fields from ERS-1 scatterometer measurements. The Global Atmosphere and Ocean System, Vol. **4**, pp. 1-29.

Boyd, A. J., 1987. The Oceanography of the Namibian Shelf. PhD. Thesis, University of Cape Town, 190 pp.

Boyd, A. J., J. Salat & M. Maseo, 1987. The seasonal intrusion of relative saline water on the shelf off northern & central Namibia. In: *The Benguela and Comparable Ecosystems*, A. I. L. Payne, J. A. Gulland & K. H. Brink (Eds.), *S. Afr. J. Mar. Sci.*, **5,** pp.107-120.

Brink, K. H., D. Halpern & R. L. Smith, 1980. Circulation in the Peruvian upwelling system near 15°S. *J. Geophys. Res.*, **85**, pp. 4036 - 4048.

Brink, K. H., 1983. The near-surface dynamics of coastal upwelling. *Prog. Oceanogr.* **12(3)**, pp. 223 – 257.

Brink, K. H., D. Halpern, A. Huyer & R. L. Smith, 1983. The physical environment of the Peruvian upwelling system. *Prog. Oceanogr.*, **12,** 285 – 305.

Brink, K. H. & R. D. Muench, 1986. Circulation in the Point Conception-Santa Barbara Channel region. *J. Geophys. Res.*, **91**(C1), pp. 877-895.

Brink, K. H. & T. J. Cowles, 1991. The Coastal Zone Transition Program. *J. Geophys. Res.*, **90 (C8)**, pp. 14637 – 14647.

Brundrit, G.B., Shannon L. V. 1989. Storms & the Agulhas Current: a glimpse of the future. *S. Afr. J Sci.*, **84**, pp. 584-586.

Carr, M., 2002. Estimation of potential productivity in Eastern Boundary Currents using remote sensing. Deep-Sea Res II., **49**, pp. 59-80.

Chapman P. & L.V. Shannon, 1985. The Benguela ecosystem Part II. Chemistry and related processes. In: *Oceanogr. Mar. Biol. Ann. Rev.* **23**, M. Barnes (Ed.), Aberdeen University Press, Aberdeen, Scotland, pp. 183–251.

Chelton, D. B., 1984. Seasonal variability of along-shelf geostrophic velocity off California. *J. Phys. Oceanogr.*, **12,** pp. 757-784.

Chelton, D. B. & R. E. Davis, 1982. Monthly mean sea-level variability along the west coast of Northern America. *J. Phys. Oceanogr.*, **12,** pp. 757-784.

Chelton, D. B., P. A. Bernal & J. A. McGowen, 1982. Large-scale interannual physical and biological interaction in the California current. *J. Mar. Res.*, **40,** pp. 1095-1125.

Christensen, N., J. & N. Rodriguez, 1979. A study of sea level variations and currents off Baja California. *J. Phys. Oceanogr.*, **9,** pp. 631-638.

Clarke, A. J., 1989. Theoretical understanding of Eastern Ocean Boundary Poleward undercurrents. In: *Poleward flows along Eastern Ocean Boundaries*, S. J. Neshyba, C. N. K. Mooers, R. L. Smith and R. T. Barber (Eds.), Springer-Verlag, Berlin, pp. 110 – 130.

Cole, J. & McGlade, J. 1998. Temporal and spatial patterning of sea surface temperature in the Northern Benguela upwelling system: possible environmental indicators of clupeoid production. South Afr. J. Mar. Sci. **19**: pp. 143-157.

Cucalón, E., 1987. Oceanographic variability off Ecuador associated with an El Niño event in 1982 – 1983, *J. Geophys. Res.*, **92**, pp. 14309-14322.

Davenport, R., S Neuer, P. Helmke, J. Perez-Marrerro, O. Llinas., 2002. Primary productivity in the northern Canary Island region as infrared from the SeaWiFS imagery, *Deep-Sea Research* II, **49,** Pergamon. pp. 3481-3496.

Djurfeldt, L., 1989. Circulation and mixing in a coastal upwelling embayment; Gulf of Arauco, Chile. *J. Cont. Shelf Res.,* **9(II)**, pp. 1003 – 1016.

Eastman, J. 1992. Time series map analysis using standardised principal components. ASPRS ACSM RT technical papers **1**: pp. 195-204.

Enfield, D. B. & J. S. Allen, 1980. On the structure of dynamics of monthly mean sea level anomalies along the Pacific coast of North & South America. *J. Phys. Oceanogr.,* **10**, pp. 557-578.

Enfield, D., 1981. Thermally driven wind variability in the planetary boundary layer above Lima, Peru. *J. Geophys. Res.*, **86**, pp. 2005 – 2016.

Enfield, D. B., M. P. Cornejo-Rodríguez, R. L. Smith & P. A. Newberger, 1987. The equatorial source of propagating variability along the Peru coast during the 1982-1983 El Niño. *J. Geophys. Res.*, **92**, pp. 14335-14346

Emery, W. J. and R. E. Thompson, 2001. Data Analysis Methods in Physical Oceanography, New York, Elsevier.

Florenchie, P., Lutjeharms, J. R. E., Reason, C. J. C., Masson, S., Rouault, M., 2003. The source of Benguela Niños in the South Atlantic Ocean. Geophys. Res. Lett., **30** (10), pp. 12.1-12.4.

Florenchie, P., Reason, C. J. C., Lutjeharms, J. R. E., Rouault, M., Roy, C., Masson, S., 2004. Evolution of Interannual Warm and Cold Events in the Southeast Atlantic Ocean. J. Climate, **17**, pp. 2318-2334.

Fonseca, T.,1989. An overview of the Poleward Undercurrent and upwelling along the Chilean coast. In *Poleward Flows Along Eastern Ocean Boundaries,* S. J. Neshyba, C. N. K. Mooers, R. L. Smith and R. T. Barbar, eds. Springle-Verlag, New York, pp. 203-228.

Freeland, H. J. & K. L. Denman, 1982. A topographically controlled upwelling centre off southern Vancouver Island. *J. Mar. Res.*, **4**(4)**,** pp. 1069-1093.

Frouin, R., A. F. G. Fiúza, I. Ambar and T. J. Boyd, 1990. Observations of a poleward surface current off the coasts of Portugal and Spain during winter. *J. Geophys. Res.*, **95**, pp. 679 – 691.

Fung, T & LeDrew, E. 1987. Application of Principal Component Analysis to change detection. Photogrammetric Engineering and Remote Sensing 53 (**12**): pp. 1649-1658.

Gamelsrød, T., C. H. Bartholomae, D. C. Boyer, V. L. L. Filipe & M. J. O'Toole, 1998. Intrusion of Warm Surface Water Along the Angolan-Namibian Coast in February – March 1995: The 1995 Benguela Niño. In: *Benguela Dynamic.* S. C. Pillar, C. L. Moloney, A. I. L. Payne & F. A. Shillington (Eds.). *S. Afr. J. Mar. Sci.*: **19,** pp. 41-56.

Gallaudet, T.C. & Simpson, J.J. 1994. An empirical orthogonal function analysis of remotely sensed sea-surface temperature variability and its relation to interior oceanic processes of Baja-California. Remote Sensing of the Environment 47 (**3**): pp. 375-389.

Gordon A. L. & K. T. Bosley, 1991. Cyclone gyre in the tropical South Atlantic. *Deep-Sea Res.,* 38-Supplement 1A, pp. S323-S343.

Hagen, E., 2001. Northwest African upwelling scenario. *Oceanologica Acta* **24-Supplement**, pp. 113-128.

Hamman, I., H. C. John and E. Mittelstaedt, 1981. Hydrography and its effects on fish larvae in the Mauritanian Upwelling Area. *Deep-Sea Res.*, **28A**, pp. 561-575.

Hardman-Mountford, N.J. & McGlade, J.M. 2002. Defining Ecosystem Structure from Natural Variability: Application of Principal Component Analysis to Remotely Sensed SST. *In:* The Gulf of Guinea Large Marine Ecosystem. J.M. McGlade, P. Cury, K.A. Koranteng and N.J. Hardman-Mountford (Editors). Elsevier, New York, pp. 67-82.

Hart T. J. & R. I. Currie, 1960. The Benguela Current. *Discovery Rep.,* **31,** pp. 123-297.

Haynes, R. and E. D. Barton, 1990. A poleward flow along the Atlantic coast of the Iberian Peninsula. *J. Geophys. Res.,* **95**, 11425 – 11442.

Haynes, R., E. D. Barton & I. Pilling, 1993. Development, persistence and variability of upwelling filaments off the Atlantic coast of Iberia. *J. Geophys. Res.,* **98,** pp. 22681-22692.

Hill, A.E., B. M. Hickey, F. A. Shillington, P. T. Strub, K. H. Brink, E. D. Barton & A. C. Thomas, 1998. Eastern Ocean Boundaries. The Sea: 11, A. R. Robinson & K. H. Brink (Eds.), John Wiley & Son, New York, pp. 29-67.

Hickey, B. M., 1979. The California current system: hypotheses and facts. *Prog. Oceanogr.,* **8,** pp. 191-279.

Hickey, B. M., 1989. Poleward flow at the northern and southern boundary of the U. S. In *Poleward Flows Along Eastern Boundaries,* S. J. Neshyba, C. N. K. Mooers, R. L. Smith and R. T. Barbar, Eds. Coastal Estuary Studies. Springle-Verlag, New York, pp. 160 – 175.

Hickey, B. M., 1992. Circulation over the Santa Monica - San Pedro basin and shelf. *Prog. Oceanogr.*, **30,** pp. 37-115.

Hickey, B. M. & N. E. Pola, 1983. The seasonal along-shelf pressure gradient on the west coast of the United States. *J. Geophys. Res.,* **88**(C12), pp. 7623-7633.

Hickey, B. M., 1998. Coastal oceanography of western North America from the tip of Baja California to Vancouver Island. In: *The Sea,* **11,** A. R. Robinson & K. H. Brink, John Wiley & Sons Inc. pp. 345 – 393.

Hugget, J., Fréon, P., Mullon, C., Penven, P., 2003. Modelling the transport success of anchovy Engraulis encrasicolus eggs and larvae in the southern Benguela: the effect of spatio-temporal spawning patterns. Mar. Ecol. Prog. Ser., Vol. **250**, pp. 247-262.

Hughes, P. and E. D. Barton, 1974. Stratification and water mass structure in the upwelling area off northwest Africa in April-May 1969. *Deep-Sea Res.*, **21**, pp.611 – 628.

Hutchings, L. & J. Taunton-Clark, 1990. The monitoring of gradual change in areas of high mesoscale variability. *S. Afr. J. Sci.*, **86**, pp. 9 – 37.

Huyer, A., 1983. Upwelling in the California Current System. *Prog. Oceanogr.*, **12,** pp. 259-284.

Huyer, A. & P. M. Korso, 1987. Mesoscale surveys over the shelf and slope in the upwelling region near Point Arena, California. *J. Geophys. Res.,* **90**(C6)**,** pp. 7680-7690.

Huyer, A., R.L. Smith & T Paluszkiewicz, 1987. Coastal upwelling off Peru during normal El Niño times, 1981-1984. *J. Geophys. Res.*, **92**, pp. 14297-14307.

Huyer, A., M. Knoll, T Paluszkiewicz & R. L. Smith, 1991. The Peru Undercurrent: a study in variability. *Deep-Sea Res.,* **38**(Suppl. 1), S247 – S271.

Huyer, A. & R. L. Smith, 1974. A subsurface ribbon of cool water over the continental shelf off Oregon. *J. Phys. Oceanogr.*, **4,** pp. 381-391.

Huyer, A. & R. L. Smith, 1984. The signature of El Niño off Oregon, 1982-1983. *J. Geophys. Res.*, **90**(C4)**,** pp. 7133-7142.

Huyer, A., P. M. Kosro, S. J. Lentz & R. C. Beardsley, 1989. Poleward flow in the California Current system. In *Poleward Flows Along Eastern Boundaries,* S. J. Neshyba, C. N. K. Mooers, R. L. Smith and R. T. Barbar, Eds. Coastal Estuary Studies. Springle-Verlag, New York, pp. 315-330.

Huyer, A., P. M. Kosro, J. Fleischbein, S. R. Ramp, T. Stanton, L. Washburn, F. Chavez, T. Cowles, S. Pierce and R. L. Smith, 1991. Currents and water masses of the coastal transition zone off northern California, June to August, 1988. *J. Geophys. Res.*, **96 (C80)**, pp. 14809 – 14832.

Johnson, D. R., T Fonseca & H. Sievers, 1980. Upwelling in the Humboldt Coastal Current near Valparaiso, Chile. *J. Mar. Res.,* **38**(1), pp. 1-15.

Johnson, M. A. & J. J. O'Brien, 1990. The northeast Pacific Ocean response to the 1982-83 El Niño. *J. Geophys. Res.,* **95**(C5)**,** pp. 7155-7166.

Johnson, A. S. & G. Nelson, 1999. Ekman estimates of upwelling at Cape Columbine based on measurements of longshore wind from a 35-year time-series. *S. Afr. J. Mar. Sci.*, **21**, pp. 433 – 436.

JPL Physical Oceanography Distributed Active Archive Center (PO.DAAC) Data Availability, Version 1-94, *JPL Publication 90-49*, rev. 5.

Jury M. R., F. Kamstra, Taunton-Clark, J., 1985a. Diumal wind cycles & upwelling off the northern portion of the Cape Peninsula in summer. *S. Afr. J. Mar. Sci.,* **3,** pp. 1-10.

Jury M. R., F. Kamstra, Taunton-Clark, J., 1985b. Synoptic summer wind cycles & upwelling off the southern portion of the Cape Peninsula. *S. Afr. J. Mar. Sci.,* **3,** pp. 33-42.

Jury M. R., 1988. Case studies of the response & spatial distribution of wind-driven upwelling off the coast of Africa: 29-34°S. *Continent. Shelf Res.* 8(11), pp. 1257-1271.

Jury, M. R., C. I. MacArthur and G. B. Brundrit, 1990. Pulsing of the Benguela region: Large-scale atmospheric controls. *S. Afr. J. Mar. Sci.,* **9**, pp. 27 – 41.

Jury, M. R. and G. B. Brundrit, 1992. Temporal organisation of upwelling in the southern Benguela ecosystem by resonant coastal trapped waves in the ocean and atmosphere. In: *Benguela Trophic Functioning*, A. I. L. Payne, K. H. Brink, K. H. Mann and R. Hilborn (Eds.), *S. Afr. J. Mar. Sci.,* **12**, pp. 219 – 224.

Kamstra, F., 1985. Environmental features of the Southern Benguela with special reference to wind stress. South African Ocean Colour Experiment. L.V. Shannon (Ed.), Cape Town, Sea Fisheries Research Institute, pp. 13 – 27.

Kelly K. A., 1985. The influence of winds and topography on the sea surface temperature pattern over the northern California slope. *J. Geophys. Res.,* **90**(C3)**,** pp. 4945-4950.

Kilpatrick, K.A., G.P. Podesta and R. Evans, 2001. Overview of the NOAA/NASA Advanced Very High Resolution Radiometer Pathfinder algorithm for sea surface temperature and associated matchup database, *J Geophys Res*, 106 (C5), pp. 9179-9197.

Largier, J. L., B. A. Magnell and C. D. Winant, 1993. Subtidal circulation over the Northern California Shelf. *J. Geophys. Res.,* **98**(C10)**,** pp. 18147-18180.

Lillesand, T.M. & Keifer, R.W. 1987. Remote Sensing and Image Interpretation (2nd edition). John Wiley & Sons, New York. 552 p.

Lukas, R., 1986. The termination of the Equatorial Undercurrent in the eastern Pacific. *Prog. Oceanogr.,* **16,** pp. 63-90.

Lutjeharms, J. R. E. & P. L. Stockton, 1987. Kinematics of the upwelling front off Southern Africa. In: *The Benguela & Comparable Ecosystems,* A. I. L. Payne, J. A. Gulland & K. H. Brink. Eds. *S. Afr. J. Mar. Sci.,* **5,** 35-49.

Lutjeharms, J. R. E., 1988. Example of extreme circulation events at the Agulhas retroflection. *S. Afr. J. Mar. Sci.,* **84,** pp. 584-586.

Lutjeharms, J. R. E., van Ballegooyen R. C., 1988. The retroflection of the Agulhas Current. *J. Phys. Oceanogr.* 18(11), pp. 1570-1583.

Lutjeharms, J. R. E., F. A. Shillington & C. M. Duncombe Rae, 1991. Observations of extreme upwelling filaments in the southeast Atlantic Ocean. *Science* (N.Y.), **253**(5021), pp. 774-776.

McClain E. P., W. G. Pichel, and C. C. Walton, 1985. Comparative performance of AVHRR based multichannel sea surface termperatures, *J Geophys Res* 90, pp. 11587-11601.

Meeuwis J. M. & J. R. E. Lutjeharms, 1990. Surface thermal characteristics of the Angola-Benguela Front. *S. Afr. J. Mar. Sci.,* **9,** pp. 261-279.

Mittelstaedt, E., 1983. The upwelling area off northwest Africa: a description of phenomena related to coastal upwelling. *Prog. Oceanogr.,* **12,** 307-331

Mittelstaedt, E., 1991. The ocean boundary along the northwest African coast Circulation and oceanographic properties at the sea surface. *Prog. in Oceanogr.* **34**, pp. 307–355.

Nelson, G., 1985. Notes on the physical oceanography of the Cape Peninsula upwelling system. In: *South African Ocean Colour and Upwelling Experiment*, L. V. Shannon (Ed.), Sea Fisheries Research Institute, Cape Town, South Africa, pp. 63 – 95.

Nelson, G., 1989. Poleward motion in the Benguela area. In: *Poleward flows along Eastern Ocean Boundaries*, S. J. Neshyba, C. N. K. Mooers, R. L. Smith and R. T. Barber (Eds.), Coastal and Estuarine Studies, **34**, Springer-Verlag, New York, pp. 110 – 130.

Nelson, G. & L. Hutchings, 1983. The Benguela Upwelling Area: *Prog. Oceanogr.* 12(3), pp. 333 – 356.

Nelson, G. & A. Polito, 1987. Information on currents in the Cape Peninsula area, South Africa. In: *The Benguela and Comparable Ecosystems*, A. I. L. Payne, J. A. Gulland and K. H. Brink (Eds.), *S. Afr. J. Mar. Sci.*, **5**, pp. 287 – 304.

Philander, S. G. H., 1990. *El Niño, La Niña, & the Southern Oscillation.* Academic Press, San Diego, California, 293pp.

Preston-Whyte, R. A. & P. D. Tyson, 1988. The Atmospheric & Weather of Southern Africa. Oxford University Press, Cape Town, South Africa, 375pp.

Parada, C., 2003. Modelling the effects of environmental and ecological processes on the transport, mortality, growth and distribution of early stages of Cape Anchovy (Engraulis Encrasicolus) in the Benguela system. Phd Thesis. Department of Oceanography, University of Cape Town. 125pp.

Pavlova, Y. V., 1966. Seasonal variations of the California Current. *Oceanology,* **6,** pp.806-814.

Ramp, S. R., J. L. Mc Clean, C. A. Collins, A. J. Semtner & K. A. S. Hays, 1997. Observations and modelling of the 1991-1992 El Niño signal off northern California. *J. Geophys. Res.,* **102**(C3), pp. 5553-5582.

Roemmich, D. & J. McGowan, 1995. Climatic warming and the decline of zooplankton in the California Current. *Science*, **267**, pp. 1324 – 1326.

Schwartzlose, R. A., Alheit, J., Bakun, A., Baumgartner, T., Cloete, R., Crawford, R. J. M., Fletcher, W. J., Green-Ruiz, Y., Hagen, E., Kawasaki, T., Lluch-Belda, D., Lluch-Cota, S. E., MacCall, A.. D., Matsuura, Y., Nevarez-Martinez, M. O., Parrish, R. H., Roy, C., Serra, R., Shust, K. V., Ward, M. N., Zuzunaga, J.Z., 1999. World-wide large-scale fluctuations of sardine and anchovy populations. *South Afr. J. Mar. Sci.*, **21**, pp. 289 – 347.

Schiff, K. C., M. James Allen, E. Y. Zeng and Steven M. Bay, 2000. Southern California. *Marine Pollution Bulletin*, **40**, pp. 76 – 93.

Schumann, E. H., Perrins L. A. & Hunter I. T., 1982. Upwelling along the south coast of the Cape Province, South Africa. *S. Afr. J. Mar. Sci.*, 78(6), pp. 238-242.

Servain, J., Picaut, J., Merle, J., 1982. Evidence of remote forcing in the equatorial Atlantic Ocean. *J. Phys. Oceanogr.*, **12**, pp. 457 – 463.

Shaffer, G., 1982. On the upwelling over the wide shelf off Peru. 1. Circulation. *J. Mar Res.,* **40,** pp. 293-314.

Shannon, L.V., Mostert S. A., Walters N. M., Anderson F. P. 1983. Chlorophyll concentrations in the southern Benguela Current region as determined by satellite. (Nimbus-7 coastal zone colour scanner*), J. Plankt Res.* **5(4)**, pp. 565-583.

Shannon L.V., 1985. The Benguela ecosystem Part I. Evolution of the Benguela, physical features and processes. *Oceanogr. Mar. Biol. Ann. Rev.* **23** (1985), pp. 105–182.

Shannon L. V., J. J. Agenbag & M. E. L. Buys, 1987. Large- & mesoscale feature if the Angola-Benguela Front. In: *The Benguela & Ecosystems,* A. I. L. Payne, J. A. Gulland and K. H. Brink (Eds.), *S. Afr. J. Mar. Sci.*, **5,** pp. 11-34.

Shannon, L.V., J. J. Agenbag, N. D. Walker & J. R. E. Lutjeharms, 1990. A major perturbation in the Agulhas Retroflection area in 1986. *Deep-Sea Res.*, 37(3), pp. 493-512.

Shannon L. V. and P. Chapman, 1991. Evidence of Antarctic bottom water in the Angola Basin at 32°S, *Deep-Sea Res.* **38(10)**, pp. 1299 – 1204.

Shannon, L. V., R. J. M. Crawford, D. E. Pollock, L. Hutchings, A. J. Boyd, J. Taunton-Clark, A. Badenhorst, R. Melville-Smith, C. J. Augustyn, K. L. Cochrane, I. Hampton, G. Nelson, D. W. Japp and R. J. Q. Tarr, 1992. The 1980's: a decade of change in the Benguela ecosystem. In: *Benguela Trophic Functioning*, A. I. L. Payne, K. H. Brink, K. H. Mann and R. Hilborn (Eds.), *S. Afr. J. Mar. Sci.,* **12**, pp. 271 – 296.

Shannon, L.V. & G. Nelson, 1996. The Benguela: large scale features and processes and system variability. In: *The South Atlantic: Past and Present Circulation.* G. Wefer, H. Berger, G. Siedler and D.J Webb (Eds.), Springer Verlag, Berlin, Heidelberg, pp. 163–210.

Shillington, F. A., W. T. Peterson, L. Hutchings, T. A. Probyn, H. N. Waldron & J. J. Agenbag, 1990. A cool upwelling filament off Namibia, southwest Africa: preliminary measurements of physical & biological properties: *Deep-Sea Res.* **37(11A)**, pp. 1753-1772.

Shillington, F. A., L. Hutchings, T. A. Probyn, H. N. Waldron and W. T. Peterson, 1992. Filaments and the Benguela Frontal zone: offshore advection or recirculating loops? In: *Benguela Trophic Functioning*, A. I. L. Payne, K. H. Brink, K. H. Mann and R. Hilborn (Eds.), *S. Afr. J. Mar. Sci.,* **12**, pp. 207 – 218.

Shillington, F. A. 1998. The Benguela Upwelling System off Southwest Africa. In: *The Sea*, **11**, Robinson, A. R., Brink, K. H., (Eds.), John Wiley & Sons Inc., New York, pp. 538 – 604.

Silva, N. & S. Neshyba, 1979. On the southernmost extension of the Peru-Chile Undercurrent. *Deep-Sea Res.,* **42A,** pp. 1387-1393.

Smith R. L., 1986. Upwelling. In: Oceanogrophy & Marine Biology: An Annual Review, 6, H. Barnes, (Ed.), Allen & Unwin, Landon. pp. 11-46.

Smith, R. L., 1983. Peru coastal currents during El Niño: 1976 and 1982. *Science,* **221,** pp.1397-1399.

Stramma, L., 1984. Geostrophic transport in the warm water sphere of the eastern subtropical Atlantic. *J. Mar. Res.*, **42**, pp. 537 – 558.

Stramma, L. & H.-J. Isemer, 1988. Seasonal variability of meridional temperature fluxes in the eastern North Atlantic Ocean. *J. Mar. Res.,* **46**, pp. 281 – 289.

Stramma, L. & G. Siedler, 1988. Seasonal changes in the North Atlantic Subtropical Gyre. *J. Geophys. Res.,* **93**, pp. 8111 – 8118.

Stramma L. and R. G. Peterson, 1989. Geostrophic transport in the Benguela Current region. *J. Phys. Oceanogr.*, **19,** pp. 1440-1448.

Strub, P. T., P. M. Kosro, A. Huyer et al., 1991. The nature of cold filaments in the California Current system. *J. Geophys. Res.*, **96 (C8)**, pp. 14743 – 14768.

Strub, P. T. & C. James, 1995a. The large-scale summer circulation of the California Current. *Geophys. Res. Lett.,* **22**(3), pp. 207-210.

Strub P.T., J. M. Mesías, C. James, 1995b. Altimeter observations of the Peru-Chile Countercurrent. *Geophys. Res. Lett.,* **22**(3), pp. 211-214.

Strub P.T., J. M. Mesías, V. Montecino, J. Rutllant & S Salines, 1998. Coastal Ocean Circulation off Western South America. In: *The Sea,* **11,** A. R. Robinson & K. H. Brink, John Wiley & Sons Inc. pp. 273 – 313.

Taunton-Clark, J., 1990. Environmental events within the South-East Atlantic (1906-1986) identified by analysis of sea surface temperature and wind data. *S. Afr. J. Sci.,* **86(7-10)**, pp. 470-472.

Tsuchiya, M., 1980. Inshore circulation in the Southern California Bight, 1974-1977. *Deep-Sea Res.*, **27a**, pp. 99 – 118.

Van Camp, L., L. Nykjaer, E. Mittelstaedt and P. Schlittenhardt, 1991. Upwelling and boundary circulation off Northwest Africa as depicted by infrared and visible satellite observations. *Prog. Oceanogr.* **9**, pp. 357–402.

Van Foreest D., F. A. Shillington & R. Legeckis, 1984. Large Scale, stationary, frontal features in the Benguela current system. *Cont. Shelf Res.*, **3(4)**, pp. 465-474.

Veitch, J. A., Florenchie, P., Shillington, F. A., 2005. Seasonal and interannual fluctuations of the Angola-Benguela Frontal Zone (ABFZ) using 4.5km resolution satellite imagery from 1982 to 1999. Int. J. Rem. Sens., IN PRESS.

Walker N. D., 1986. Satellite observations of the Agulhas Current & episodic upwelling south of Africa. *Deep-Sea Res.*, **33(8A)**, pp. 1083-1106.

Wilkin, J. L. and D. C. Chapman, 1990. Scattering of coastal-trapped waves by irregularities in coastline and topography. *J. Phys. Oceanogr.*, **20 (3)**, pp. 396 – 421.

Wooster, W. S., & T. J. Reid Jr., 1963. Eastern Boundary Current. In: The Sea, 2, edited by M. N. Hill, Interscience Publishers, New York, pp. 253-280.

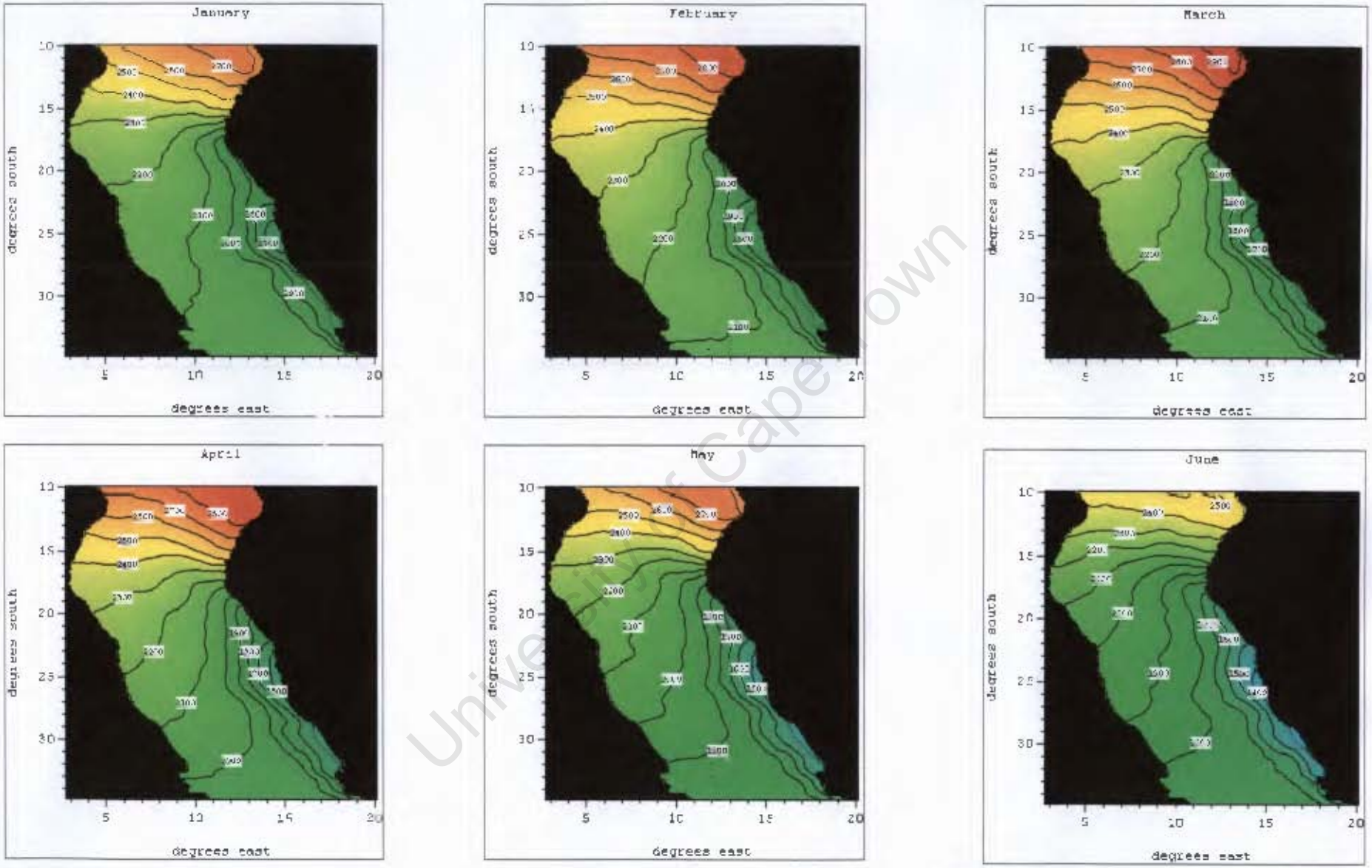

Appendix 1: Mean seasonal pattern of SST in the Benguela region.

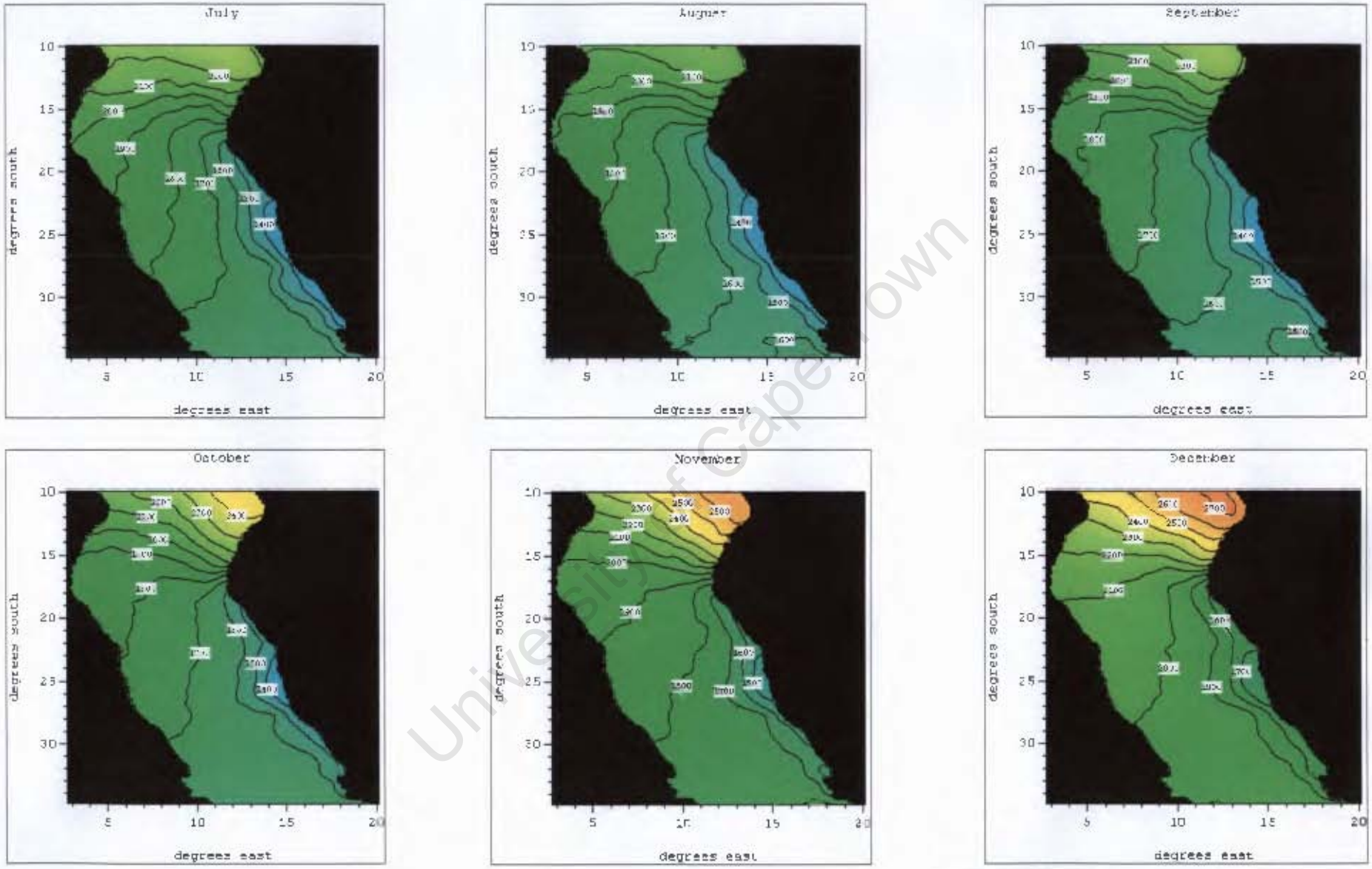

Appendix 1 cont.: Mean seasonal pattern of SST in the Benguela region.

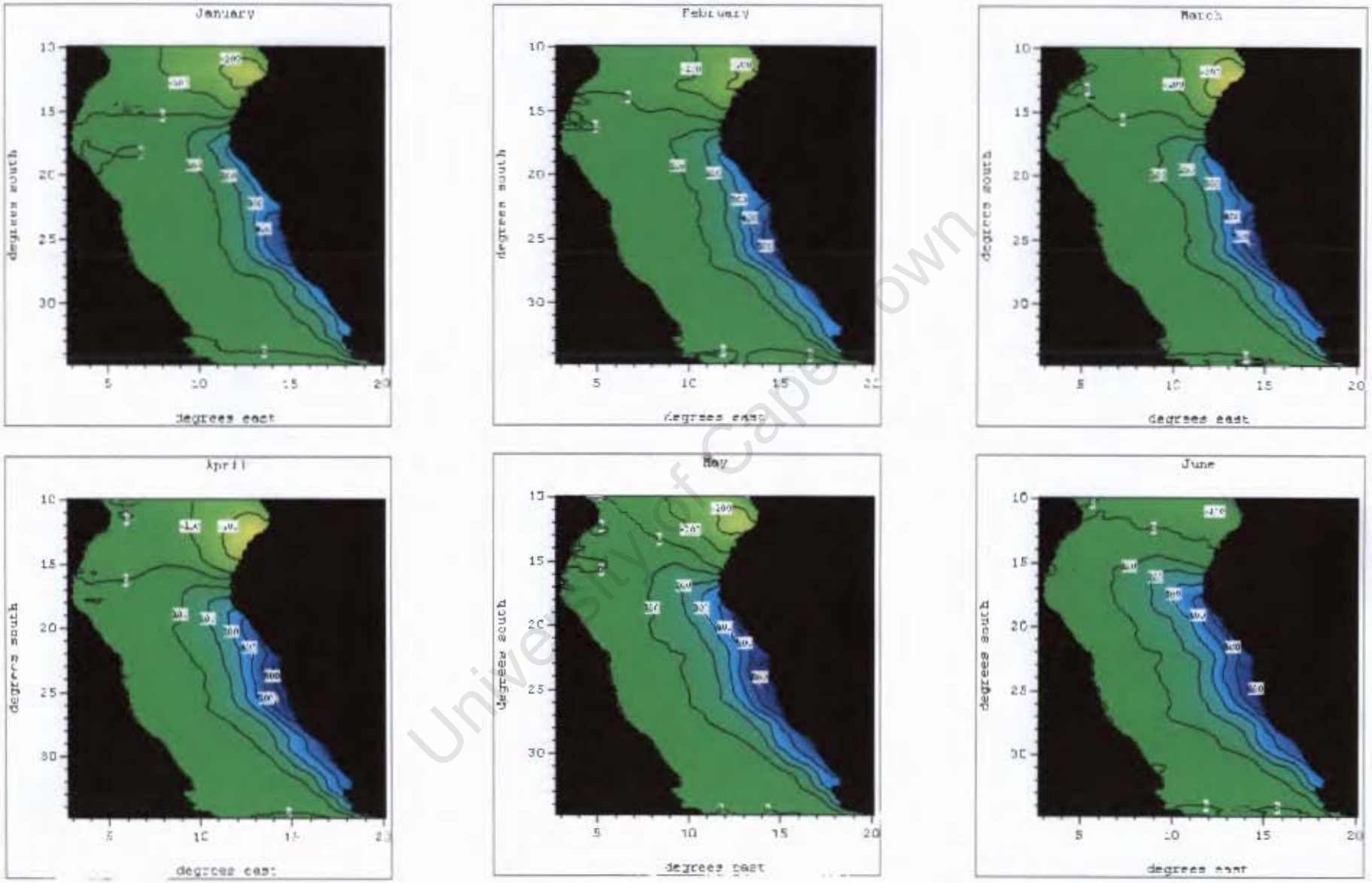

Appendix 2: Mean seasonal pattern of DSST in the Benguela region.

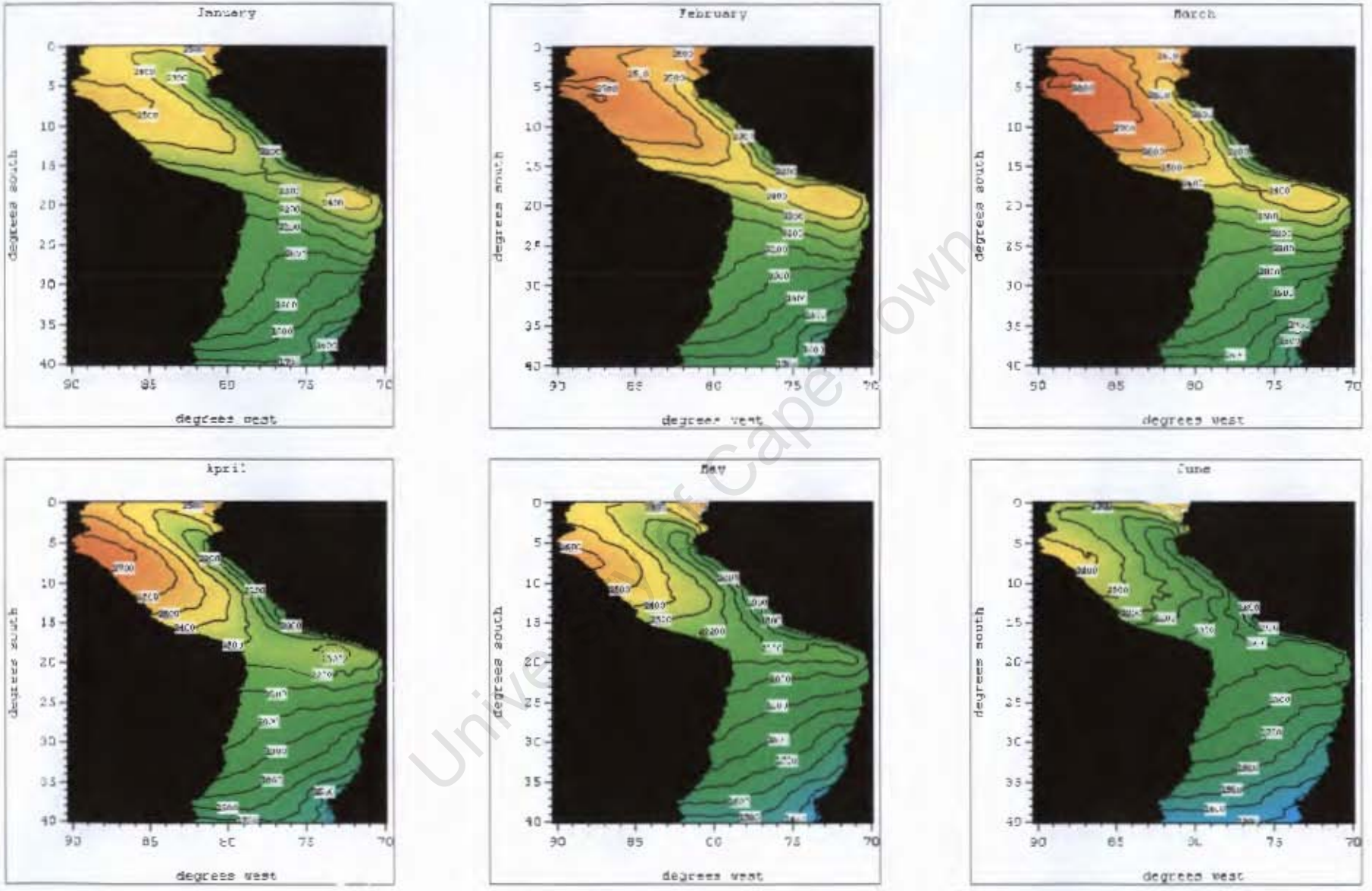

Appendix 3: Mean seasonal pattern of SST in the Peru-Chile region.

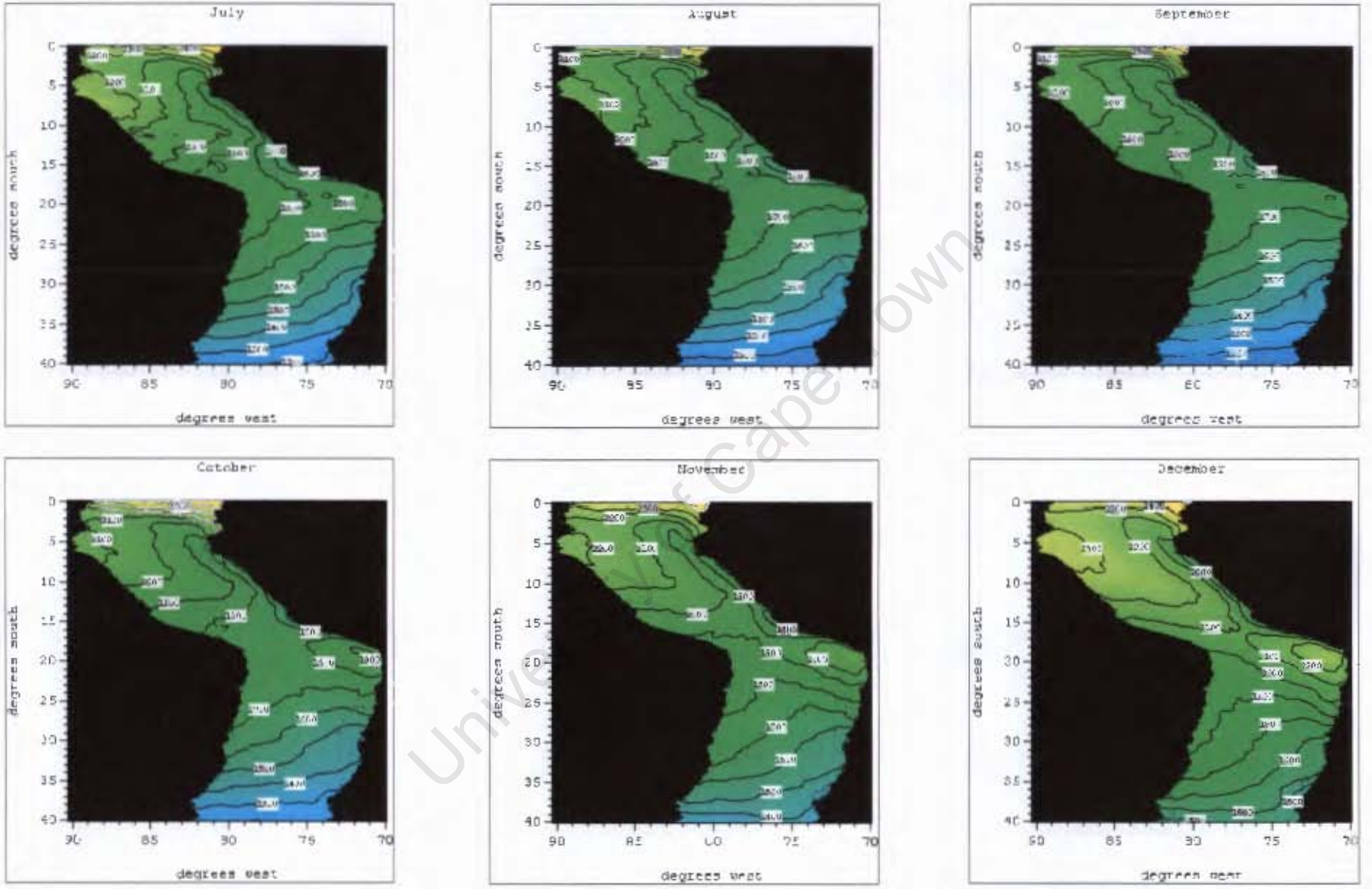

Appendix 3 cont: Mean seasonal pattern of SST in the Peru-Chile region.

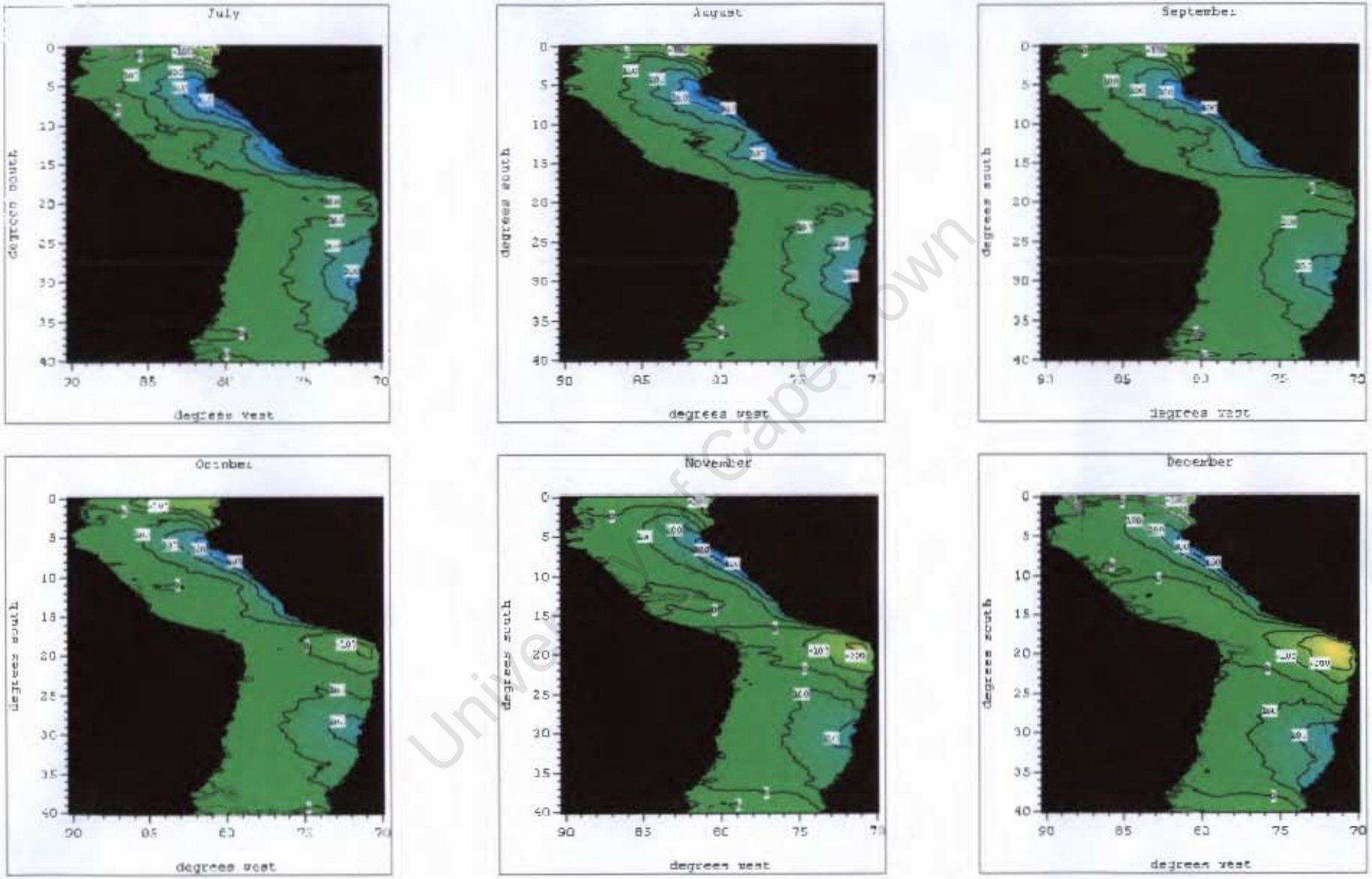

Appendix 4 cont.: Mean seasonal pattern of DSST in the Peru-Chile region.

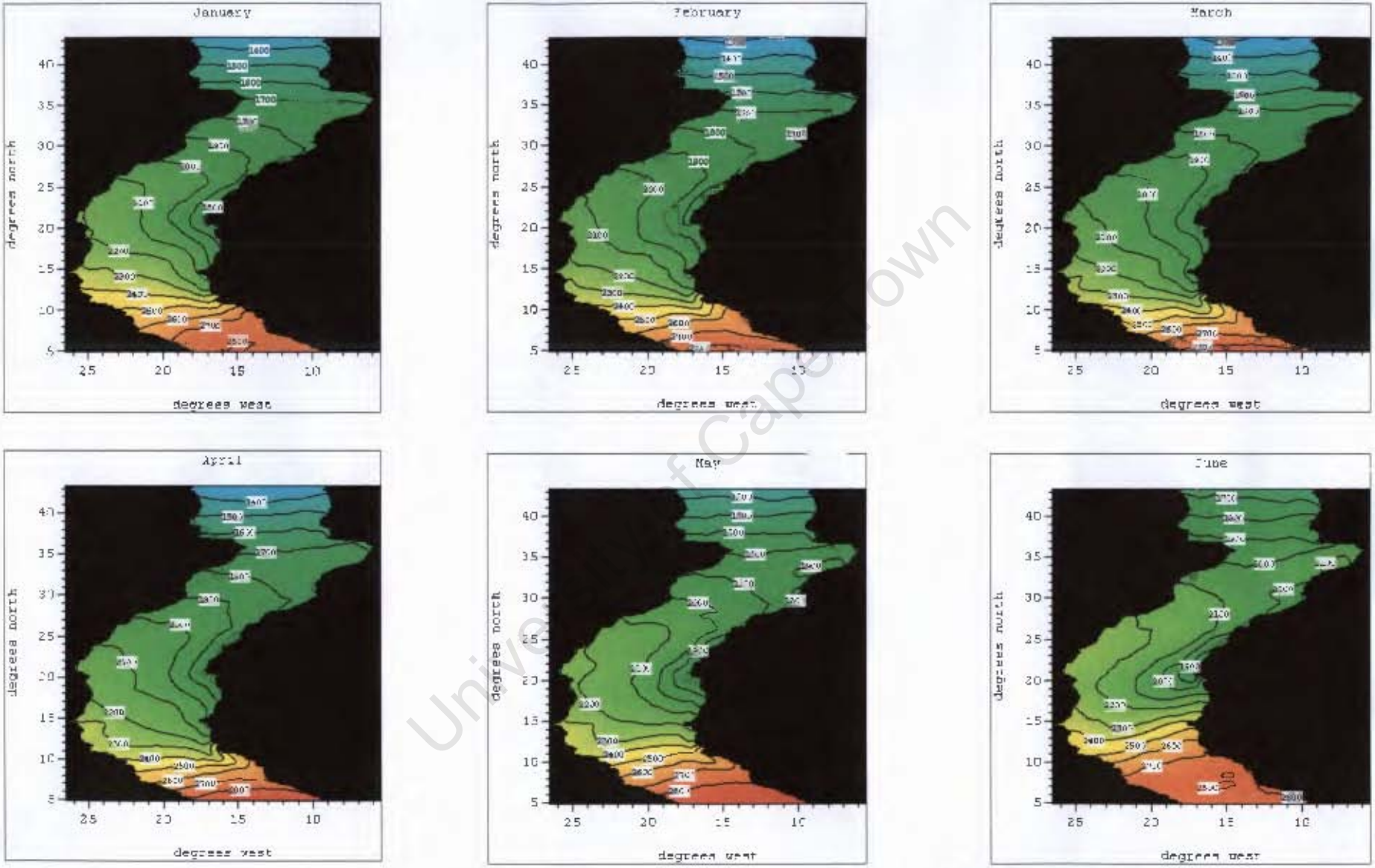

Appendix 5: Mean seasonal pattern of SST in the Canary region.

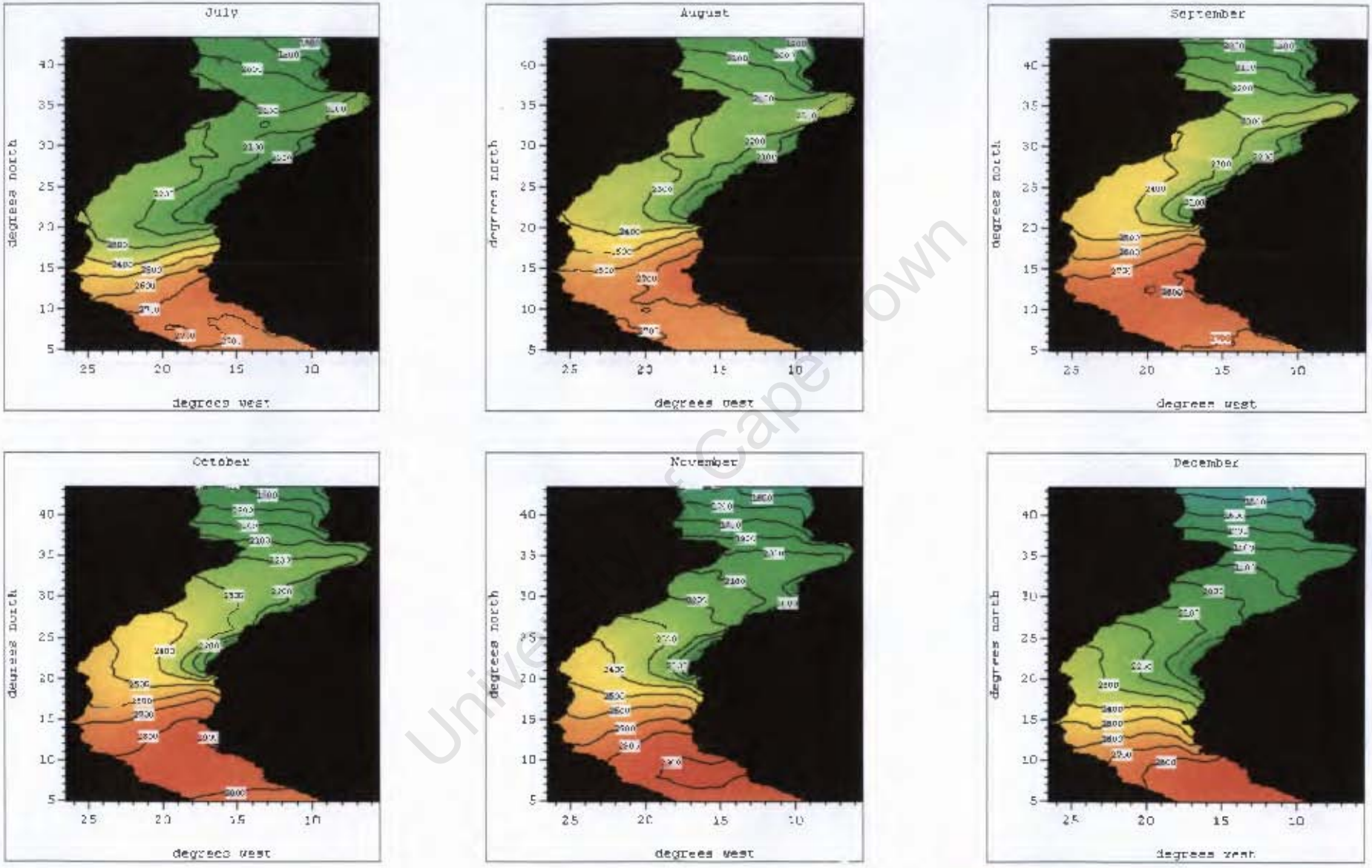

Appendix 5 cont.: Mean seasonal pattern of SST in the Canary region.

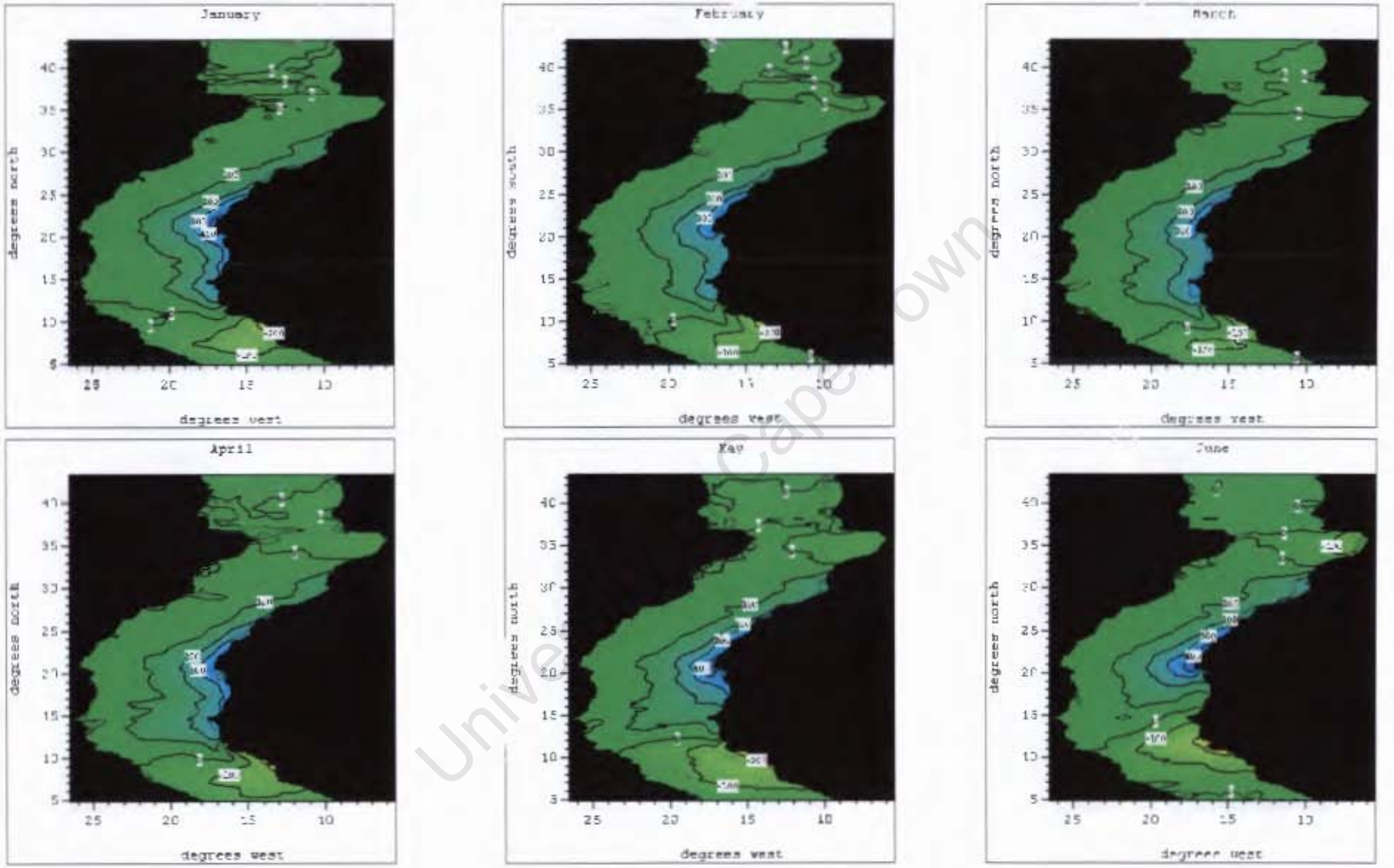

Appendix 6: Mean seasonal pattern of DSST in the Canary region.

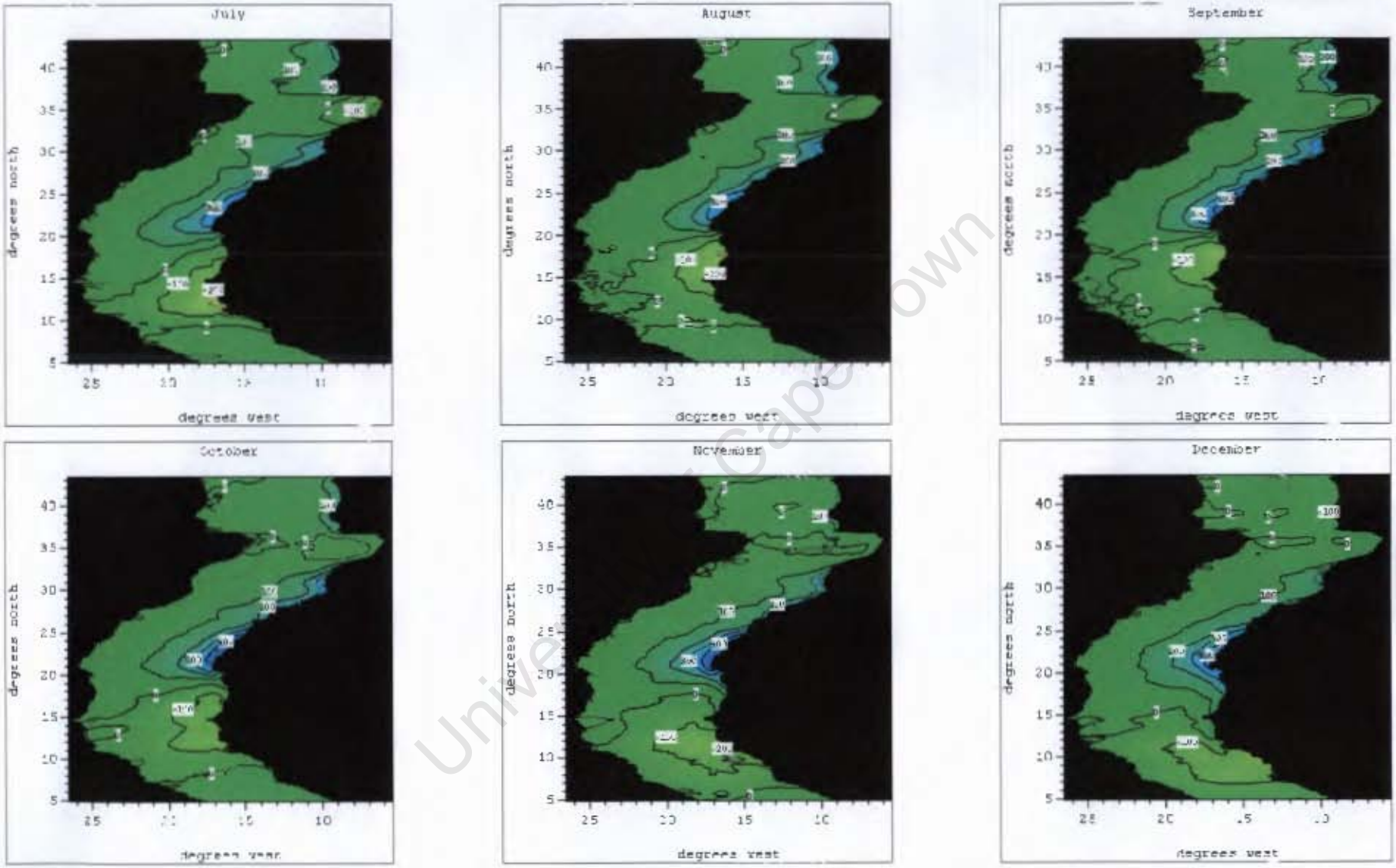

Appendix 6 cont.: Mean seasonal pattern of DSST in the Canary region.

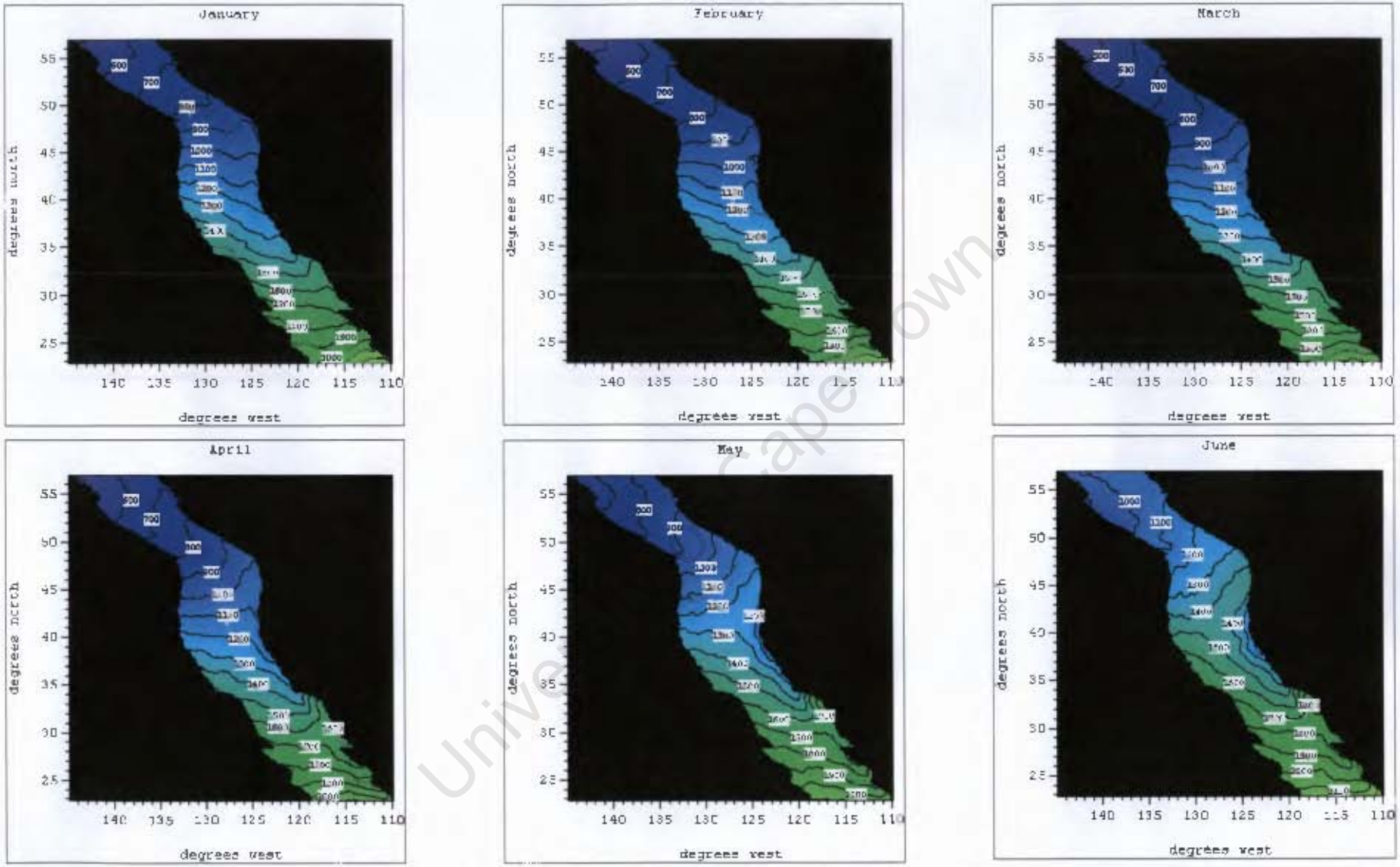

Appendix 7: Mean seasonal pattern of SST in the California region.

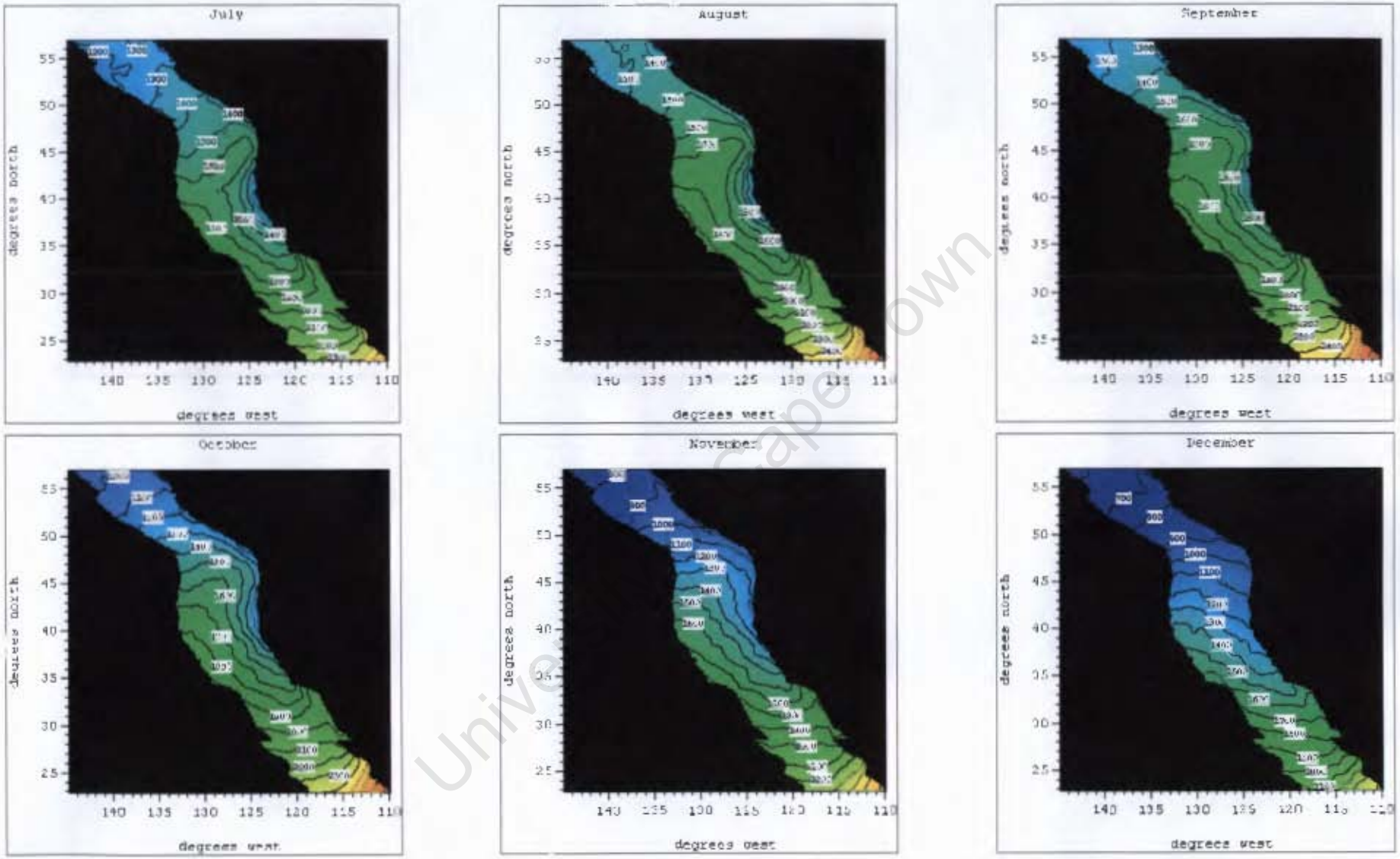

Appendix 7 cont.: Mean seasonal pattern of SST in the California region.

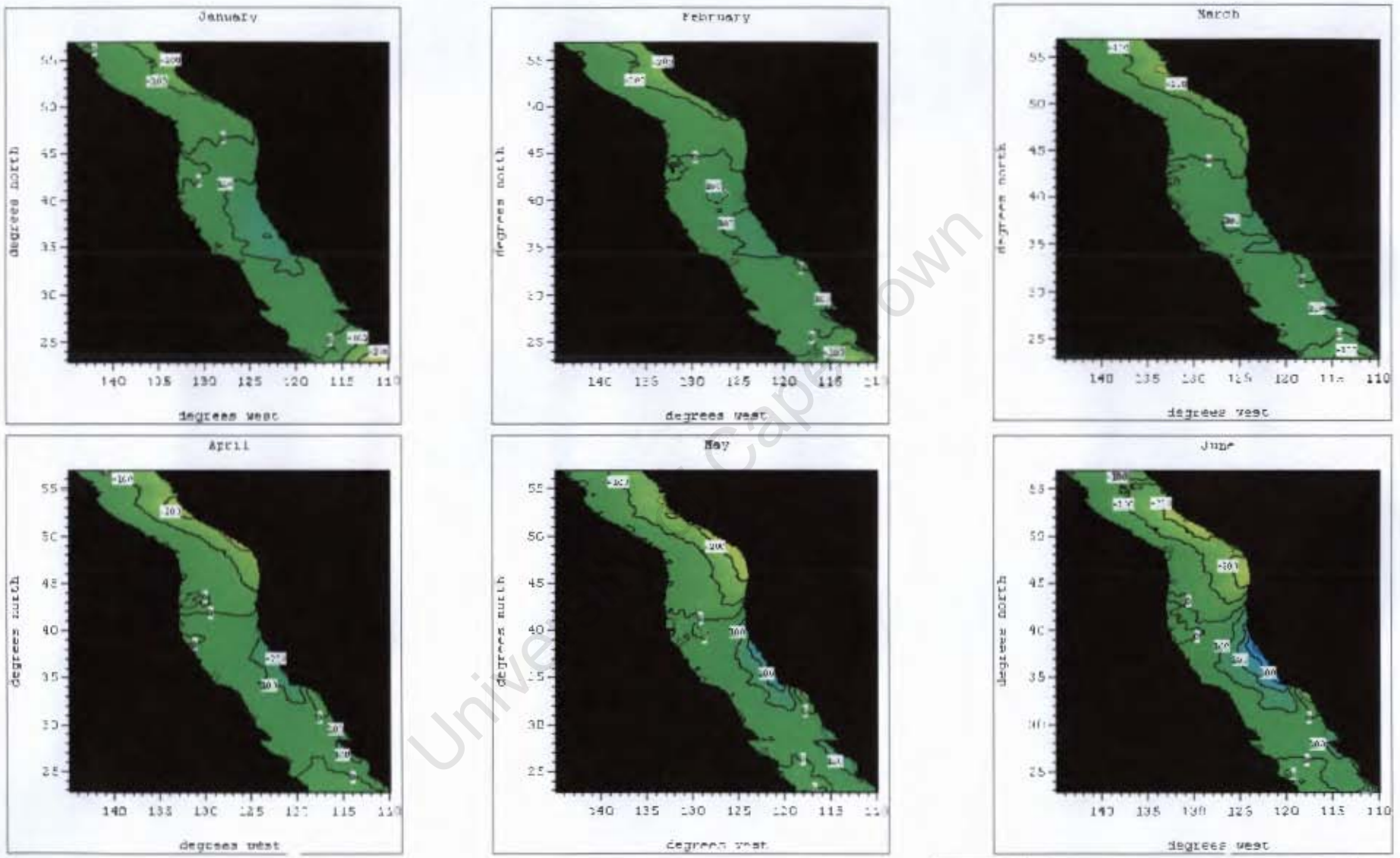

Appendix 8: Mean seasonal pattern of DSST in the California region.

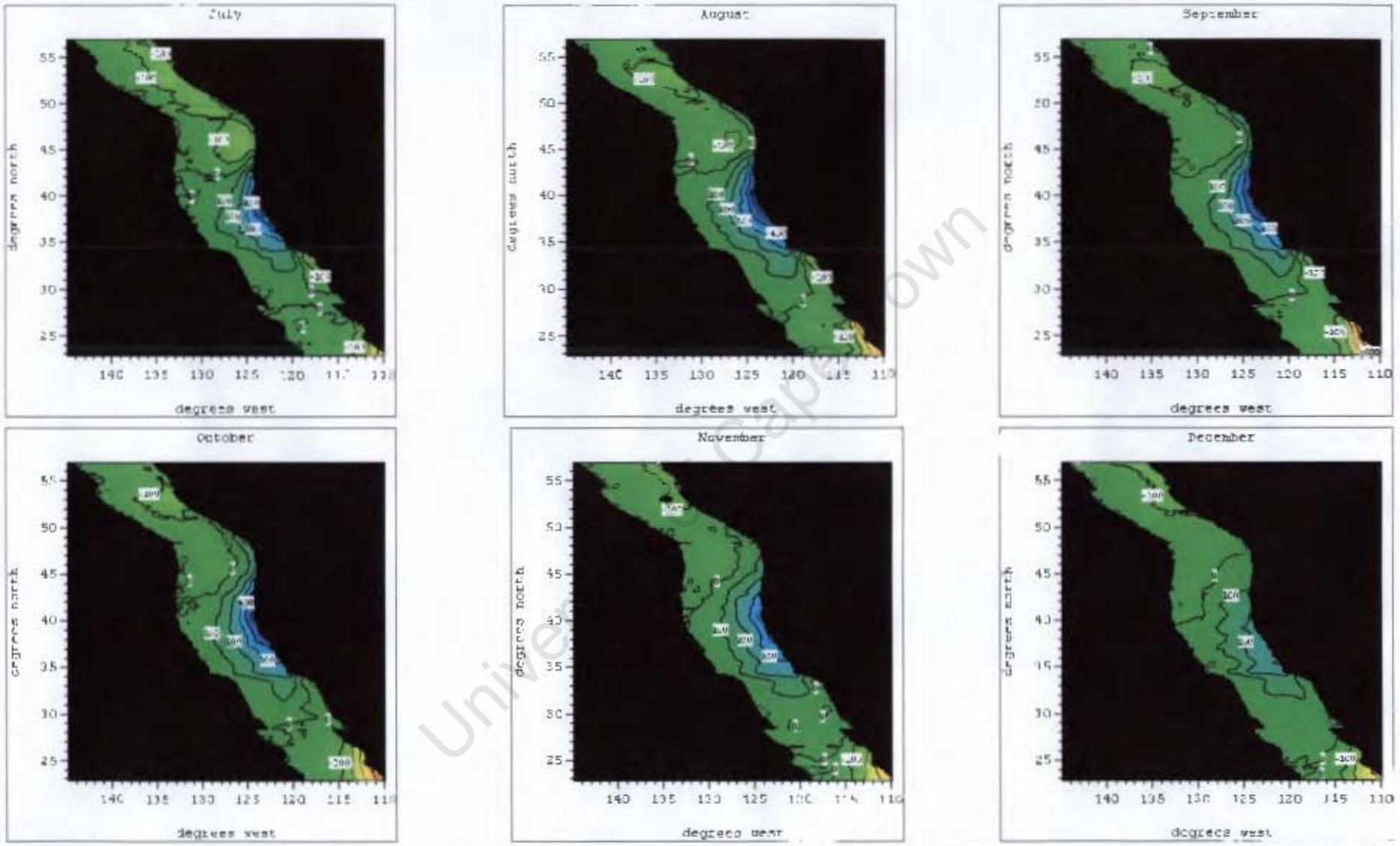

Appendix 8 cont.: Mean seasonal pattern of DSST in the California region.